New Ionization and Detection Technologies for Mass Spectrometry Imaging

From Small Molecules to Intact Proteins

ISBN/EAN: 978-90-77209-77-6

An electronic version of this thesis is available at www.amolf.nl/publications. Paper copies are available from the library of the FOM Institute AMOLF (library@amolf.nl).

New Ionization and Detection Technologies for Mass Spectrometry Imaging

From Small Molecules to Intact Proteins

Nieuwe Ionisatie en Detectie Technologieën voor Massaspectrometrie Imaging

(met een samenvatting in het Nederlands)

Proefschrift

ter verkrijging van de graad van doctor aan de Universiteit Utrecht op gezag van de rector magnificus, prof.dr. G.J. van der Zwaan, ingevolge het besluit van het college voor promoties in het openbaar te verdedigen op woensdag 8 januari 2014 des middags te 2.30 uur

door

András Kiss

geboren op 20 december 1985
te Tatabánya, Hongarije

Promotor: Prof. dr. R. M. A. Heeren

Co-promotor: Dr. D. F. Smith

The work described in this thesis was performed at the FOM Institute AMOLF, Science Park 104, 1098 XG Amsterdam, The Netherlands.
This work is part of the research programme of the Foundation for Fundamental Research on Matter (FOM), which is part of the Netherlands Organisation for Scientific Research (NWO). This work is supported by the Netherlands Proteomics Centre. Part of this research is supported by the Dutch Technology Foundation STW, which is the applied science division of NWO, and the Technology Programme of the Ministry of Economic Affairs, Project OTP 11956.

Vizsgálódás nélkül nincs tudomány, tudomány nélkül nincs kultúra.

There is no science without research; there is no culture without science.

Ferenc Kölcsey

Családomnak

To my family

Contents

Introduction 11
1.1 Mass Spectrometry 12
1.2 Mass Spectrometry imaging 12
1.3 The scope of this thesis 13
Size, weight and position: ion mobility and MS imaging combined 15
2.1 Introduction 15
2.2 Secondary Ion Mass Spectrometry 18
2.2.1 Metal assisted-SIMS (MetA-SIMS) 20
2.2.2 Matrix-Enhanced SIMS (ME-SIMS) 20
2.3 Matrix Assisted Laser Desorption Ionization 25
2.4 Size: the basics of IMS 27
2.4.1 Drift-time IMS 28
2.4.2 Travelling-wave IMS 31
2.4.3 Differential mobility analysers 34
2.5 Weight: IM-MS coupled with a MALDI ion source 37
2.6 Position: IM-MS in imaging experiments 39
2.7 Summary and outlook 43
Microscope Mode Secondary Ion Mass Spectrometry Imaging with a Timepix Detector 45
3.1 Introduction 45
3.2 Experimental 49
3.2.1 The Medipix/ Timepix Detectors 49
3.2.2 Imaging setup on the ion microscope 50
3.2.3 Reference measurement system 51
3.2.4 Timepix-generated spectra and images 51
3.2.5 Samples 52
3.3 Results 53
3.3.1 Ion imaging: Medipix versus time-over-threshold mode acquisitions 53

3.3.2 Spatial resolving power: Timepix versus standard TRIFT images 54
3.3.3 Mass Spectra: Timepix versus TRIFT TDC 56
3.3.4 Time- and space-resolved microscope mode SIMS imaging 58
3.3.5 SIMS-MSI on biological samples with the Timepix 59
3.4 Conclusion 60
Cluster SIMS Microscope Mode Mass Spectrometry Imaging 63
4.1 Introduction 63
4.2 Materials and methods 66
4.2.1 The Medipix/Timepix detectors 66
4.2.2 Microscope mode mass spectrometer 67
4.2.3 Samples 68
4.3 Results and discussion 69
4.3.1 Effects of the high voltage 69
4.3.2 Positive mode imaging 72
4.3.3 Negative mode imaging 74
4.3.4 Tissue imaging 75
4.4 Conclusions 76
Lipid imaging by secondary ion mass spectrometry in a cardiac tissue following myocardial infarction 79
5.1 Introduction 79
5.2 Materials and methods 82
5.2.1 Sample preparation 82
5.2.3 Data analysis 83
5.3 Results and discussion 84
5.3.1 Positive-Ion mode SIMS imaging 84
5.3.2 Negative-ion mode SIMS imaging 89
5.4 Conclusion 91
Top-Down Mass Spectrometry Imaging of Intact Proteins by LAESI FT-ICR MS 93
6.1 Introduction 93

6.2 Materials and methods 96
6.2.1 Samples 96
6.2.2 Mass spectrometry 97
6.2.3 Synchronization of the mass spectrometer and the LAESI source 98
6.3 Results and discussion 100
6.3.1 ESI and LAESI of a protein standard 100
6.3.2 MS imaging of intact proteins 102
6.3.3 CID imaging of an intact protein 105
6.3.4 IRMPD imaging of an intact protein 108
6.4 Conclusion 110
References 111
Appendix 133
Summary 137
Samenvatting 141
Acknowledgements 145
List of publications 147
Curriculum Vitae 153

Chapter 1

Introduction

Curiosity is, without any doubt, one of the most important human traits. We try to understand more and more about how the world around us works. This curiosity is the main driving force behind science. Experiments have a key role in obtaining the answers for the existing scientific questions, testing hypotheses and also unexpected results may lead to new questions. Thus, experiments have a key role in scientific progress. This importance of the experimental work in science and thus in human culture is reflected in the quote chosen for the first page of this thesis from the Hungarian poet Ferenc Kölcsey.

As experimental method is important part of the scientific method, its roots are present in the work of some of the Greek philosophers. Later, experiments played a significant role in the work of a number of philosophers and scientists such as Alhazen, Avicenna or Roger Bacon. However, the first philosophical system that stressed the central role of experience and thus experiments in gaining knowledge was empiricism. Thus, the first experimental method became the integral part of the scientific method was in the work of one of the first empiricist philosophers, Francis Bacon. Because of this he is sometimes called the "father of the experimental method".

Two equally important aspects of experimental research are instrument development and applications. The development of state of the art instrumentation is necessary to be able to push the boundaries of science. New instrumentation can lead to new fields of science. A prime example is the connection between new ion sources for mass spectrometry and the subsequent success of mass spectrometry based proteomics. Also, the application of these new instruments is equally important for further scientific progress. This thesis presents work from both the instrument development and application in the field of mass spectrometry imaging.

1.1 Mass Spectrometry

Probably the first description of mass spectrometry is J. J. Thomson's 100 year old work published in his book titled "The Rays of Positive Electricity" in 1913. Mass spectrometry was able to continuously redefine itself and move in new directions from a method to determine structure of small organic and inorganic compounds to an essential tool in analytical chemistry due to several new improvements in instrumentation. This constant evolution of the field is the main reason for its continuous success during its 100 years of history. These 100 years resulted in several Nobel-prizes for mass spectrometry related scientific discoveries in both the fields of physics and chemistry. These included Thomson in 1906 for his research on electrons, Aston in 1922 for his discovery of isotopes and Wolfgang Paul in 1989 for the discovery of the ion traps[1]. The most recent mass spectrometry related Nobel Prize was awarded to Fenn and Tanaka in 2002 for the development of electrospray ionization and MALDI, respectively[1]. The discovery of these new ion sources revolutionized mass spectrometry and more specifically bio-molecule mass spectrometry. Both ion sources gave "wings to molecular elephants" as Fenn said in the title of his Nobel Lecture[2] and enabled the measurement of intact proteins. Additionally, Electrospray Ionization proved to be a good solution for the problems with the combination of liquid chromatography and mass spectrometry. Thus, these new ion sources started such new and rapidly expanding fields such as mass spectrometry based proteomics and mass spectrometry imaging.

1.2 Mass Spectrometry Imaging

Mass spectrometry imaging is a mass spectrometry technique capable of detecting multiple analytes simultaneously from complex surfaces; determining their identity and location on the surface at the same time. The first examples of the technique for the analysis of inorganic surfaces can be found from the 1960s[3]. However, MALDI mass spectrometry imaging started in the late 1990s[4]. Since then the field evolved into an essential method for biomedical research and the number of applications is still quickly expanding. The main challenges of the field include the increase of measurement speed, spatial resolution and

information content of the measured datasets. Thus, new developments in instrumentation and methodology are crucial for the further progress of mass spectrometry imaging.

1.3 The scope of this thesis

This thesis presents examples to improve both the detection (Chapters 3 and 4) and generation of ions (Chapter 6) for mass spectrometry imaging. Additionally, it gives an example of the application of mass spectrometry imaging to study a complex disease, myocardial infarction, in Chapter 5. Thus, it exemplifies both sides of the research carried out in the *Biomolecular Imaging Mass Spectrometry* (BIMS) *group* at the *FOM Institute AMOLF* in Amsterdam.

Chapter 2 focuses on the evolution of ion-mobility based mass spectrometry imaging and provides examples of its application in analytical studies of biological surfaces. In addition, it reviews Matrix Assisted Laser Desorption Ionization and Secondary Ion Mass Spectrometry, the two main ionization methods for mass spectrometry imaging with a focus on matrix-enhanced SIMS.

Chapter 3 presents the first example of microscope mode Secondary Ion Mass Spectrometry imaging with the Timepix detector, a novel pixelated detector system. This is a proof-of-concept study that evaluates the spectral and imaging performance of the system. This work also proves the feasibility of microscope mode SIMS imaging of biological samples.

Chapter 4 is an extension of the research presented in Chapter 3. The work employs a cluster primary ion source and the high voltage version of the Timepix detector setup. This results in improved speed, sensitivity and mass range of the microscope mode SIMS setup. Also, this work presents the first negative microscope mode imaging data with a pixelated detector from both benchmark samples and tissue sections.

Chapter 5 presents an example of the application of mass spectrometry imaging in biomedical research. The work in the chapter focuses on the study of myocardial infarction. It uncovers the changes in the

distribution of different lipid species and small ions as a result of heart attack.

Chapter 6 demonstrates how an ambient pressure ion source, a Laser Ablation Electrospray Ionization source combined with an FT-ICR mass spectrometer can be used to image multiply charged intact proteins from tissue sections. Also, the first example of top-down imaging of an intact protein is presented with both CID and IRMPD fragmentation.

Chapter 2

Size, weight and position: ion mobility and MS imaging combined

Size, weight and position are three of the most important parameters that describe a molecule in a biological system. Ion mobility spectrometry is capable of separating molecules on the basis of their size or shape, whereas mass spectrometry imaging is an effective tool to measure the molecular weight and spatial distribution of molecules. Recent developments in both fields enabled the combination of the two technologies. As a result, ion-mobility-based mass spectrometry imaging is gaining more and more popularity as a (bio-)analytical tool enabling the determination of the size, weight and position of several molecules simultaneously on biological surfaces. This chapter reviews the evolution of ion-mobility based mass spectrometry imaging and provides examples of its application in analytical studies of biological surfaces.

2.1 Introduction

Key questions in analytical biology and biochemistry evolve around the determination of three basic molecular properties: size, weight and position. The complex interplay between molecules in living systems results in a continuous alteration of these properties at the molecular level. The need for analytical approaches that provide better insight into these processes is growing, as understanding of these systems is increasing. A cell, a tissue section, a tissue extract or a body fluid contains a huge amount of chemical and biological information. A single analytical method is usually insufficient when a better understanding of the function of these

different biological systems is targeted. This is caused by the complexity of these systems. For that reason, a combination of different instruments is extensively used in biochemical research. Ion mobility spectrometry (IMS) coupled with mass spectrometry imaging (MSI) is one of these combined approaches that have the potential to provide direct insight into the shape, structure and position of biomolecules. The combination of MS with IMS has already proven to be an extremely successful technique for determining the structures of ions in the gas phase as it allows the separation of different structural isomers. The addition of a molecular imaging component enhances the molecular detail provided.

The basics of IMS have been known for a long time. Rutherford[5] was one of the first researchers who performed measurements based on the mobility of ions when he measured the velocity of different gas ions. Still, the first ion mobility spectrometers that enabled the separation of ions on the basis of their physical collision cross-section were built only in the 1960s. Ions were simply forced to drift in a gas cell. The first ion mobility mass spectrometers coupled with magnetic sector instruments were also built in the 1960s[6], almost immediately after the development of the first ion mobility spectrometers. Since then the combination of ion mobility cells with both continuous and pulsed ion sources has been solved and ion mobility spectrometers have been coupled with many different kinds of mass analyzers, including time-of-flight (TOF) analyzers[7, 8] magnetic sector instruments[6], quadrupoles[9, 10], ion traps[11-13] and Fourier transform ion cyclotron resonance instruments[14-16]. The first ion mobility instruments were pure drift-time instruments. Two other types of ion mobility spectrometers evolved, differential mobility analyzers (also called high-field asymmetric ion mobility spectrometers) and recently travelling-wave instruments.

Initially, ion mobility spectrometers were used only in the field of physical chemistry and for plasma physics research. The development of the matrix-assisted laser desorption and ionization (MALDI)[17-19] and electrospray ionization (ESI)[20, 21] methods in the late 1980s enabled the measurement of large biomolecules by MS. This also resulted in a major breakthrough in the field of ion mobility MS (IM-MS) in the 1990s. The first work where the mobility of biomolecules was measured was undertaken by Clemmer et al.[22]. In this publication, the possibility of measuring the conformation of proteins with IM-MS was demonstrated.

These results led to the maturation of the technique and since then IM-MS has been used for structural studies of several different biomolecules, such as proteins[22-24], lipids[25-30], carbohydrates[31-34] and even intact viruses[35-37]. It was also shown in several works that the separation of optical isomers is possible using chiral modifiers in the collision gas[38-40]. The potential of using ion mobility mass spectrometers in biological and biochemical research accelerated the development of the instrumentation and moved the field from custom-built instruments to commercially available instruments. Nowadays, several vendors sell ion mobility mass spectrometers and these instruments are becoming more and more popular.

In parallel to the development of IM-MS, another bioanalytical technology has emerged: MS imaging[41, 42]. MS imaging is an MS technique where the spatial distribution of different classes of molecules can be determined on a surface. It is perceived as one of the emerging tools in proteomics, lipidomics and metabolomics. Recent developments in MS imaging allow the direct detection of biomolecules such as proteins, lipids and drugs from thin tissue sections. Label-free imaging with MS uses an intrinsic molecular parameter, the molecular mass, to identify and visualize the distribution of a wide variety of biomolecules on surfaces. This allows the combined determination of molecular weight and localization. An MS imaging experiment requires surface molecules to be desorbed and ionized. Two general approaches can be distinguished in MS imaging. The first and oldest approach uses energetic charged particles to generate ions from a surface for mass analysis. This approach is common to secondary ion MS (SIMS). The second approach uses photons to generate ions from a surface for mass analysis. This is the domain of laser-based MS technologies such as MALDI. There is a continuous stream of new desorption and ionization technologies that extend the capabilities of MS imaging. Desorption ESI and laserspray are examples of recently conceived ambient desorption and ionization methods that further the application areas of MS imaging. The interested reader is referred to recent MS imaging reviews[41, 42] for an overview of all relevant innovation in desorption and ionization for MS imaging. Here we will briefly introduce the key concepts of SIMS and MALDI for MS imaging.

2.2 Secondary Ion Mass Spectrometry

SIMS involves the analysis of secondary ions generated from a surface when this surface is bombarded with high energy primary particles. These primary particles are typically elemental ions generated from a liquid metal ion source. The 'sputtered' secondary particles will be electrons, neutrals and ions. These ions are amenable to analysis with a mass spectrometer and provide insight into the chemical composition of the surface. As a rule of thumb, with a primary ion dose below 10^{13} ions/cm^2, each individual primary ion samples a fresh spot on the surface. This is referred to as the 'static limit'. An ion-induced modification of the surface is sampled with a primary ion dose above this static limit. Under these conditions the surface changes rapidly and is sputtered with a fixed sputter rate. The regime where the primary ion dose exceeds the static limit is hence referred to as 'dynamic SIMS'. Traditionally, SIMS has been applied in the domain of surface physics and solid-state physics. Over recent decades, SIMS has developed more and more as an analytical tool for biological materials such as cells and tissue. Abundant lipids and small peptides can be studied from these surfaces through the use of sample modification strategies[43] and new polyatomic ion sources (Au_n^{m+}, Bi_n^{m+} and C_{60}^+)[44]. Simulations[45] show that the larger primary ions have shallower penetration depth in the sample compared to the monoatomic primary ions (Figure 2.1) and they distribute their energy over a larger area. Thus, the fragmentation of the molecules is less prominent with the cluster ion sources and this makes possible the detection of intact phospholipids and small peptides.

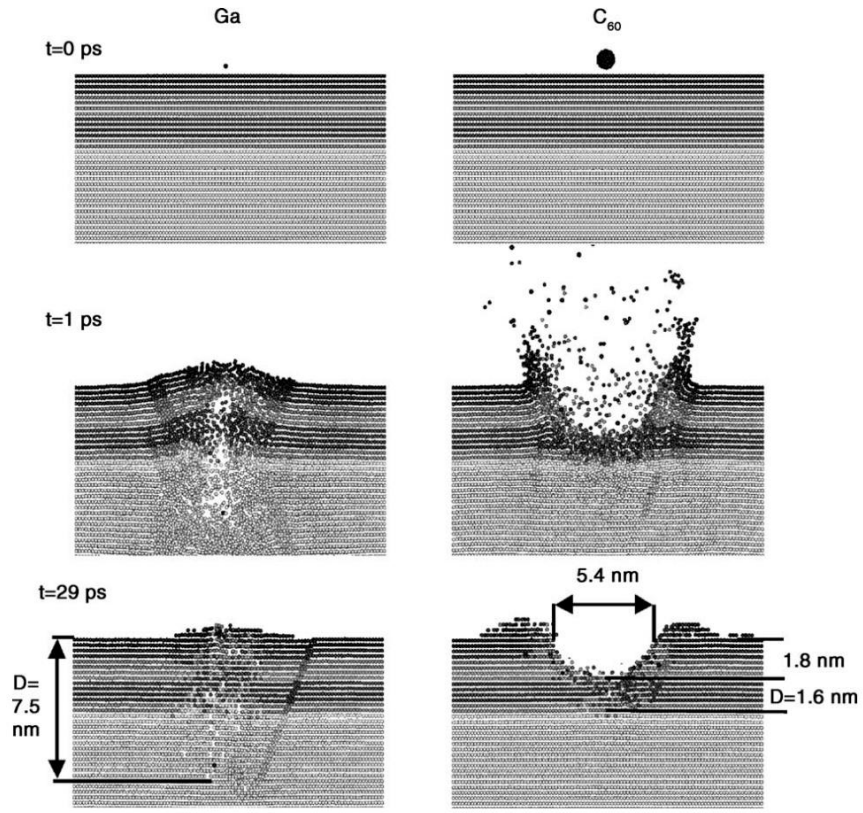

Figure 2.1 ***A cross sectional view showing molecular dynamics simulations on the temporal evolution of collision events for Ga and C_{60} bombardement at 15 keV energy at normal ion incidence. The figure also shows molecular damage as atomic volume mixing. D is the maximum depth at which this mixing is observed. Figure taken from literature[45]***

Traditionally SIMS instruments are single time-of-flight mass spectrometers. As a result, they lack MS/MS capabilities. This makes the identification of the detected ions challenging. It is mostly restricted to the comparison of the spectra with SIMS databases from the measurement of standard samples. Recent developments such as the SIMS quadrupole orthogonal TOF hybrid mass spectrometer built by the Winograd group[46-48] made MS/MS identification possible. The other option is to combine SIMS with a high mass resolution and high mass accuracy FT-ICR mass spectrometer. In the literature there are several examples of the combination of an external SIMS ion source and an FT-ICR mass spectrometer[49-52]. The first SIMS FT-ICR system for imaging was built by Smith et al[53, 54] by combining a 40 keV C_{60}^{+} primary ion source with a Bruker solariX FT-ICR

mass spectrometer. Thus, in this work the high spatial resolution capabilities of SIMS were combined with the high performance of an FT-ICR mass spectrometer for tissue imaging.

2.2.1 Metal Assisted SIMS (MetA-SIMS)

In SIMS imaging the sample preparation is usually simpler than in MALDI. SIMS is frequently used for the study of small molecules such as lipids and drugs. Thus, washing of the sample is not beneficial. However, there is an additional phenomenon in SIMS that one needs to take into account during sample preparation. Most of the samples analyzed by SIMS are insulating. During the SIMS process, the deposited charges can build-up on the surface and the secondary ions can then be deflected. This prevents them to enter to the analyzer region of the mass spectrometer. In order to avoid the charging of the sample several methods can be used. One is the use of an electron flood gun between SIMS pulses to neutralize the charges on the surface. Another common method is to coat the sample surface with a few nm thick metal layer. This method is called metal assisted SIMS (MetA-SIMS)[55-57]. The most common coating material is gold but other metals such as silver can be used as well[56]. It was also shown that MetA-SIMS positively influences the detection of some ions such as cholesterol or intact phospholipids[55] while adversely affects others such as the phosphocholine headgroup. Additionally, MetA-SIMS suffers from the appearance of different gold clusters. Due to the lack of MS/MS capabilities on most of the SIMS instrument, the identification of these compounds can be challenging. One possible solution is to measure adjacent samples with gold coating and with a different coating material such as silver. In this case the cluster ions will be shifted by the mass difference between gold and silver. Thus, the metal clusters can be identified.

2.2.2 Matrix-Enhanced SIMS (ME-SIMS)

One approach to address the problem of low secondary ion yields is to use matrices in SIMS, which is referred to as Matrix-Enhanced SIMS (ME-SIMS)[58, 59]. A wide variety of matrix compounds have been investigated. Frozen noble gases[60], ammonium chloride[61], carbon[62],

nitrocellulose[63], frozen organic solvents[64], ice[65], trehalose[66] and classical MALDI matrices[59], such as α-cyano-4-hydroxycinnamic acid (CHCA) and 2,5-dihydroxybenzoic acid (DHB) have been tested. Nowadays, the term ME-SIMS mainly refers to SIMS experiments that are using typical MALDI matrices and sample preparation protocols. The underlying mechanism by which the matrices improve the performance of SIMS experiments is not precisely known. It has been suggested that, upon primary ion impact, matrix and analyte molecules and ions are sputtered in clusters. Dissociation of these clusters cools and stabilizes the incorporated analyte species, yielding lower internal energy secondary analyte ions and thereby reducing fragmentation[67]. Another contributing mechanism might be that polymeric chains of larger analytes are disentangled by the matrix and that the matrix leads to a lower overall cohesiveness of the sample, possibly also leading to a separation of reactive molecules from each other[68].

It was recently experimentally verified that protonated matrix molecules are the species necessary for analyte ionization in MALDI[69]. It was already assumed before that alleviated proton transfer reactions from protonated matrix molecules enable higher analyte ion yields[70] which led to the halogenated α-cyanocinnamic acid derivatives 4-chloro-α-cyanocinnamic acid (ClCCA)[70, 71] and α-cyano-2,4-difluorocinnamic acid (DiFCCA)[72] This was recently shown for the compounds α-cyano-4-trifluoromethylcinnamic acid (F_3C-CCA) and α-cyano-2,3,4,5,6-pentafluorocinnamic acid (PentaF-CCA) which allow for very high analyte sensitivities at MALDI-MS using optimized irradiation wavelengths but are completely unsuited as MALDI matrices at the standard wavelengths[73].

CHCA derivatives

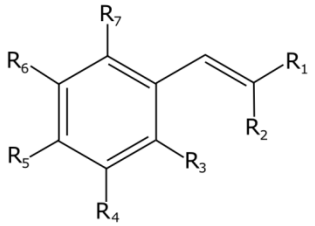

Matrix	R_1	R_2	R_3	R_4	R_5	R_6	R_7
2,4-di-F-CCA	COOH	CN	F	H	F	H	H
2,6-di-F-CCA	COOH	CN	F	H	H	H	F
2,6-di-F-CCAAmide	$CONH_2$	CN	F	H	H	H	F
2,4-di-F-CCAAmide	$CONH_2$	CN	F	H	F	H	H
penta-F-CCA	COOH	CN	F	F	F	F	F
penta-Br-CCA	COOH	CN	Br	Br	Br	Br	Br
4-NO_2 -CCA	COOH	CN	H	H	NO_2	H	H
4-CN-CCA	COOH	CN	H	H	CN	H	H
3,5-di-F-CCA	COOH	CN	H	F	H	F	H
4-(2,2-dicyanovinyl)-BA	CN	CN	H	H	COOH	H	H
4-Br-CCA	COOH	CN	H	H	Br	H	H
2,4-di-Cl-CCA	COOH	CN	Cl	H	Cl	H	H
4-CF3-CCA	COOH	CN	H	H	CF_3	H	H
2,4,6-tri-F-CCA	COOH	CN	F	H	F	H	F
3,5-di-Cl-CCA	COOH	CN	H	Cl	H	Cl	H
4-(2,2-dicyanovinyl)-phenol	CN	CN	H	H	OH	H	H
4-Cl-CCA	COOH	CN	H	H	Cl	H	H
CHCA	COOH	CN	H	H	OH	H	H

DHB derivatives

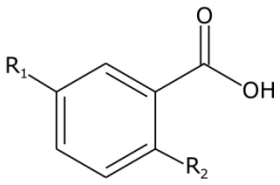

Matrix	R_1	R_2
2,5-di-CN-BA	CN	CN
5-CN-2-OH-BA	CN	OH
DHB	OH	OH

Figure 2.2 List of CHCA and DHB derivatives tested for ME-SIMS

Since no such constraint exists in ME-SIMS, a larger number of potentially reactive derivatives of the classical MALDI matrices may prove beneficial in ME-SIMS. Consequently, the concept of increasing the matrix sensitivity by lowering their PA with the help of electron-withdrawing substituents[70] was extendable to even more reactive compounds. In addition to the highly reactive halogenated α-cyanocinnamic acid derivatives mentioned above, a set of 14 novel matrices (see Figure 2.2) were characterized with respect to their performance in ME-SIMS of peptide samples, where all derivatives were from CHCA or DHB with assumed low PAs.

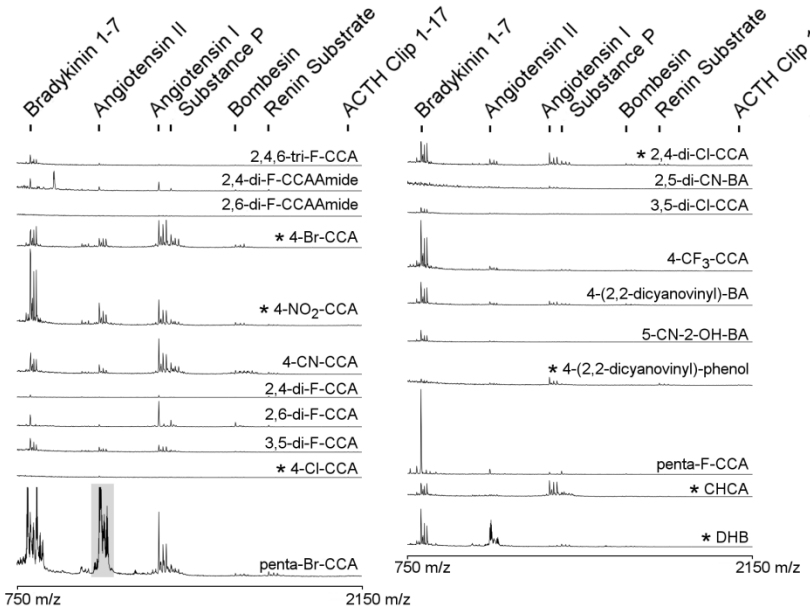

Figure 2.3 ME-SIMS spectra of dried droplets of the Bruker Peptide Calibration Standard II measured with several different matrix compounds. Stars next to compound names indicate that some peptide detection was also achieved from the same sample on a MALDI instrument. Areas labeled in gray indicate intense interfering matrix-related peak distributions.

The matrix compounds were evaluated by dried droplet preparations of matrix solution mixed with a commercial calibration standard (Bruker Peptide Calibration Standard II) and a tryptic digest of casein (Bacto™ Tryptone) and recording the ME-SIMS spectra in positive ion mode, using a post-acceleration voltage of 9 kV to detect higher mass analytes more efficiently. Three replicates were measured per matrix compound. Figure 2.3 shows representative ME-SIMS spectra for the calibration standard using different reactive matrices for ME-SIMS. Analyte labels at the top of Figure 2.3 refer to the *m/z* ratios of singly protonated species. Significant differences in performance between the matrices were observed, with many compounds yielding higher analyte intensities than the classical matrices CHCA and DHB. Additionally, certain matrices favor certain analytes, for example, penta-F-CCA afforded relatively high signal intensities for the singly protonated Bradykinin 1-7 peak, but performed less well than many other matrices for the remaining peptides in the sample.

Casein digest	Bruker Peptide Standard	Combined
4-NO_2-CCA	penta-Br-CCA	4-NO_2-CCA
penta-F-CCA	4-NO_2-CCA	penta-Br-CCA
2,4,6-tri-F-CCA	4-CN-CCA	2,4-di-Cl-CCA
2,4-di-Cl-CCA	2,4-di-Cl-CCA	CHCA
CHCA	2,4-di-F-CCAAmide	penta-F-CCA
3,5-di-Cl-CCA	CHCA	4-CN-CCA
4-CF_3-CCA	DHB	2,4-di-F-CCAAmide
penta-Br-CCA	4-(2,2-dicyanovinyl)-BA	4-CF_3-CCA
2,5-di-CN-BA	penta-F-CCA	2,4,6-tri-F-CCA
2,4-di-F-CCA	4-Br-CCA	4-(2,2-dicyanovinyl)-BA

Table 2.1. Relative rankings of the experimental matrices derived from peptide samples. Rank positions are based on the number of occurrences among the top 6 performers for a selection of 8 clearly detected analytes for each sample.

Overall rankings have been derived by ranking by intensity for single analytes first, followed by counting the occurrences among the top six matrices for every analyte, weighing the top two with 3, the next two with 2 and the last two with 1. Weighing all compounds equally lead to largely comparable results, but analyte intensity differences between the first few rank positions can be large and thus the weighing has been expected to better reflect the actual matrix performance. The results are shown in Table 2.1. For the peptide calibration standard, the six lowest mass singly protonated peptide peaks were used for the ranking.

It was demonstrated that some of these compounds afford significant increases in signal intensity. These findings support the hypothesis that the gas-phase basicity is an important parameter in the SIMS desorption and ionization process and may lead to further structural optimizations of ME-SIMS matrices in the future. ME-SIMS has the potential to enable the analysis of peptides directly from tissue with sub-micron spatial resolution.

2.3 Matrix Assisted Laser Desorption Ionization

MALDI was discovered in the late 1980s by Hillenkamp and Karas[17-19, 74]. It was one of the two ionization methods that revolutionized mass spectrometry, since it was one of the first ionization methods that were able to ionize large intact proteins. As a result, new fields opened up for mass spectrometry such as proteomics or biomolecular mass spectrometry imaging.

MALDI is a versatile, effective and sensitive method to desorb and ionize a wide variety of compounds such as polymers, small organic molecules, lipids and amino acids but also especially biopolymers such as peptides, proteins and oligonucleotides[75]. The basic experiment involves irradiating the sample with a pulsed laser to generate analyte ions from the surface. A matrix solution is applied to the tissue sample to facilitate effective MALDI analysis. In MS imaging, these solutions are used for the extraction of the analyte molecules from a tissue section and to create analyte doped matrix crystals.

During the analysis, the surface is irradiated by a pulsed laser, thus inducing ablation of these analyte-rich crystals, which results in cooperative motion of the analyte and matrix ions into the vacuum. The role of the matrix compound which is commonly a small organic compound is to absorb the laser light to assist the desorption process. They also interact with the desorbed neutrals in gas phase and ionize them in ion-molecule reactions. Also, they absorb most of the laser energy and help to prevent the fragmentation of the analytes.

MALDI can be applied directly for the analysis of biological surfaces and tissue sections. This makes it a key technology for MS imaging. The advantages of MALDI for imaging are the high sensitivity and the wide range of possible analytes, while the main disadvantage of the method is the lower achievable spatial resolution. In microprobe mode imaging the maximum spatial resolution is determined by laser spot size. The routinely achievable spot size is in the range of tens of microns and the minimum spot size is around 5 µm[76]. The other disadvantage is that MALDI requires an additional sample preparation step, namely the deposition of the matrix. This step can be time consuming, it can result in additional diffusion of the analytes and the size of the matrix crystals can

negatively influence the achievable spatial resolution. The added separation power of IMS has its advantages for MS imaging. Several research groups are combining these technologies to enable ion-mobility-based MS imaging.

This chapter describes the evolution of ion-mobility based MS imaging from a historical perspective to the current state of the art. The developments described have resulted in an innovative (bio-)analytical technology for the analysis of complex surfaces. Ion-mobility-based MS imaging enables the direct determination of three of the most important parameters of molecules on the surface of biological systems: size, weight and position.

2.4 Size: the basics of IMS

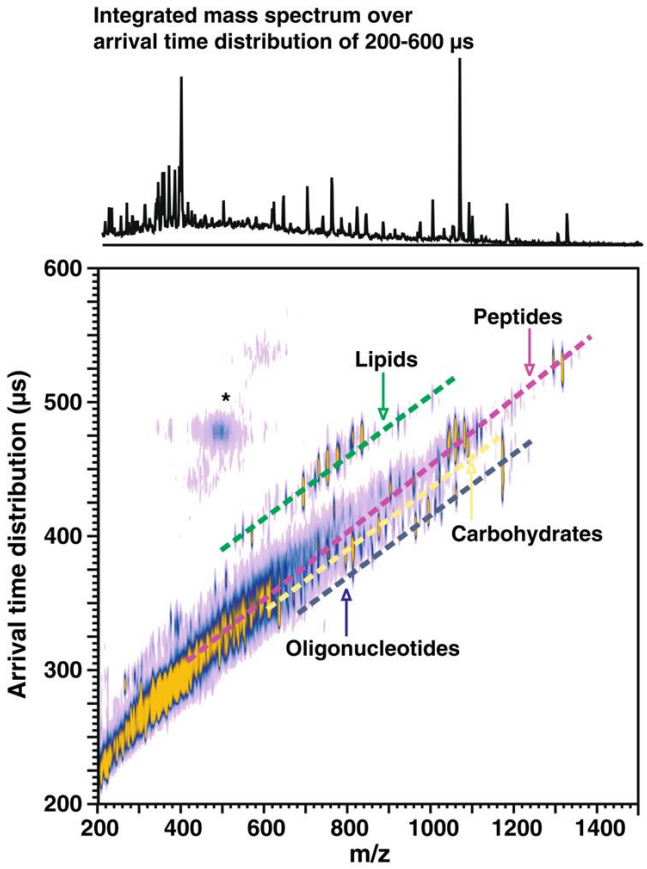

Figure 2.4 Matrix-assisted laser desorption and ionization (MALDI)–ion mobility mass spectrometry (MS) conformation space obtained for a mixture of model species representing each molecular class (ranging from seven to 17 model species for each class, spanning a range of masses up to 1,500 Da). Dashed lines are for visualization purposes, where each molecular class occurs in conformation space. Signals in the vicinity of the asterisk arise from limited post-ion-mobility fragmentation of the parent ion species. (Reproduced with permission from[77])

The main physical phenomenon behind all of the ion mobility methods is the collision of the ions with neutral gas molecules or atoms. The change in the speed of the ions due to the collisions is influenced by the collision cross-section of the ions. Thus, IMS separates the ions on the basis of their size, conformation and charge state instead of their mass. In this

way it provides complementary shape information when it is coupled with MS. The time frame of an ion mobility separation is in the millisecond range, which is significantly slower than the average time it takes to acquire a mass spectrum. This makes the coupling of the two methods easy because for every ion-mobility-separated peak several mass spectra can be measured. A given molecular class usually follows a trend line when the ion mobility is plotted as the function of the *m/z* of the ions. This is illustrated in Figure 2.4 with the different trend lines for peptides and lipids. The various ion mobility methods can be grouped on the basis of whether their ion separation selectivity is based on spatial dispersion such as in drift tubes or travelling-wave instruments or on temporal dispersion such as in high-field asymmetric IMS (FAIMS) instruments.

2.4.1 Drift-time IMS

The first and simplest design ion mobility spectrometers were drift-tube instruments. In this type of spectrometer the ion mobility cell consists of series of stacked-ring electrodes (Figure 2.5). With use of these electrodes a near-uniform electric field is created along the axis of the cell. An important part of the drift tube is the collision gas, which is usually nitrogen, helium or argon. During the measurement, ion packets are injected into the cell and the ions drift from one end of the cell to the other in the electric field. During their drift they collide with the particles of the collision gas. Thus, the time that it takes the ions to travel through the cell is affected by their average collision cross-section. This is the basic principle behind ion mobility separation. In drift-time spectrometers, the field strength is usually chosen such that the diffusion processes will be dominant. To achieve this, the electric field should be low enough so the thermal energy the ions obtain from the collisions with the buffer gas is larger than the energy they obtain from the electric field. This is called the ‘low-field limit’. In this case the velocity of the ions is directly proportional to the electric field.

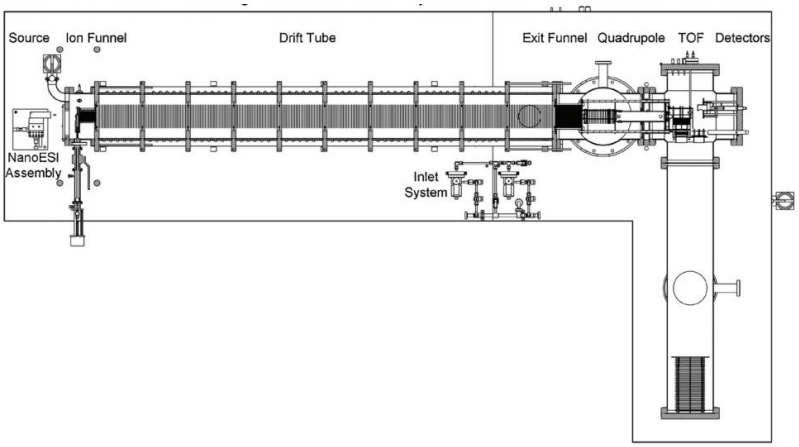

Figure 2.5 A high-resolution drift time ion mobility mass spectrometer. ESI electrospray ionization, TOF time-of-flight analyzer. (Reproduced with permission from[78])

This is one of the main advantages of the drift-time ion mobility methods because the proportionality constant, called the 'ion mobility constant' is directly related to the collision cross-section of the ions. This way the collision cross-sections can be determined directly from the drift time using only the experimental parameters with the following formula:

$$K = \left(\frac{3q}{16N}\right)\left(\frac{2\pi}{kT}\right)^{1/2}\left(\frac{m+M}{mM}\right)^{1/2}\left(\frac{1}{\Omega}\right)$$

where K is the ion mobility constant, which is directly proportional to the electric field and the velocity of the ions, q is the charge on the ion, N is the number density of the buffer gas, k is Boltzmann's constant, T is the absolute temperature, m is the mass of the buffer gas, M is the mass of the ion and Ω is the collision cross-section of the ion. Drift-time ion mobility spectrometers can be either ambient-pressure or reduced-pressure devices. The ambient-pressure configuration provides better resolution and greater separation selectivity, but because of the inefficient transfer of the ions from the ion mobility cell to the mass spectrometer such instruments suffer from reduced sensitivity. Because of this, ambient-pressure instruments are mostly used as standalone ion mobility spectrometers for field analytical applications such as the detection of explosives or dangerous chemicals at airports.

In addition to the ion transfer issues with the ambient pressure devices, both types of instruments suffer from the need for narrow ion packets for the separation. This seriously compromises their sensitivity, especially when they are coupled to continuous ion sources. This problem can be reduced using a trap cell preceding the drift tube that traps the ions and releases them as narrow ion packets. Still, with this ion accumulation the duty cycle of these instruments is low. Thus, their sensitivity is lower than that of the other type of instruments. Several attempts were made to improve the ion transmission to the drift tube. These include the use of various ion funnel designs[79] or the use of multiplex methods such as Fourier transform[80] and Hadamard transform[81, 82] to deconvolve the signals after the continuous introduction of ions into the ion mobility cell instead of using ion packets and thus improving the duty cycle of the instrument.

The other direction in which ion mobility spectrometers have been improved is the resolution of the separation. Several developments have recently been reported in this field as well, such as the so-called ion cyclotron mobility spectrometer developed by Clemmer and co-workers[83]. This device consists of four curved drift tubes and four ion funnels in cyclotron geometry. In this configuration the flight path of the ions in the drift tube can be increased significantly since it depends on the number of cycles in the spectrometer. There have been several developments to overcome the sensitivity issues of the drift-time instruments, such as overtone ion mobility spectrometers, another recent development by Clemmer and co-workers[84, 85]. Their goal was to build a drift-tube instrument which operates as a continuous ion mobility filter rather than using the above-mentioned gating of ion packets, which results in decreased sensitivity. To achieve this, they divided the linear drift tube into multiple segmented regions and they created two sawtooth voltage gradients by applying the electric field to pairs of segments. The sawtooth voltage is offset by one segment across the whole drift tube and the voltages are alternated during the separation. This way the ion transmission will be a function of the frequency, so an intensity–frequency plot is used to visualize the measured data. The interesting feature of the method is that a given ion gives a signal not only at the fundamental frequency but also at multiples of the fundamental frequency and usually the resolution of these so-called overtone peaks is better than that at the fundamental frequency.

It is possible to couple two drift cells and to do IMS2 experiments[86-88]. In this case the ions are excited between the two ion mobility cells, so their conformation will be different. These types of experiments can provide valuable information about the energetics of conformational changes of gas-phase ions. This way the peak capacity of the method can be further increased as well as making possible the high-throughput analysis of proteins in biological samples such as human plasma.

2.4.2 Travelling-wave IMS

Travelling-wave IMS is the youngest of the ion mobility separation methods. The idea is based on a patent from 1993 by Kirchner[89] but the first commercial instruments were produced only in 2004[90]. Travelling-wave IMS is based on the use of stacked-ring ion guides (SRIGs) similar to the configuration in drift-time instruments. In these devices an opposite phase of RF is applied to consecutive ring electrodes. The potential generated in one of these ion guides can be seen in Figure 2.6.

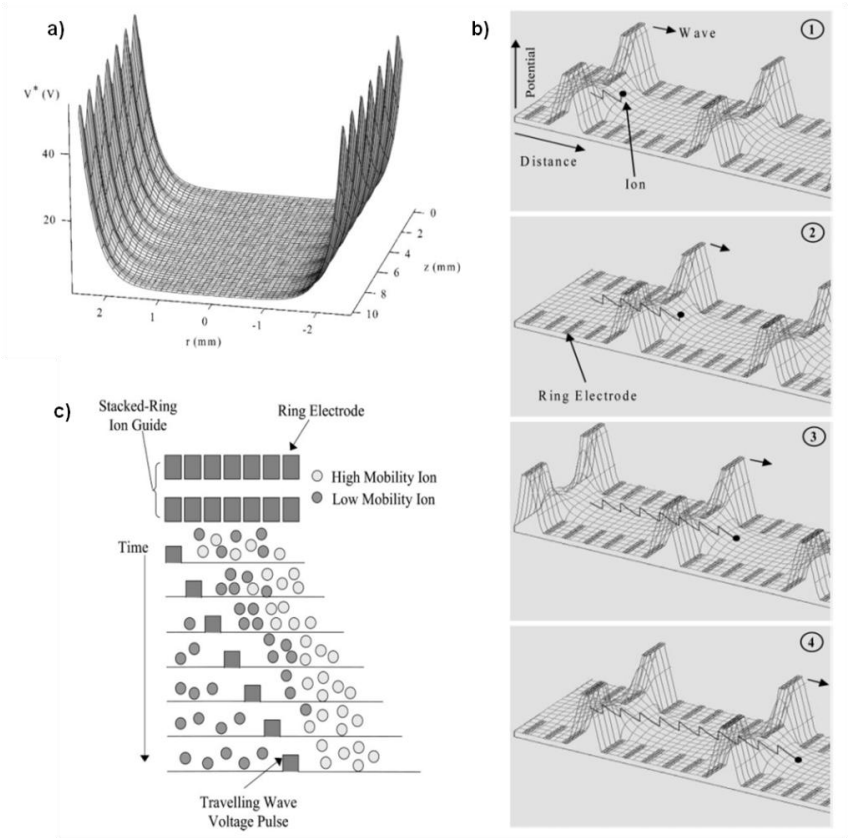

Figure 2.6 Calculated effective potential (a) for a stacked-ring ion guide (SRIG). Series of SIMION plots showing an ion surfing on the front of a travelling wave as it passes along the SRIG (b). Mobility separation in the travelling-wave ion guide (c). (Reproduced with permission from[90])

The main flaw of this design is that there are undulations in the potential surface in the z direction where ions can be trapped. This can significantly slow down the progress of the ions through the ion guide or can even prevent their exiting the cell. As a result, the ions need to be propelled through the ion guide. In travelling-wave instruments a DC potential is superimposed on the RF of an electrode which is subsequently swept over successive electrodes. This creates a moving electric field called a 'travelling wave'[90]. The simulation of the ion trajectories indicates that the ions roll down the potential gradient, then the potential pulse moves forward and the process is repeated (Figure 2.6b). This way the ions are propelled through the cell by the wave. For ion mobility separations one of these ion guides is filled with a neutral gas, usually nitrogen or argon. In

this case the ions not only 'surf' on the waves as described above but they also roll over the waves owing to collisions with the gas particles. Low-mobility ions roll over the waves more often than high-mobility ions; thus, they leave the cell later, as can be seen in Figure 2.6.

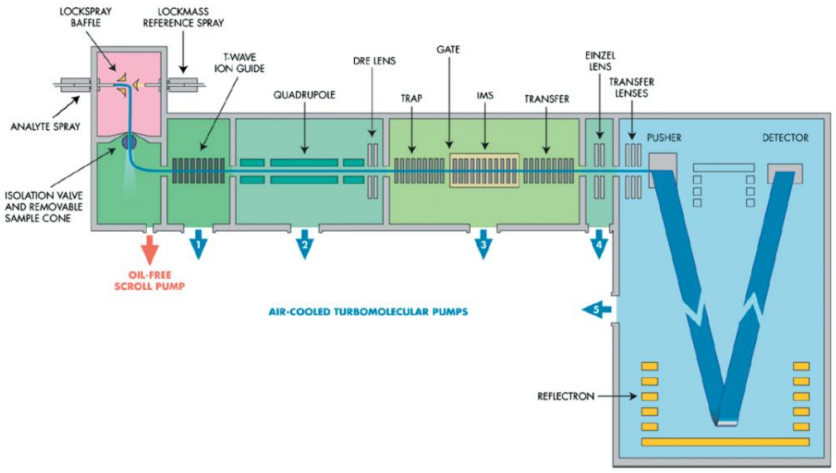

Figure 2.7 The Waters SYNAPT ESI HDMS mass spectrometer equipped with a travelling-wave ion mobility cell. The abbreviation IMS refers to the ion mobility separation device. (Reproduced with permission from[91])

There is one commercially available instrument equipped with a travelling-wave cell as shown in Figure 2.7. This is essentially a quadrupole TOF MS instrument where the travelling wave ion mobility cell is located between the quadrupole and the TOF analyzer. The ion mobility cell consists of three consecutive SRIGs. The first is called 'the trap cell', intended to trap the ions and to release them in packets in the mobility cell. In the second one the actual ion mobility separation takes place. The third one is called 'the transfer cell' and its role is to transfer mobility-separated ion packets to the TOF analyzer (Figure 2.7). The advantages of this design are the relatively high duty cycle because of the trap SRIG and the quadrupole analyzer before the ion mobility cell, and the possibility to enhance the detection of certain mobility separated ions by synchronizing the pusher of the TOF and the release of the ions by the transfer cell.

Also, these instruments are capable of performing collision-induced dissociation fragmentation before the ion mobility separation in the trap cell or after the mobility separation in the transfer region, which has the advantage that the fragments will have the same drift time as the

corresponding parent ions. It is also possible to fragment the ions in both cells, which leads to MS^3-like experiments.

The main issue with this type of instrument is the relatively low resolution, although with recent developments it was increased to around 40 $\Omega/\Delta\Omega$. This was achieved by increasing the length of the mobility region and adding an additional region filled with helium before the mobility ion guide.

Another drawback of the method is the lack of a simple relation between the drift times and the collision cross sections of the analytes. There have been recent attempts to find the relation between these two parameters. Shvartsburg and Smith[92] have proposed a physical model to describe the properties of a travelling-wave cell that addresses this issue. Despite these attempts, the experimental collision cross-sections are still determined using different compounds with known collision cross-sections as calibration standards[93, 94]. Since this is the youngest of the three ion mobility separation methods, it is expected that the above-mentioned issues will be dramatically reduced in the future.

2.4.3 Differential mobility analysers

The idea of the method first appeared in a Soviet patent in the 1980s[95] and was published in referenced literature in 1993[96]. The mobility of ions depends on the ratio of the electric field intensity and the gas number density. The electric field density between two electrodes oscillates between high and low field and the ions are separated on the basis of their mobility difference in high and low field. This is achieved by passing the ions between two parallel electrodes through a carrier gas while on one electrode a voltage waveform is applied. This causes an oscillation of the ions. Their mobility difference between the high and low field will force them to drift in the direction of an electrode, where they will be neutralized. For each species a given compensation voltage has to be applied to one electrode to allow those ions to pass between the electrodes. It is possible to scan with the compensation voltage over a wide range of species with their respective mobility differences, which results in mobility spectrometry. Alternatively, one compensation voltage can be set that enables the exclusive transmission of ions with a specific mobility difference, i.e.

mobility filtering. This is why this type of ion mobility analyzer is often considered to be analogous to quadrupole mass analyzers.

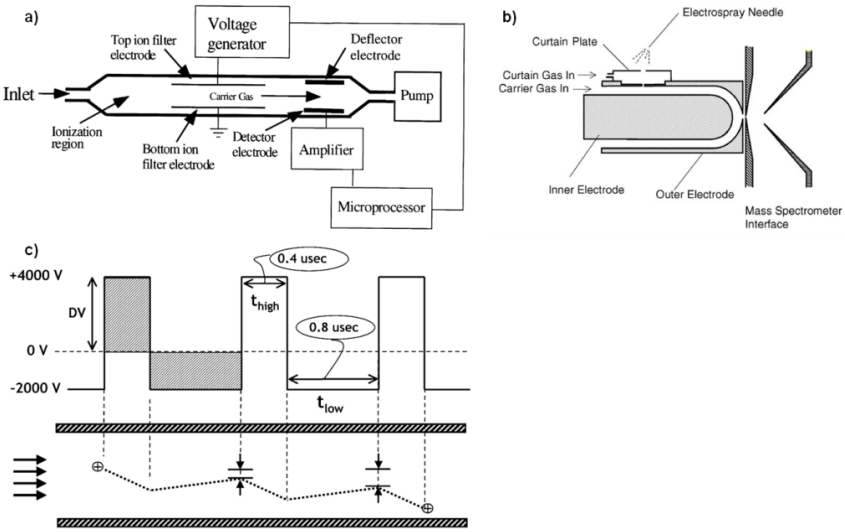

Figure 2.8 Planar geometry (a) and cylindrical geometry (b) high-field asymmetric ion mobility spectrometry (FAIMS) analysers and the ion motion in a planar FAIMS device (c). (a Reproduced with permission from[97]; b and c reproduced with permission from[98])

Mainly two electrode geometries are used: plate electrodes (Figure 2.8a) or electrodes with cylindrical geometry (Figure 2.8b). The latter design not only separates the ions on the basis of their mobility but also focuses the ions and reduces ion loss due to diffusion and Coulomb repulsion[99]. One concern regarding the disadvantages of this design is the limited resolution. This is a direct result from the wider compensation voltage range needed to keep the ions stable and allowing them to pass the analyzer. Although simulations indicate that the optimal resolution/sensitivity balance can be achieved with planar geometry[100], it is important to improve the sensitivity of these instruments. One solution is to use a slit aperture instead of the common circular orifice between the ion mobility analyzer and the mass spectrometer, which will improve the ion transmission and refocus the ions in the mass spectrometer in an electrodynamic ion funnel[101].

One of the main advantages of the method is the size of the instrument. Field asymmetric ion mobility spectrometers can be produced

with dimensions under a few centimeters without seriously compromising the resolution of the instruments. This makes these devices well suited for the production of portable ion mobility spectrometers. One of the potential applications of such instruments is the detection of explosives[102, 103].

Owing to their slightly differing principles, FAIMS and the other ion mobility methods provide slightly different conformational information about the ions. Tandem ion mobility separation becomes possible through the coupling of FAIMS with another ion mobility method[104]. This is especially advantageous as there are currently no means to extract structural information from FAIMS results. A 2D-FAIMS/IMS measurement will reveal the ion geometry separated by FAIMS. Despite their low resolution, isomers or isobars are often distinguished by FAIMS better than by conventional IMS. This is because the differential mobility is much more weakly correlated with the ion mass than the absolute mobility.

Two directions of development were made possible by the miniaturization of the FAIMS analyzer. One is increasing the speed of the method by applying higher fields on the two electrodes[105, 106]. The separation speed scales with the fourth to sixth power of the electric field, so this way the separation speed can be increased extensively (about 100–10,000 times higher when the electric field intensity is increased to over 60 kV/cm) although the resolution of these devices is lower than that of the other designs. The other method was proposed to increase the resolution of FAIMS instruments[107, 108]. It has been known for a relatively long time that using He/N_2 mixtures in these instruments, with as high He content as possible, can increase the resolution. A typical planar high-field asymmetric IM spectrometer design with a 2-mm gap between the two electrodes precludes the use of gas mixtures with He content higher than 65%. Electrical breakdown has been observed between the two electrodes at higher He contents. Shvartsburg et al.[107, 108] proved with a slightly modified instrument that He/N_2 gas mixtures up to 75% He content can be used without observing electrical breakdown. This way the resolution of the instruments can be increased to around 100, in line with the resolution of common drift tube IMS instruments.

2.5 Weight: IM-MS coupled with a MALDI ion source

Since its development in the late 1980s by Karas et al.[17-19, 74], MALDI has become one of the main ionization techniques used in the field of mass spectrometry based proteomics. The method has several advantages over ESI-MS, such as its speed and tolerance of salts. It mostly produces singly charged ions, whereas during the electrospray process several multiply charged species arise, making the mass spectra and also the ion mobility spectra more complex. Because of the lack of separation, usually ion suppression and significant chemical noise such as matrix-related peaks can decrease the sensitivity of MALDI. Combined with low-resolution MS, it is difficult to separate ions that are nominally isobaric. Although it is possible to use off-line high-performance liquid chromatography (HPLC) separation before MALDI-MS measurements, this solution has some disadvantages, mainly the significantly increased measurement time needed to analyze a sample. Most of these limitations can be overcome or at least reduced when IM-MS is used with a MALDI ion source. MALDI ion sources operate in pulsed mode, so they are more easily coupled with ion mobility devices than are electrospray ion sources. One of the first examples where a MALDI ion source and IM-MS were coupled was the instrument developed by the group of Bowers[109] in 1995. They used a magnetic sector instrument equipped with a MALDI ion source and they coupled a drift-time ion mobility spectrometer after it. They used this instrument to study the conformation of several polymer ions, namely sodiated poly (ethylene glycol) ions. Since then several papers have been published wherein it was reported that ion mobility mass spectrometers were used to examine even biomolecules and biological mixtures.

Koomen et al.[110] developed a method for rapid screening of oligonucleotides. This work in 2002 was the first where MALDI-IM-MS was used for the study of different oligonucleotides. It was demonstrated that an ion mobility cell with a mobility resolution of 20–30 is sufficient to separate oligonucleotides of different length and to remove the chemical noise caused by matrix signals. However, they did not have enough resolution to separate different structural isomers. The resolution of the ion mobility cells alone is also not enough to separate oligonucleotides with the same length but different mass; in this case the MS data have to be used to differentiate between the species. Also, they studied the separation of different DNA fragment ions and determined chemical modifications of

DNA using MALDI-IM-MS. Their results suggest that MALDI-IM-MS can be used to study chemically modified DNA oligonucleotides and DNA–drug and DNA–metal complexes.

McLean and Russell[111] proved in a publication from 2003 that sub-femtomole amounts of peptides can be detected using MALDI-IM-MS. They used a high repetition-rate laser to increase the duty cycle of the instrument. Sub-femtomole amounts of angiotensin I and angiotensin II and also a tryptic digest of bovine hemoglobin were measured. This proved that using IM-MS with a MALDI ion source will not decrease the detection sensitivity significantly owing to the pulsed nature of the ion source.

In 2004 Woods et al.[30] demonstrated that it is possible to use MALDI-IM-MS for the separation of complex biological mixtures. It was shown in this work that peptides, lipids and oligonucleotides form distinct trend lines which make possible the rapid separation of these different compound classes. Also, MALDI-IM-MS was used for the rapid screening of drugs in saliva.

One of the fields that can benefit tremendously from the use of MALDI-IM-MS is proteomics[112]. One of the main advantages of the method compared with classic HPLC-MS workflows is its speed. The liquid chromatography separation of complex biological mixtures can take from several minutes to hours, whereas ion mobility separation takes only milliseconds. There are several proteomics experiments where IM-MS can be effectively used, such as increasing the confidence of protein identification by separating isobaric tryptic peptides. In conventional experiments to determine post-translational modifications the interpretation of the mass spectra can be difficult because of neutral losses and the small concentration of the modified protein. Some simulations suggest that, for example, phosphorylation changes the protein conformation, leading to a more compact structure, which can thus be beneficial for the study of such modifications by IM-MS; thus, IM-MS is potentially a powerful tool to study post-translational modifications and protein–small molecule complexes. IM-MS also provides a means to study the conformation of gas-phase ions and with variable temperature ion mobility separation protein folding and unfolding processes, which can be important to understand diseases that are related to protein misfolding such as Parkinson’s or

Alzheimer's disease. Another technique that can benefit from IM-MS is MS imaging. This technique will be discussed in detail in the next section.

In a recent paper, the McLean group[113] reported a custom-built drift-time instrument with interchangeable MALDI and nano-ESI sources and evaluated the instrument for comparison of the mobility of ions produced by ESI and MALDI processes. These experiments can be beneficial to better understand how the conformation of the ions will change during the ionization process in different ion sources. This information is crucial for biochemical studies where the conformation of biomolecules is investigated by IM-MS.

2.6 Position: IM-MS in imaging experiments

MS imaging has emerged in recent years as a powerful discovery tool for biochemical studies. However, the performance of the technique is compromised by the complexity of the sample. This can cause ion suppression and also several nominally isobaric species can be present that cannot be resolved using TOF analyzers. Recently, it was demonstrated that this can be improved using a Fourier transform ion cyclotron resonance mass spectrometer, an instrument which has mass resolution far superior to that of TOF instruments[114]. Another solution is the use of a separation technique, but because of the nature of the samples, chromatographic techniques cannot be used. An effective way to solve this problem is to add a separation step after the ionization; thus, the use of IM-MS can address some of the aforementioned limitations. With IMS it is possible to separate isobaric species, although it will not prevent ion suppression because the separation takes place after the ionization process. Another useful property of the method is the possibility to remove chemical noise such as matrix-related peaks, this way simplifying the interpretation of the spectra and also improving the contrast of the ion images.

Lipids are one of the most abundant biomolecules in tissue sections. They also ionize easily; thus, they can be easily studied by MS imaging. They can also be associated with several diseases, so they are interesting also from a medical point of view. The imaging of lipids can benefit from ion mobility separations since different classes and structures of possible isobaric species exist. It is not surprising that there are several published

reports of the study of the distribution of lipids, especially phospholipids, using ion mobility separation before the mass-spectrometric detection. One work was by Jackson et al.[25] and another was by the McLean group[115], both from 2007, where the possibility and usefulness of using ion mobility separation for the imaging of different lipid classes, mainly phospholipids from brain samples, were demonstrated.

One of the main advantages of MS imaging is the capability to measure the distribution of drugs and their metabolites selectively and simultaneously in whole-body sections without using labeling[116, 117], thus giving information complementary to that obtained from conventional whole-body autoradiography measurements. Trim et al.[118] investigated whether the coupling of ion mobility separation with MS imaging has additional benefits for pharmaceutical studies. The distribution of vinblastine and its metabolites was studied in mouse whole-body sections using ion mobility MS imaging and MS/MS. An endogenous lipid isobaric to vinblastine and also one isobaric to one of its metabolites were observed. Removing these isobaric backgrounds by ion mobility separation alters the spatial distribution of the mass related to vinblastine or its metabolite and increases the confidence in the results (Figure 2.9).

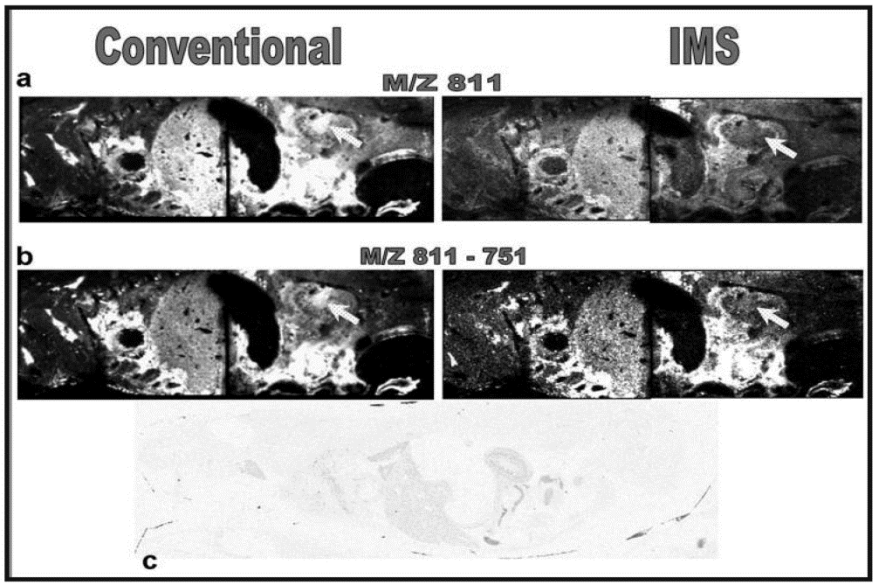

Figure 2.9 Comparison of *m/z* 811 (a) and *m/z* 811-751 (b) images obtained using MALDI–ion mobility spectrometry (IMS)–MS/MS and conventional MALDI-MS/MS. These images clearly demonstrate the advantages of ion mobility separation within MALDI xenobiotic imaging. The main difference observed is indicated: the distribution of the ions of interest within the renal pelvis. Whole-body autoradiograph (c) showing the distribution of 3H in a 1-h post dose rat dosed with 6 mg/kg 3H-vinblastine intravenously, confirming the distribution observed with MALDI IMS-MS/MS. (Reproduced with permission from[118])

In 2010 Ridenour et al.[28] described a method to determine the collision cross-section of phospholipids and tryptic peptides directly from tissue using MALDI-T-wave-IM-MS data. It was indicated that it is important to calibrate the instrument with the same class of compounds. They observed that if the instrument was calibrated with the drift time collision cross-section values of peptides for phospholipid measurement, then the average difference between the drift time and the T-wave collision cross-section values was 7%, whereas with phospholipid drift-time data this value can be decreased below 0.5%.

Recently, the use of MALDI-IM-MS was reported for on-tissue bottom-up proteomics experiments using formalin-fixed, paraffin-embedded (FFPE) tissue samples in several papers. FFPE samples are amongst the most challenging samples. However, formalin fixing and

paraffin embedding is the standard protocol that pathologists use to fix tissue sections for storage and these samples are available in great numbers for the study of different diseases. One of the problems is that FFPE samples require extensive washing with different solvents to remove the paraffin, but this can easily damage the sample. The formalin fixing cross-links the proteins, so enzymatic digestion is necessary to study these tissue sections.

In one report, a 78-kDa protein called glucose-regulated protein 78 kDa (Grp78) was identified from pancreatic adenocarcinoma tissue after tryptic digestion. The spatial distribution of the tryptic peptides related to Grp78 suggested high expression of the protein in the adenocarcinoma cells [119]. This result demonstrates that the use of MALDI-IM-MS imaging allows the localization of a tumor biomarker in on-tissue-digested FFPE samples.

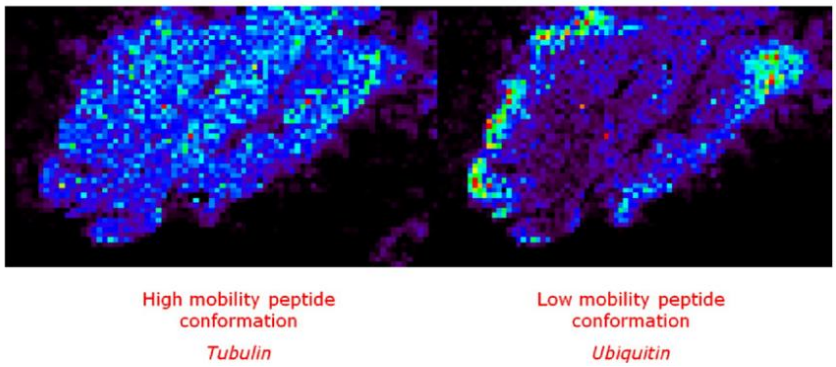

Figure 2.10 Images of separated and identified isobaric ions of tubulin and ubiquitin peptide fragments (1,039 *m/z*) are presented directly on tissue by ion mobility MS imaging (BioMap). For these images, two different drift times were selected: 100–127 and 133–148 bins to reconstruct the respective images. Without any ion mobility, one image is obtained corresponding to the superposition of these two images. (Reproduced with permission from[120])

In other work, FFPE rat brain and frozen human brain samples were analyzed after on-tissue digestion of the proteins[120]. It was shown that with the additional ion mobility separation the number of detected peaks increased owing to the separation of isobaric species. Also the improved confidence of protein identification was proved when ion mobility separation is used. Tubulin and ubiquitin have isobaric tryptic peptides at 1,039 *m/z* that have different spatial distributions in the brain (Figure 2.10).

If an MS/MS experiment without ion mobility separation is performed, the resulting spectrum will contain a mixture of fragment peaks from the fragmentation of both species. MASCOT identification of the proteins is severely hampered by this phenomenon. Imaging experiments without ion mobility result in an average image of the two proteins. With drift-time separation the fragmentation products of the two peptides are separated, thus providing higher scores for a MASCOT search and increasing the confidence of the identification of the proteins. It reveals different spatial organization of the proteins as well.

Also, recent work by Djidja et al.[121] used imaging combined with ion mobility separation for tumor classification. The samples studied were pancreatic cancer tissue microarray (TMA) samples and human FFPE tissue sections. After tryptic digestion of the TMA samples, MALDI-IM-MS, MALDI-IM-MS/MS and principal component analysis–discriminant analysis (PCA-DA) were employed to generate tumor classification models. It was found that the use of IM-MS is beneficial for similar studies as it provides the exact distribution of proteins as a result of minimization of peak interferences. This also results in better protein identification from database searches. The classification model they built up was verified after statistical analysis of the TMA results by measuring the digested FFPE tissue sections with MALDI-IM-MS. The distribution of characteristic peptides of the tumor region highlighted by the PCA-DA was in good agreement with the histological data, thus confirming the results of the PCA-DA statistical method.

2.7 Summary and outlook

The importance of IM-MS has increased during the past decade and most likely this trend will continue. The separation speed obtainable, the possibility to acquire additional information about the structure of different molecular classes and the easy coupling with MS contributes to the maturation of this technique. We have described some of the technological developments that have contributed to the growing importance of IM-MS. Several research areas have been described that can benefit from the use of IM-MS. These examples also demonstrate the utility of IM-MS to address the need for additional separation steps in imaging and MALDI proteomics

applications. Another possible utilization of imaging IM-MS is in the field of quantitative imaging. Quantitation of molecules on tissue is seriously hampered by ion suppression and nominally isobaric species present. With use of ion mobility separation the precision of the quantitation can be increased through the removal of the nominally isobaric ions. This approach has great potential in future quantitative molecular imaging experiments using MS.

As we have shown IM-MS has several limitations, such as the significantly decreased sensitivity that needs to be overcome to study low-abundance species with IM-MS. There is a strong need to further increase the resolution of the existing IM-MS methods to obtain more structural separation. Most of the current instrumental developments aim at improving these areas.

Besides the instrumental developments, we expect better understanding of the connection between ion drift times and collision cross-sections, especially in the case of the T-wave[92] and FAIMS[122] devices. There is growing interest in predicting the collision cross-sections of peptides on the basis of their sequence[123]. In the future, developments in bioinformatics may also help to handle the increased datasets resulting from the use of ion mobility separation as an additional dimension in the data.

It was shown that the combination of IMS and MS imaging is capable of determining the size, weight and position of biomolecules simultaneously from complex samples, rendering it an essential tool in the field of analytical biochemistry.

Chapter 3

Microscope Mode Secondary Ion Mass Spectrometry Imaging with a Timepix Detector

In-vacuum active pixel detectors enable high sensitivity, highly parallel time- and space-resolved detection of ions from complex surfaces. For the first time, a Timepix detector assembly was combined with a Secondary Ion Mass Spectrometer for microscope mode SIMS imaging. Time resolved images from various benchmark samples demonstrate the imaging capabilities of the detector system. The main advantages of the active pixel detector are the higher signal-to-noise ratio and parallel acquisition of arrival time and position. Microscope mode SIMS imaging of biomolecules is demonstrated from tissue sections with the Timepix detector.

3.1 Introduction

Atoms, molecules and molecular complexes form the basis of life. They are the building blocks of bio-molecules like peptides, proteins, lipids and DNA. The investigation of the interaction of these macromolecules reveals insights into the dynamic processes that determine the state of biological systems. It is crucial to understand how biological (mal-) function is related to molecular organization. Neurodegenerative diseases, like Alzheimer's and cancer, for instance, change the cellular biochemistry. Therefore, disease studies and diagnosis can benefit from a fundamental understanding of protein identity, distribution and modification. The investigation of this relationship has given rise to several molecular imaging techniques. In particular, the complexity of biological systems both in the healthy and in the diseased state calls for high spatial resolution molecular imaging techniques that can identify a wide range of biological analytes simultaneously.

Several imaging techniques, such as atomic force microscopy and scanning electron microscopy, enable high spatial resolution analysis of biological systems, but lack chemical identification capabilities. Other techniques, such as fluorescent, antibody or radioactive labeling require prior knowledge about the sample composition and target pre-defined analytes.

Mass spectrometry imaging (MSI)[41, 42] is used to determine the identity and location of many different molecular species from complex surfaces. In particular, this hybrid technique, i.e. mass spectrometry combined with imaging, identifies compounds based on the atomic composition of the sample molecules and their charge state (mass spectrometry) and detects the analytes in a position-correlated way (imaging) without any prior knowledge of the composition of the imaging target. At this point, large-area surface analysis by MSI is used in several areas of research. In particular, it is applied in the fields of proteomics[124, 125], lipidomics[126-128] and metabolomics[129-131]. Disease studies like the fundamental understanding of the bio-chemistry of neurodegenerative diseases[116, 132] or cancer[133], drug distribution studies[118, 131] and forensics[134, 135], among others, also benefit from the information revealed by MSI.

There are two different approaches for mass spectrometry imaging. Microprobe mode imaging is the most common approach. It uses a highly focused ionization source and every individual pixel of the image is measured separately. Secondary ion mass spectrometry (SIMS) uses a charged primary ion beam for ionization, while matrix-assisted laser desorption/ionization (MALDI) uses a focused laser light source. Many commercial microprobe mode instruments are available for both SIMS and MALDI microprobe MS imaging. It is possible to obtain images with a pixel size below 50 nm with highly focused primary ion beams in SIMS[136, 137] and 5 µm with UV laser probes in MALDI[76, 138, 139].

An alternative approach is microscope mode imaging. In this case, the laser or primary ion beam is defocused to irradiate a larger area, typically 100-300 µm in diameter. In this way, microscope mode can reduce analysis time by several orders of magnitude[140]. For example, the analysis of a 100×100 µm area with a 1 µm primary ion beam spot size takes 10,000 individual microprobe mode experiments, while it only takes a single

microscope mode experiment that targets an area of 100 μm^2. This greatly reduces the measurement time and increases the sample throughput, which is advantageous to the analysis of degrading (biological) samples.

Another advantage of microscope mode MSI in SIMS is that the primary ion gun can be operated with a high primary ion current optimized for higher secondary ion generation. Small primary ion beam spot sizes in microprobe mode (on the order of 500 nm–1 µm) often require relatively low primary ion current (thus low secondary ion count rates), in order to achieve such a spot size and to stay under the static SIMS limit (~10^{13} ions/cm^2) and ensure the sample surface is not damaged by the primary ion beam. If the primary ion dose stays below the SIMS static limit, each primary ion samples a fresh position on the surface.

While microprobe mode MSI relies on position-correlated image reconstruction, the microscope mode approach requires that the ion cloud retains its spatial organization in the mass spectrometer and that a position-sensitive detector is used. This means that the obtainable spatial resolution is now decoupled from the ionization source. Thus, the spatial resolution is dependent on the quality of the ion optics in the mass spectrometer, as well as the "magnification factor" of the instrument combined with the capabilities of the position-sensitive detector. The most common detector for this purpose, and the simplest, is the combination of a microchannel plate (MCP) with a phosphor screen and a charge-coupled device (CCD) camera behind the screen[140]. Recently, also the direct detection of ions with a specialized CCD camera has been shown[141]. However, these systems cannot simultaneously measure the spatial information and the time-of-flight of different ions. Thus, to spatially map the ion of interest it is necessary to blank out all other ions using an electrostatic blanker. To still obtain the spatial localization of multiple analytes, the sample analysis has to be repeated for each desired analyte. This approach is highly repetitive and hence time-consuming, and additionally not very practical on depleting (biological) samples. On the way towards both position- and time-sensitive measurements, delay-line detectors are another option for microscope mode imaging. These detectors provide both time and space information for all ions simultaneously[142, 143]. However, they lack sufficient multi-hit capability and the image reconstruction is time-consuming. The latter makes the instrument tuning and optimization difficult because of a lack of direct image feedback.

A recent development for microscope mode detection employs in-vacuum pixel detectors, where every pixel acts as an individual detector. The main advantage of these detector systems is the capability to obtain position-[144] and time-resolved[145-147] ion images. The small pixel size of such a detector (here, 55 µm), combined with a high quality ion microscope mass spectrometer with a good magnification factor (typically up to 100×), make these detectors very well-suited for high spatial resolution microscope mode imaging, i.e. a detector pixel (with a physical dimension of 55×55 µm) probes 550 nm on the sample surface at a magnification factor of 100×. Further, such a system provides parallel detection of thousands of ion hits simultaneously. The pixelated detector offers "multiplexed" ion detection capabilities, where each ion hit is detected by multiple pixels, which results in better sensitivity. It also offers direct image acquisition (i.e. no complex instrumental operation or image reconstruction is needed to spatially map all ions from the surface). Furthermore, this class of detectors bears the potential for a fast readout (up to 1 kHz) and hence high experimental repetition rates. The advantages of a pixelated detector have been previously demonstrated using a MALDI ion microscope[144, 146, 148]. However, this technology and its benefits have not yet been applied for SIMS imaging.

Secondary ion mass spectrometry was the first mass spectrometry imaging approach. It utilizes high energy charged particles to generate secondary ions from a surface. These high energy particles are usually elemental ions from a liquid metal ion source (LMIS). Further, the primary ion beam can easily be focused to micrometer and nanometer probe sizes. Compared to MALDI, SIMS suffers from extensive fragmentation of secondary ions and from low secondary ion yield. Also, ion counts steeply drop at higher masses. This limits its use mostly to the analysis of low mass molecular and elemental ions. Recent developments in sample preparation methods[43, 59, 149] and the introduction of cluster primary ion sources (Au_n^{m+}, Bi_n^{m+}, C_{60}^{+})[44, 150, 151] have improved the secondary ion yields for lipids and small peptides. These developments have helped move the technique from applications in the domains of surface physics and solid state physics to the study of biological samples such as cells and tissue sections, where it proved to have an outstanding spatial resolution of few hundred nanometers compared to other mass spectrometry imaging methods.

In this work, we present the first example of an in-vacuum pixelated detector for microscope mode SIMS imaging. The detector used was a member of the Medipix/Timepix family in combination with a chevron MCP stack. The advantages of the Timepix pixelated detector for microscope mode MSI, i.e. position- and time-sensitive measurements, measurement of different masses simultaneously, high dynamic range, high throughput and high spatial resolution, are transferred to SIMS microscope mode MSI. The detector was evaluated for SIMS imaging with a benchmark sample, as well as biological tissue sections. The different acquisition modes of the Timepix active pixel detector, i.e. the particle counting mode and the time-over-threshold (both in microprobe mode) and the time-of-flight modes (in microscope mode), are evaluated for SIMS imaging. Whenever applicable, the performance of the new detection system is compared to that of an established detector system.

3.2 Experimental

3.2.1 The Medipix/ Timepix Detectors

The detectors in the Medipix/Timepix family are based on complementary metal-oxide-semiconductor (CMOS) technology[152]. The detectors have been developed by the Medipix collaboration hosted by CERN[153]. A single chip contains 256×256 pixels (pixel size=55 μm×55 μm) and it is possible to build chip arrays of 2×2n (n=1,2…) chips.

The Timepix chip[154] is the successor of the Medipix2 chip[155], where each pixel contains an additional clock with a maximum clock speed of 100 MHz and measurement interval of 118 μs. This makes it possible to use the Timepix chip in three different operating modes. The first is Medipix counting mode, which simply counts the number of particles that hit the individual pixels of the chip in a set time frame (“particle counting”). The second is called time-over-threshold (TOT) mode where the time that a pixel spends above a certain charge threshold (“intensity distribution” of how much charge is deposited per pixel) is measured. Finally, the Timepix has a time-of-flight (TOF) mode that is capable of measuring the arrival time of particles with respect to an external trigger signal. This mode is particularly well-suited for time-of-flight mass spectrometry (TOF-MS), since every pixel functions as an individual TOF detector.

The data is read out by a 1 Gbit/s read-out system developed by the ReLAXD project (high Resolution Large Area X-ray Detector[156, 157]) for 2×2 chip assemblies. It reads out the four chips in parallel, which results in a maximum frame rate of 30 frames/s. The chips are controlled by a dedicated acquisition and control software package, Pixelman[158, 159].

3.2.2 Imaging setup on the ion microscope

All experiments were performed on a Triple Focusing Time-of-Flight mass spectrometer (TRIFT-II, Physical Electronics, INC., Chanhassen, USA) equipped with a gold Liquid Metal Ion Gun (LMIG) primary ion source. All experiments were performed in the positive-ion mode with 22 keV Au^+ primary ions. The ion source routinely operates with a repetition rate in the kHz range. Thus, to synchronize the mass spectrometer with the Timepix detector (in TOF mode), the original trigger signal from the instrument needed to be down-sampled to 30 Hz (the maximum readout rate of this setup). The Timepix detector can only collect one measurement frame before it must be readout (i.e. it is single-stop) and cannot measure during the readout phase. Thus, an experimental repetition rate higher than the maximum readout rate would not result in any additional measurements on the Timepix. For the evaluation of the particle counting and TOT mode (sections 3.3.1 and 3.3.2), the mass spectrometer is operated in "quasi" microprobe mode, i.e. the primary ion source is rastered with a 100-200 µm wide square tile with a raster speed in the MHz range, where every tile measures 256×256 pixels. However, the images are directly acquired with the position-sensitive Timepix detection system and need not be reconstructed by position-correlation, as is required with traditional microscope mode experiments. Note that for these experiments, the Timepix detection system and the TRIFT instrument run completely asynchronously. The primary ion source runs at a repetition rate of 8 kHz, while the Timepix detector collects data at 30 Hz. Hence, the Timepix collects ions from multiple primary ion gun raster positions in one acquisition frame.

For time-resolved measurements (evaluation of the TOF mode, sections 3.3.3-3.3.5), the rastering was disabled and the ion beam was defocused for microscope mode operation. In this way, the imaged area was about 100 µm wide and 300 µm high.

The detection system was a chip assembly consisting of bare Timepix ASIC (application-specific integrated circuit) in a 2×2 array mounted 2 mm behind a chevron MCP stack (ϕ = 4 cm, 12 µm pores, 15 µm pitch). Details of the detector assembly can be found elsewhere[146]. The MCP was used at a bias of 1.9 kV (gain: $5 \cdot 10^6$) unless stated otherwise. The potential between the backside of the MCP and the chip was 600 V.

3.2.3 Reference measurement system

The high voltage line from the MCP backside was decoupled into the original electronics rack of the TRIFT-II mass spectrometer, which consists of a constant-fraction discriminator (CFD) and a multi-stop time-to-digital converter (TDC) with 138 ps time bins. This setup makes it possible to acquire reference spectra with an established method simultaneously with the Timepix measurements. Reference images are acquired by position-correlated registration of the ion current, i.e. traditional microprobe mode.

3.2.4 Timepix-generated spectra and images

The Timepix detector was operated in all of its possible operating modes. In all modes, a typical, sparse data frame contains the x- and y-coordinate of every triggered pixel. Additionally, per acquisition mode, the data file lists the number of particles counted by the pixel (counting mode), the time during which the pixel was over threshold (TOT mode) or the time-of-flight (TOF mode). The Medipix counting and the TOT mode are imaging modes (used in combination with the microprobe mode). Images are integrated by adding the Medipix or TOT counts of several image frames, respectively. In the TOF mode, every measurement frame contains the TOF information obtained from a single primary ion pulse. The mass spectrum is reconstructed by making a histogram of the TOF values from the separate frames. Standards were used to calculate mass calibration parameters, which were then applied to the TOF spectra. Total ion images were constructed by summing all of the individual frames. Selected ion images were plotted by extracting the pixel positions for a selected mass spectral peak.

3.2.5 Samples

An organic dye (green Staedtler Lumocolor 318-5 permanent marker, Staedtler Mars GmbH & Co. KG, Nürnberg, Germany) and a solution of polyethylene glycol (2 mg/ml PEG; 200-3500 dissolved in methanol) spotted on an indium tin oxide (ITO) coated glass slide (4-8 Ω resistance, Delta Technologies, Stillwater, MN) were used for initial evaluation of the new experimental setup. A hexagonal thin bar transmission electron microscopy (TEM) grid (700 mesh, G2760N, 3.05 mm diameter, 37 µm pitch, 8 µm bar width; Agar Scientific Limited, Stansted, United Kingdom) was placed on top of the wet solutions, which allowed the standards to be detected from underneath the grid.

Mouse testis tissue (male balb/c mouse; Harlan Laboratories, Boxmeer, The Netherlands) was sectioned into 12 µm thin sections using a Microm HM525 cryomicrotome (Thermo Fisher Scientific, Walldorf, Germany) and then thaw-mounted on an ITO slide. After sectioning, the tissue sections were kept at -20 °C until further use. The sample was dried in a vacuum desiccator for 30 minutes and then coated with 1 nm gold layer using a sputter coater equipped with a FT7607 quartz crystal microbalance stage and a FT690 film thickness monitor (Quorum Technologies SC7640, New Haven, East Sussex, United Kingdom) prior to measurement.

3.3 Results

3.3.1 Ion imaging: Medipix versus time-over-threshold mode acquisitions

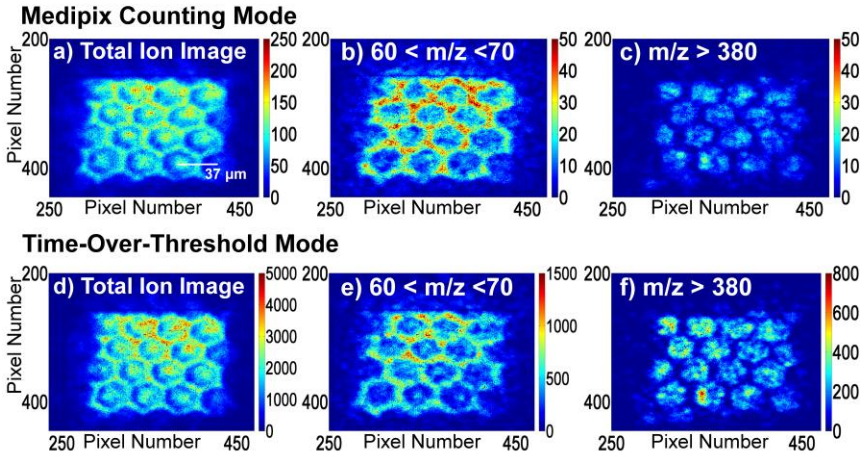

Figure 3.1. Comparison of Medipix counting mode (a-c) and Time-Over-Threshold mode (d-f) of the Timepix detector using the total ion image (a,d) and the selected ion images of copper (b,e) and the organic dye (c,f).

Experiments were performed to assess the image quality of the Timepix. Therefore, the TEM grid/organic dye sample was measured in both ion counting mode and TOT mode ("intensity mode"). The results of these experiments are shown in Figure 3.1.

Both modes return TEM grid images with a very good image quality and contrast (Figure 3.1). A comparison of the images of the two modes reveals that the contrast in TOT mode is better than in the counting mode. In TOT mode, the time each pixel spends above a certain signal threshold is measured which results in a better signal-to-noise ratio (S/N) and better image contrast than in the counting mode.

When the Timepix is run in the Medipix counting or the TOT imaging mode, mass-selected images can only be created by selectively blanking all unwanted ions by the use of an electrostatic blanker[140] (unlike

in the Timepix TOF mode, sections 3.3.3-3.3.5). As stated earlier, mass-selection by an electrostatic blanker is suboptimal. However, it can readily be employed for the evaluation of the image quality delivered by the Timepix system. The motivation is to assess if the image quality (image resolution) of the Timepix is acceptable or better than current approaches for SIMS imaging. Thus, later experiments could include "dual" or even "triple" mode experiments, in which different pixels of the detection system are programmed to operate in the counting, the TOT or the TOF mode (which will again remove the need for mass-selection with the blanker).

As expected, the selection of the copper ion mass range ($60<m/z<70$) yields a high contrast and high resolution image of the grid bars (Figure 3.1, b,e), while a selection of ions above $m/z=380$ results in a complementary ion image of green dye in the holes (Figure 3.1 c,f).

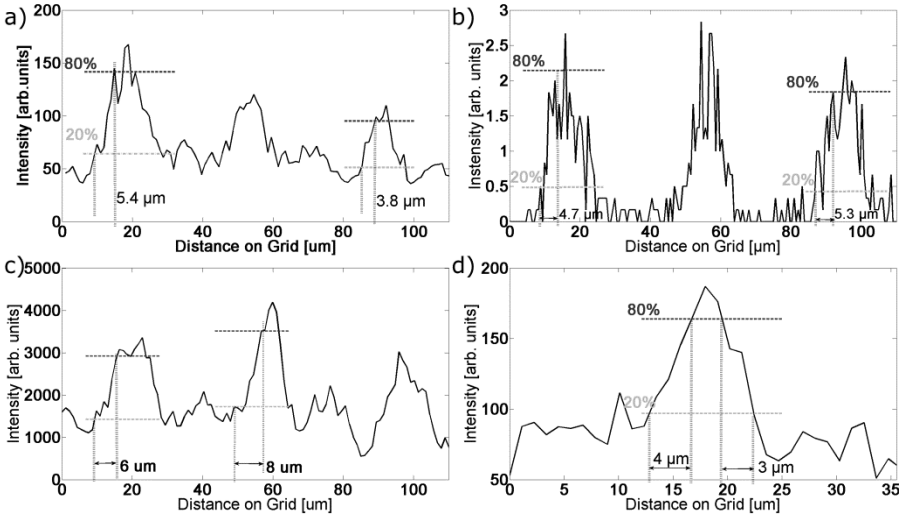

Figure 3.2. Line scans from the copper signal of a TEM grid used to calculate the spatial resolving power. Acquired with the Timepix detector in Medipix mode (a), the original MCP and TDC detector system (b), the Timepix detector in Time-over-Threshold mode (c) and in Time-of-Flight mode (d).

3.3.2 Spatial resolving power: Timepix versus standard TRIFT images

The spatial resolving power, rather than the spatial resolution (1 detector pixel corresponds to 550 nm-1µm on the sample surface depending on the ion optical magnification factor in the TRIFT-II MS), of the images

shown in Figure 3.1 is investigated and compared to the spatial resolving power that is obtained in the equivalent "postion-correlated" microprobe experiment. Generally, the spatial resolving power is determined by generating an intensity profile across features of the sample, a so-called line scan, and assessing the distance between the 20% and 80% points of the peaks in the line scan[160]. Figure 3.2a shows the result of such a line scan through Figure 3.1b (Medipix counting mode, copper ions, *m/z*=60-70), which yields a spatial resolving power of ~5 µm (Figure 3.2a). The spatial resolving power of the Timepix detector in TOT mode and the spatial resolution from Timepix TOF microscope mode imaging is similar (Figure 3.2c and 3.2d). The spatial resolving power of the position-correlated microprobe mode image reconstruction is similar but slightly inferior to the Timepix resolution (Figure 3.2b, see also Figure 3.3 for the position-correlated image of the TEM grid). Thus, the spatial resolution of the two detection methods, position-sensitive detection with the Timepix and position-correlated image reconstruction on the basis of the MCP signal, is comparable with a slight performance advantage for the Timepix. Also note that the absolute intensity of the signal obtained with the Timepix detector is much higher than the one measured with the MCP only. This is due to the multiplexed detection capabilities of the Timepix detector where a single ion hit is translated into an electron shower by the MCP which is then detected on multiple pixels on the Timepix detector. It is also worth noting that the Timepix image was measured using an MCP bias of 1.3 kV (gain of $2 \cdot 10^5$), while the standard MCP-based image detection required a bias of 1.75 kV (gain of $1.5 \cdot 10^6$) for any ion to be detected. A lower MCP bias (and hence gain) results in a longer MCP lifetime.

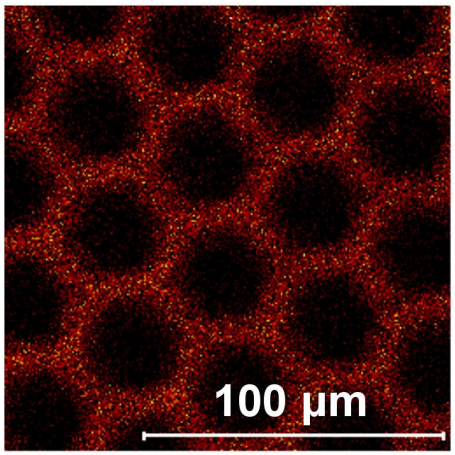

Figure 3.3. Image of the TEM grid acquired with the MCP-TDC detector system

3.3.3 Mass Spectra: Timepix versus TRIFT TDC

The previous sections evaluate the Timepix imaging quality in Medipix counting mode and TOT mode. These modes allow fast image acquisition of total ion images (see section 3.3.5 for an evaluation of the acquisition speed and obtainable repetition rates). Thus, high S/N images can be collected in a short amount of time. However, the measurement of selected ion images for every mass spectral peak are still time-consuming (i.e. only a single mass can be imaged at once) in these two imaging modes. Thus, the desired Timepix mode of operation for TOF-SIMS imaging is the TOF mode.

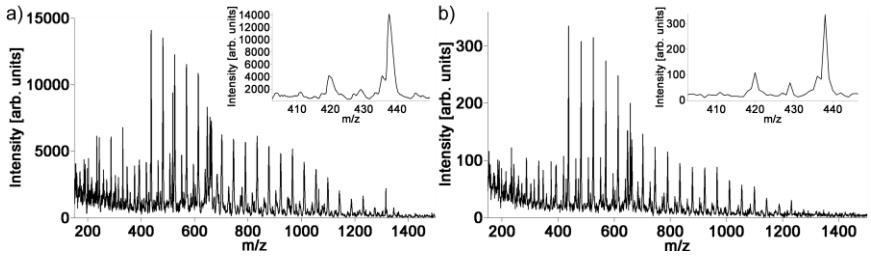

Figure 3.4. Mass spectrum of PEG mixture measured with the Timepix detector (a) and with the MCP-TDC (b). The sodiated ions of different length PEG oligomers are marked (*). Insets show a selected peak at *m/z* 437 ($[PEG_9+Na]^+$ ion).

The quality of Timepix-acquired SIMS mass spectra is evaluated with a mixture of PEG. For this measurement, the MCP was biased at a voltage of 2.3 kV (gain of 10^7) and the repetition rate of the SIMS source was down-sampled to 30 Hz. This high gain was needed in order to record a mass spectrum with the reference TDC detector system. The comparison of the two detectors shows that all peaks detected with the TDC are also present in the Timepix spectrum (Figure 3.4). The detected peaks are the sodiated ions of different length PEG oligomers. Both systems achieve the same mass range. The signal-to-noise ratio of the mass spectrum acquired with the Timepix detector (peak at *m/z*=437 detected with a S/N of 18) is almost 40% superior to the one measured with the TDC setup (peak at *m/z*=437 detected with a S/N of 13). The Timepix spectral mass resolution is slightly less, due to the relatively long clock cycles of the detector (10 ns, detailed evaluation in reference 144). Since the ion mass is determined from its time-of-flight in TOF-SIMS measurements, the minimum clock cycle length determines the obtainable mass resolution. A clock cycle of 10 ns corresponds to approximately 150 mDa for an ion around 400 Da on our ion microscope mass spectrometer

3.3.4 Time- and space-resolved microscope mode SIMS imaging

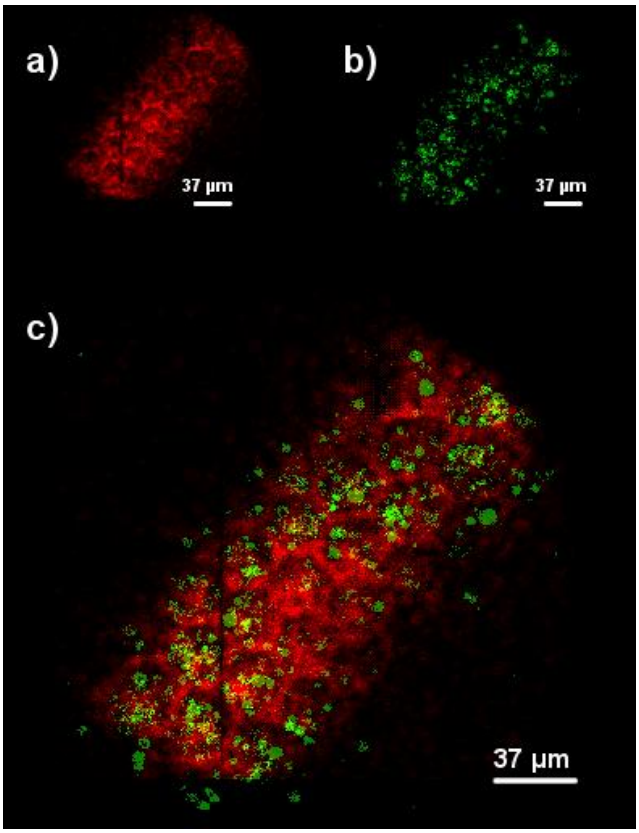

Figure 3.5. Time-resolved overlay image of the green organic dye standard below a TEM grid. The plotted masses are *m/z*=63 (copper grid, a), *m/z*=385 (organic dye, b) and the overlay of the two images (c).

Figure 3.5 illustrates time-resolved (i.e. mass-selected) imaging of the benchmark sample (green organic dye under a TEM grid) using the TOF mode of the Timepix detector. The images of the low mass copper ions show good contrast (Figure 3.5a, red). The images of the organic dye (in the holes of the grid, Figure 3.5b, green) are relatively sparse due to low ion counts. These results show that the low ion count rates encountered with SIMS result in a low S/N, especially for higher mass ions, with the Timepix detector. The low ion count rates encountered here are the result of multiple factors, the most important of which is the low repetition rate of the gold primary ion source. It was necessary to decrease the repetition rate of the

primary ion source by a factor of 266 (from 8 kHz to 30 Hz), in order to synchronize it with the Timepix detector. Since there is a linear connection between the repetition rate of the ion source and the number of ions delivered to the sample, the latter decrease by the same factor. Similarly, the aquisition time must be increased by the same factor to reach the same primary ion dose on the surface as in a microprobe experiment. Another factor that causes low ion counts is the lack of a post-acceleration voltage in this Timepix setup where the Timepix detection system is held at ground potential A post-acceleration voltage is particularly important for higher mass ions, since they impinge on the detection system with a lower momentum and hence might not be able to initiate an electron cascade in the MCP. Combined, these effects explain the observed steep drop in secondary ion counts with increasing mass. The lower ion yield (per frame) of the SIMS setup versus a MALDI experiment is clearly visible if we compare the total ion image from a single measurement frame from both SIMS and MALDI (Figure 3.6).

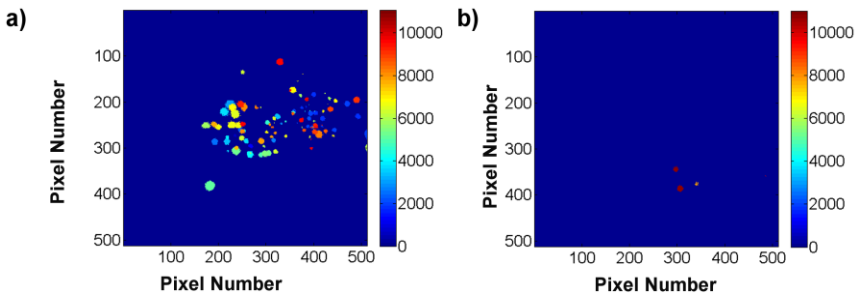

Figure 3.6. Comparison of a single frame of ion events detected on the Timepix detector using MALDI (a) and SIMS (b). Per frame, SIMS has a much lower number of ions, which necessitates many scans to be collected for sufficient signal-to-noise ratio.

3.3.5 SIMS-MSI on biological samples with the Timepix

Figure 3.7 demonstrates successful microscope mode SIMS imaging of a biological tissue section, mouse testis, with the Timepix detector in TOF mode. Here, the detector and the primary ion source are synchronized and more than 300,000 frames were collected at this one position (more than 3 h measurement at 30 Hz) due to the 30 Hz experimental repetition rate of the Timepix system. It is possible to distinguish different features in the measurement area. The selected ion

images show ions present on the tissue section, such as cholesterol (*m/z*=369, green) and another organic ion at *m/z*=358 (blue). For contrast, indium (*m/z*=115, red) was selected which was detected mostly from the surface of the ITO-coated glass slide. The diagonal "line" across the image marks the tissue boundary.

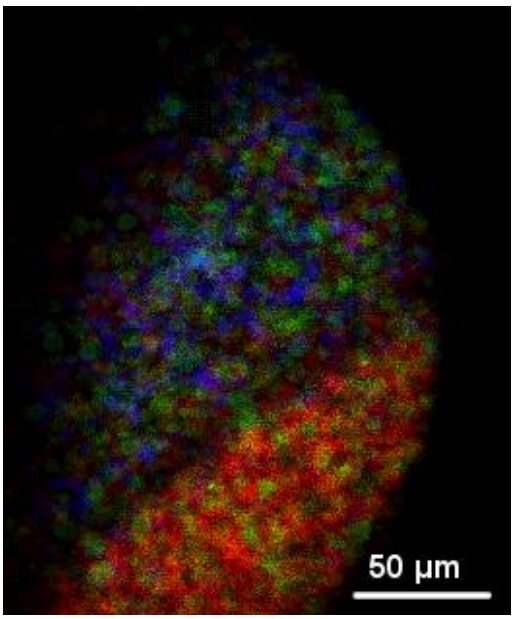

Figure 3.7. Overlay of different time resolved images of a mouse testis section. The selected ion images are *m/z* 115 (Indium, red), *m/z* 369 (cholesterol-OH, green) and *m/z* 358 (blue).

3.4 Conclusion

For the first time, a MCP/Timepix detector assembly has been combined with a SIMS mass spectrometer for microscope mode SIMS imaging. This combination enables high spatial resolution imaging of biomolecules from tissues with high sensitivity due to the parallel detection of ions achieved with the pixelated detector. The detector system's performance was compared to the established detection system of the SIMS instrument. The signal-to-noise ratio of the spectra acquired with the Timepix detector proved to be significantly better at a comparable spectral mass resolution. Also, the spatial resolving power of the Timepix-generated images is superior to the original detection system. Additionally, it is

advantageous that the MCP in the detector assembly can be run at sub-saturation gains without compromising the measurement quality, which is advantageous for the lifetime of the MCP and enables tuning the MCP gain to achieve optimal spatial resolution.

This chapter shows high quality ion images from (biological) surfaces both in ion counting and time-of-flight mode with a Timepix detector. It also shows the capability of the Timepix to easily deliver time-resolved ion images from the analysis of a tissue section using the time-of-flight mode of this active pixel detector.

The biggest challenge for the SIMS-Timepix setup is low ion counts per frame. Normally, the relatively low SIMS ion load is compensated by the use of a high repetition rate primary ion source, which allows the summation of many scans per pixel. This is currently not feasible in combination with a Timepix detection system since the data readout of the Timepix system is limited to tens of frames per second, which increases the overall measurement time. This necessitates a new version of Timepix readout electronics with a duty cycle in the kHz range. Furthermore, the use of a primary ion source with higher secondary ion yield, such as the Au LMIG in cluster mode or a C_{60} ion source should alleviate the low secondary ion count rates. Previous studies show that the use of C_{60} as a primary ion improves secondary ion yield (versus monatomic primary ions) between a factor of 13×-300×[44, 161-165]. With a mild 50-fold improvement in secondary ion yield, the time needed for the experiment shown in Figure 3.7 would be reduced from ~3 hours to only 3.6 minutes. Larger primary ion species also provide better ionization of larger molecules (and less fragmentation). Thus, the combination of such a primary ion source with the Timepix detector for microscope mode imaging is very attractive.

Chapter 4

Cluster SIMS Microscope Mode Mass Spectrometry Imaging

Microscope mode imaging for secondary ion mass spectrometry is a technique with the promise of simultaneous high spatial resolution and high speed imaging of biomolecules from complex surfaces. Technological developments such as new position-sensitive detectors, in combination with polyatomic primary ion sources, are required to exploit the full potential of microscope mode mass spectrometry imaging, i.e. to efficiently push the limits of ultra-high spatial resolution, sample throughput and sensitivity. In this chapter, a C_{60} primary ion source is combined with a commercial mass microscope for microscope mode secondary ion mass spectrometry imaging. The detector setup is a pixelated detector from the Medipix/Timepix family with high-voltage post-acceleration capabilities. The system's mass spectral and imaging performance is tested with various benchmark samples and thin tissue sections. We show that the high secondary ion yield (with respect to "traditional" monatomic primary ion sources) of the C_{60} primary ion source and the increased sensitivity of the high voltage detector setup improve microscope mode secondary ion mass spectrometry imaging. The analysis time and the signal-to-noise ratio are improved compared to other microscope mode imaging systems, all at high spatial resolution. We have demonstrated the unique capabilities of a C_{60} ion microscope with a Timepix detector for high spatial resolution microscope mode secondary ion mass spectrometry imaging.

4.1 Introduction

Mass spectrometry imaging (MSI)[41, 42] is a technique for the label free study and visualization of the distribution of multiple molecular species

on complex surfaces, such as thin tissue sections. It has two main advantages over other common imaging techniques used. First, it has chemical identification capabilities and second, no *a priori* knowledge of the sample is required. Matrix assisted laser desorption ionization (MALDI) has seen widespread use for mapping of intact biological molecules from complex surfaces. Spatial resolution in such experiments is typically limited to 10-50 μm, due to laser beam focusing. However, secondary ion mass spectrometry (SIMS) has a long history of sub-micrometer chemical imaging of a variety of sample substrates[55, 160, 166-170].

SIMS is the oldest ionization method used for mass spectrometry imaging[3]. Early primary ion sources for SIMS used atomic primary ions such as Ga^+, Cs^+ or In^+. These ion sources have the advantage that the ion beam can be focused to a very small spot size, thus a very high spatial resolution can be achieved (10s of nanometers)[136, 137] for MS imaging experiments. A drawback of these sources is the high degree of fragmentation of the secondary ions. The range of detectable ions is limited to elemental ions and small organic fragments such as CH_3^+ or CN^-, albeit at high spatial resolution. For many years, this restricted the use of SIMS to solid state physics and to the study of semiconductor surfaces. The introduction of polyatomic primary ion sources was one of the biggest advancements in the field[44, 150, 151]. It was shown by several groups that these sources have a higher secondary ion yield and they provide "softer" ionization[44, 161-165], thus opening the field of SIMS for biological research applications. However, these ion sources are more difficult to focus due to the strong space-charge effect associated with the combination of high primary ion current and small spot size. Thus, a compromise is needed between the primary ion current, which is related to the secondary ion yield, and spatial resolution. This is shown by the fact that the highest spatial resolution achieved with a C_{60} primary ion source was 1 μm, as opposed to the tens of nanometers with monoatomic primary ion beams. This was demonstrated by the Vickerman group which built a C_{60} buncher Time-of-Flight (TOF) instrument for high spatial resolution imaging[164].

Typically, mass spectrometry imaging is performed in the microprobe mode, where a focused laser (MALDI) or primary ion beam (SIMS) measures the sample pixel-by-pixel. The spatial resolution is dependent on the spot size of the ion source in microprobe mode. *Microscope* mode imaging does not require highly focused beams. Rather,

large beam sizes (usually around 200-300 µm) are used to desorb and ionize the molecules on the sample surface. After the desorption and ionization event, the spatial distribution of the ions is preserved as they travel through the mass spectrometer and then the ion image is projected onto a position-sensitive detector. The main advantage of this approach is that the spatial resolution is independent from the size of the laser focus or primary ion beam. In this way the analysis speed is significantly increased for the same area, spatial resolution and repetition rate compared to microprobe mode imaging. Additionally, it eases the difficulty of focusing the laser beam or primary ion source to very small spot sizes (few µm or less).

So far, the widespread use of microscope mode mass spectrometry imaging was limited by the lack of an appropriate position-sensitive detector with simultaneous measurement of time-of-flight and position information. The first detector used for microscope mode imaging consisted of the combination of a dual microchannel plate (MCP) with a phosphor screen and a charge-coupled device (CCD) camera[140, 171]. The main limitation of these detector systems is that they are not capable of recording the time-of-flight of the arriving ions, only their position. Thus, the selection of an ion of interest with, for instance, an electrostatic blanker in the mass spectrometer is needed to record a selected-ion image. Because of the sample damage due to the ionization process, this is only possible for a few ions before the sample is depleted. It is also very time consuming because the sample needs to be imaged separately for every ion of interest.

Recently, other detectors, such as delay-line detectors, have been tested for microscope mode imaging[142, 172]. These detectors have the capability to record the time-of-flight and the spatial position of an ion simultaneously. However, they lack multi-hit capabilities for typical mass spectrometry imaging event rates. As a result, these detection systems require low ion loads and are only well suited for SIMS experiments and not MALDI. Additionally, there is no direct feedback during measurement because of the time consuming image reconstruction process which makes optimization of measurement parameters difficult.

The latest development in the field of microscope mode mass spectrometry imaging has been the introduction of pixelated detectors, such as the Medipix/Timepix detector family[144-147, 173, 174]. In these detectors, every pixel acts as an individual detector capable of recording the time-of-

flight of the arriving ions with respect to an external trigger signal. Combined with MCPs, they offer multiplexed ion detection capabilities where every ion hit is registered by multiple pixels. This multiplexed detection results in increased sensitivity for these systems. Additionally, the spatial information is determined by the pixel address of each pixel. The capabilities of the Timepix detectors were previously demonstrated for microscope mode MALDI imaging[144, 146, 147, 174].

In the previous chapter, we presented the first example of microscope mode SIMS imaging with a Timepix detector[175]. The potential of this detection system for SIMS microscope mode MSI, namely superior spatial resolving power and signal-to-noise was demonstrated. Also, these first experiments revealed that this initial setup lacked the sensitivity and speed needed for practical use in biological studies. Limitations were the low secondary ion yield of the gold primary ion source, the lack of ion post-acceleration in the Timepix setup and the low repetition rate of the Timepix detector. Also, negative mode measurements were not possible with this setup.

This chapter presents an improved Timepix detector setup[174] with ion post-acceleration and negative ion detection capabilities in combination with a C_{60} primary ion source. This combination offers improvements in most of the crucial parts of the system such as sensitivity, speed and mass range. In particular, the use of a polyatomic C_{60} primary ion source promises improved ion yield performance as compared to the gold liquid metal ion source and is evaluated in detail in this work. The capabilities of the system for microscope mode C_{60} SIMS imaging were demonstrated with various benchmarks and thin tissue sections.

4.2 Materials and methods

4.2.1 The Medipix/Timepix detectors

The Timepix detector used for this project is the member of the Medipix/Timepix detector family[153-155, 176]. These are active pixel detectors developed by the Medipix collaboration at the European Organization for Nuclear Research (CERN, Geneva, Switzerland). They are based on Complementary Metal-Oxide Semiconductor (CMOS) technology[152]. The

Timepix application-specific integrated circuit (ASIC) is an improved version of the Medipix ASIC with two new measurement modes in addition to the simple particle counting mode. One is the Time-over-Threshold mode (TOT mode) in which every pixel registers how long it is above a certain charge threshold level. The other operating mode, and the one used for mass spectrometry, is the Time-of-Flight mode (TOF mode). One Timepix chip consists of 256×256 pixels, each capable of individually measuring the time-of-flight of ions hitting the detector with respect to an externally applied trigger signal. Each clock cycle is 10 ns wide and the maximum measurement interval of the Timepix detector is 118 μs. The size of an individual pixel is 55 μm×55 μm. It is also possible to build 2×2n arrays of Timepix chips if bigger detectors are necessary for the experiments.

4.2.2 Microscope mode mass spectrometer

A Triple Focusing Time-of-Flight (TRIFT II) mass spectrometer (Physical Electronics, Inc., Chanhassen, MN, USA) is used. The mass spectrometer is equipped with a 20 keV C_{60} primary ion source (Ionoptika, Chandlers Ford, Hampshire, United Kingdom) and a high voltage Timepix detector setup[174]. The primary ion source is operated at 20 keV primary ion energies with the C_{60}^{2+} ion selected for high primary ion beam current. The primary ion beam uses a pulse length of 60 ns and is then bunched for better spectral resolution. All the measurements are done in static SIMS mode, where the primary ion dose is well below the static limit ($1x10^{13}$ ions/cm^2).

The high voltage Timepix setup installed on the instrument has been described in details elsewhere[174]. Briefly, it consists of a 2×2 array of Timepix chips behind a chevron MCP stack. The MCPs are operated at a bias of 1.375 kV for the positive mode and 1.4 kV for the negative mode experiments, unless it is stated otherwise. The data readout system uses the ReLAXD (high Resolution Large Area X-ray Detector) readout board which has a readout speed of 1 Gbit/s[156, 157] and is operated at a frame rate of 10 frames/s. The chips are cooled with a Peltier element based active cooling system. The entire detector setup can be floated at +12 kV (for negative ion mode) or -8 kV (for positive ion mode) with the use of the TRIFT II mass spectrometer's high voltage power supply. This offers additional post-acceleration of the secondary ions before they reach the MCPs. Both the Timepix/RelaXD system and the C_{60} source are triggered

from the TRIFT II mass spectrometer master trigger, which is down sampled 100 times to 10 Hz. For data acquisition, the Pixelman data acquisition software is used[159].

The Timepix detector is operated in TOF mode. In all modes, a typical, sparse data frame contains the x- and y-coordinate of every triggered pixel. Additionally, in TOF mode, the data file lists the time-of-flight. In the TOF mode, every measurement frame contains the TOF information obtained from a single primary ion pulse. The mass spectrum is reconstructed by making a histogram of the TOF values from the separate frames. Standards are used to calculate mass calibration parameters, which are then applied to the TOF spectra. Total ion images are constructed by summing all of the individual frames. Selected ion images are plotted by extracting the pixel positions and intensities for a selected mass spectral peak.

4.2.3 Samples

Various benchmark samples are used to test the imaging and mass spectral performance of the system. These include brilliant green dye (green Staedtler Lumocolor 318-5 permanent marker, Staedtler Mars GmbH & Co. KG, Nürnberg, Germany) as well as a 1 mg/mL solution of a mixture of different chain length polyethyleneglycols (PEG 200-3500) mixed with 7 mg/mL α-cyano-4-hydroxycinnamic acid (CHCA) in 1:1 ratio (1 µL deposited). The benchmark samples are placed on an indium tin oxide coated glass slide (ITO; 4-8 Ω resistance, Delta Technologies, Stillwater, MN, USA). A hexagonal transmission electron microscopy (TEM) grid (700 mesh, G2760N, 3.05 mm diameter, 37 µm pitch, 8 µm bar width; Agar Scientific Limited, Stansted, United Kingdom) is placed on the top of the samples. For biological tissue imaging, 12 µm thick coronal mouse brain (male balb/c mouse; Harlan Laboratories, Boxmeer, The Netherlands) sections are used. The brain is sectioned in a Microm HM525 cryomicrotome (Thermo Fisher Scientific, Walldorf, Germany) and the sections are placed on an ITO coated glass slide. The sections are kept at -20 ^{o}C until further use. Before measurement the samples are dried in a vacuum desiccator and are measured without any further sample preparation steps.

4.3 Results and discussion

4.3.1 Effects of the high voltage

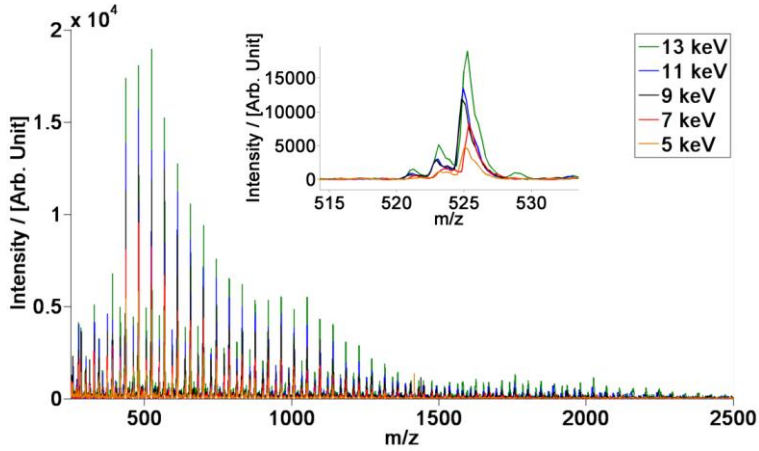

Figure 4.1. Mass spectra of a mixture of polyethylene glycol measured with C_{60} SIMS on the Timepix detector at different ion acceleration energies. The inset shows a selected PEG peak at *m/z* 525. Higher ion acceleration energies improve the signal-to-noise ratio and extend the accessible upper mass range.

As a first experiment, the system's spectral quality is assessed. Also, the effect of the increased post-acceleration of the ions on the mass spectra is systematically studied. A mixture of PEGs is used and 10,000 frames at different total ion acceleration energy values between 5 keV and 13 keV are collected. The MCP is operated at an MCP bias of 1.5 kV. Figure 4.1 shows an overlay of the PEG mass spectra obtained at the different total ion acceleration energies. The sodiated molecular ions of the PEGs are detected in this measurement. Increasing the acceleration energy of the secondary ions has a two-fold effect on the mass spectra. First, the intensity of the detected ions increases. Thus, the higher post acceleration yields a better signal-to-noise ratio (S/N of 184 for the ion at *m/z* 525 at 13 keV total acceleration energy and S/N 55 at 5 keV total acceleration energy). Also, the accessible mass range is significantly increased at the highest energy values. This is due to the higher ion energies, where more ions have a chance to start an electron cascade in the MCP. Also, higher mass ions that would not have the necessary energy to start an electron cascade can be detected due to the additional post-acceleration capabilities of the system.

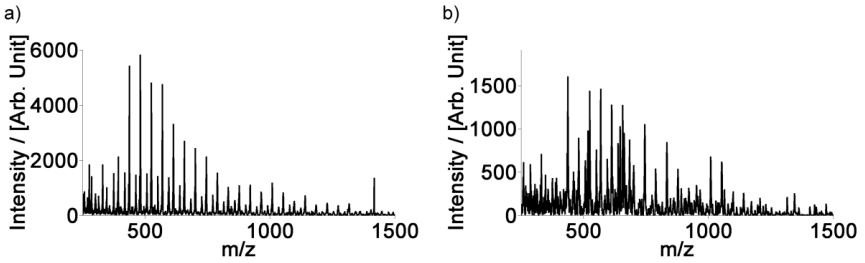

Figure 4.2. Comparison of a PEG spectra recorded with the C_{60}^+ Timepix setup (a) and with the Au^+ LMIG Timepix setup (b)

It is important to note that the same sample measured for 10,000 frames with an Au primary ion source with a higher MCP gain results in a spectrum with a S/N of 37, which is five times lower than the S/N achieved with the combination of the C_{60} source and the high voltage Timepix setup, and mass range between *m/z* 0 and 1200 (see Figure 4.2). Thus, the use of the C_{60} primary ion source results in a significant increase in spectral quality, even at low post-acceleration, due to the higher secondary ion yields associated with such polyatomic primary ion sources.

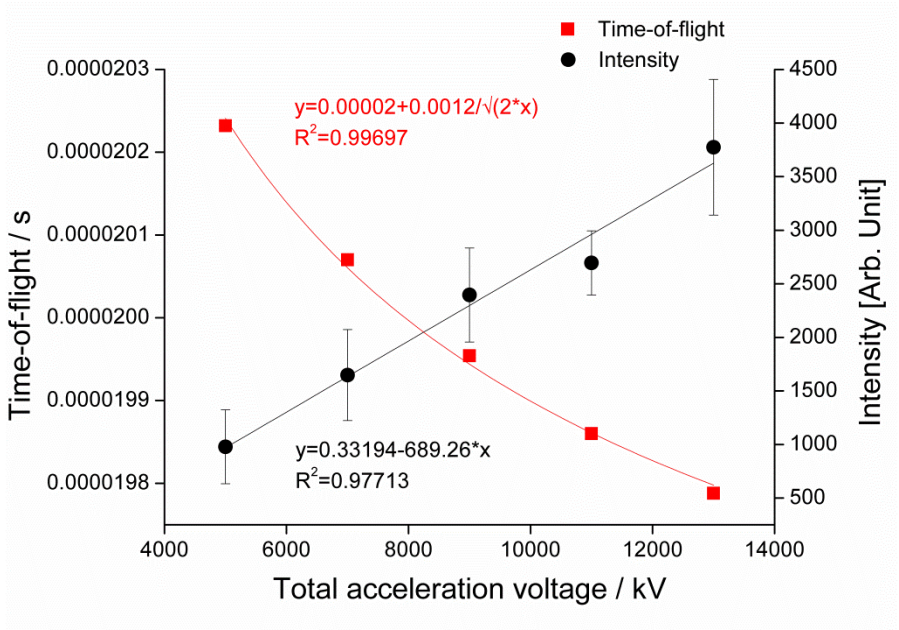

Figure 4.3. Intensity (black) and the time-of-flight (red) of the PEG ion at *m/z* 526 as a function of the ion acceleration energy.

The high voltage setup has two main effects on the spectral quality. The first one is the increase of the secondary ion intensities discussed in the previous paragraph. The second effect is a decreasing time-of-flight of the same ion as a function of the acceleration voltage. To demonstrate these effects the measurements shown in Figure 4.1 are divided into 5 x 2,000 frame segments. Figure 4.3 shows the average intensities and average time-of-flight values of these five smaller datasets as a function of the ion acceleration energies. The time-of-flight of the selected ion changes as a quadratic function of the acceleration voltage. This is in agreement with the TOF analyzers calibration equation (1)

$$t = \frac{d}{\sqrt{2U}}\sqrt{\frac{m}{q}} \qquad (1)$$

where t is the time-of-flight of the ion, d is the length of the ion's flight path, m is the mass of the ion, q is the charge of the ion and U is the acceleration voltage. Analysis of the dependence of ion intensity demonstrates a linear increase with ion kinetic energy, as expected.

4.3.2 Positive mode imaging

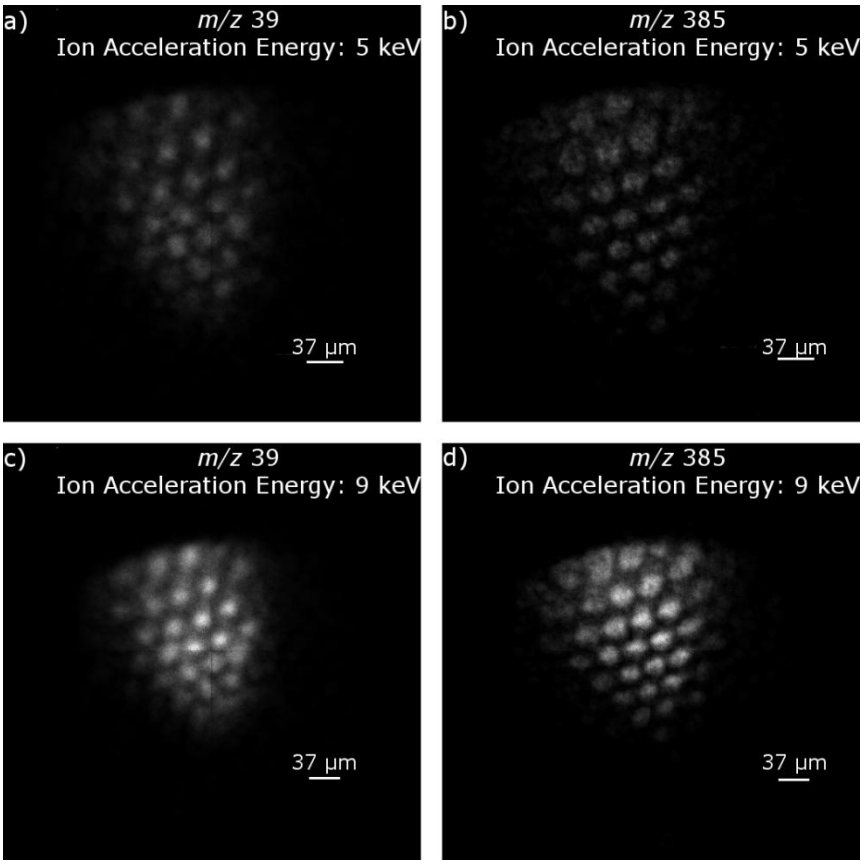

Figure 4.4. Comparison of the image quality at different ion acceleration energies. Selected-ion images of potassium at *m/z* 39 (a, c) and brilliant green dye at *m/z* 385 (b, d) are plotted on the same intensity scale. The detector is operated at total ion acceleration energies of 5 keV (a, b) or 9 keV (c, d).

Figure 4.4 demonstrates the imaging capabilities of the system on brilliant green dye underneath a TEM grid, in the positive ion mode. The same area of the sample is measured with the detector at ground (Figure 4.4a and 4.4b) and at 4 kV (Figure 4.4c and 4.4d). The selected-ion images for the comparison are the cation of the brilliant green dye (*m/z* 385) and potassium ion (*m/z* 39) which both localize in the holes of the grid. The size of the primary ion beam is ~224 µm × 272 µm and the images are reconstructed from 20,000 frames. Figure 4.4 shows that the high voltage setup is capable to provide the same image quality as the previous detector setup (where the detector is held at ground potential). The effects of the

higher ion acceleration on the image quality are a better image contrast, due to the higher S/N ratio, and a smaller magnification factor, due to the shorter time that the ions spend in the magnification region of the instrument.

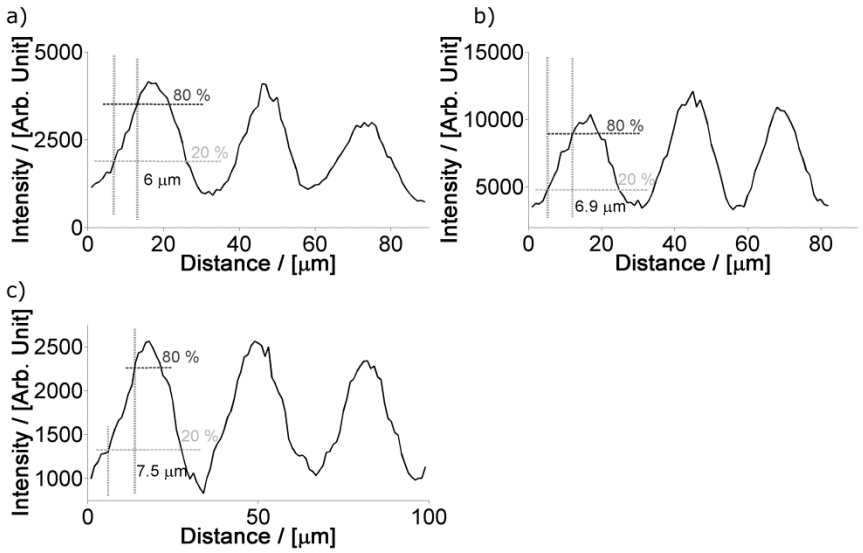

Figure 4.5. Line scans from the total ion image of the TEM grid in positive mode at a total acceleration energy of 5 keV (a) and 9 keV (b) and in negative mode at the total acceleration energy of 12.5 keV (c)

The observed spatial resolving power is ~7 µm (see Figure 4.5) with a pixel size of 900 nm. This value is close to the previously reported[175] spatial resolutions for the Timepix setup without high voltage capabilities and for a microprobe mode reference measurement system that uses the combination of an MCP with a time-to-digital converter (TDC), both on a TRIFT mass spectrometer.

4.3.3 Negative mode imaging

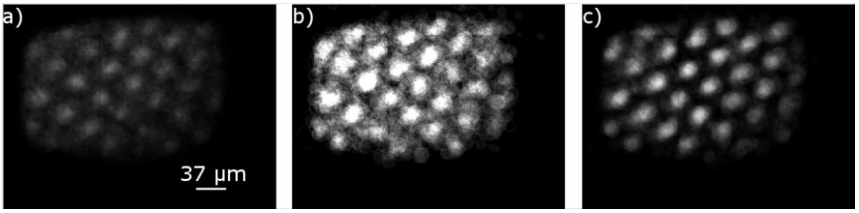

Figure 4.6. Negative mode imaging of brilliant green dye under a TEM grid. Selected-ion images show the distribution of C_2H^- at *m/z* 25 (a), C_4H^- at *m/z* 49 (b) and HSO_4^- at *m/z* 97 (c).

The previous Timepix setup was only operable in positive ion mode. One of the advantages of the new high voltage setup is the capability to detect negative ions as well. Thus, it is capable of providing complementary information to the positive mode measurements. This new functionality of the system was previously demonstrated on peptide and protein standards with MALDI ionization[174]. However, no negative mode images were recorded thus far with a pixelated detector. Figure 4.6 shows the first example of negative mode microscope mode SIMS imaging with a Timepix detector. The sample is the same grid standard used for the positive mode measurements shown in Figure 4.4. The detector is operated at an ion acceleration energy of 12.5 keV. As expected, the ions detected are mostly the standard small negative ions common to SIMS, such as C_2H^- at *m/z* 25, C_4H^- at *m/z* 49; or HSO_4^- at *m/z* 97. These ions are abundant in the holes of the sample which means they are present in the green dye underneath the grid. The image quality is similar to the positive mode image quality as can be seen in Figure 4.5. This evaluation reveals a resolving power of 7.5 µm in negative mode which is in accordance with the images acquired in positive ion mode.

4.3.4 Tissue imaging

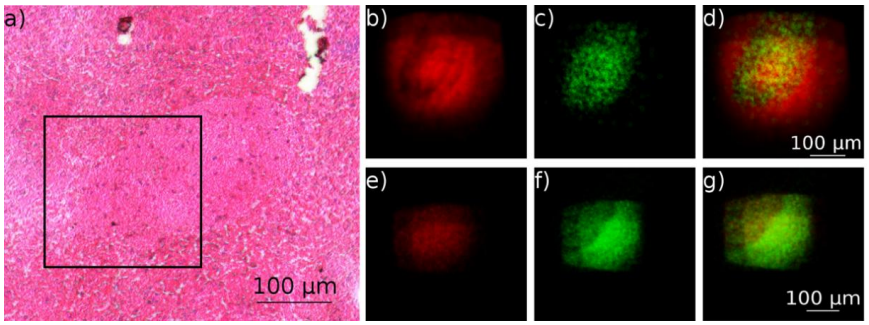

Figure 4.7. Microscope image of a H&E stained mouse brain (a), positive (b, c, d) and negative (e, f, g) microscope mode SIMS image of the anterior commissure region of the mouse brain. The selected ion images show the distribution of sodium at *m/z* 23 (b), the cholesterol fragment $[M+H-H_2O]^+$ at *m/z* 369 (c), CH^- at *m/z* 13 (e) and PO_3^- at *m/z* 79 (f) and the overlay of the two positive (d) and negative mode (g) images

The fivefold increase in sensitivity achieved with the new setup makes the imaging of biological samples possible. Figure 4.7 exemplifies the system's improvement for the imaging of biological samples. This first example of a mosaic microscope mode SIMS imaging with a pixelated detector shows complementary positive and negative ion mode images of a biological tissue sample. In particular, the sample is half of the anterior commissure area of a mouse brain section as can be seen on the hematoxylin and eosin (H&E) stained image (Figure 4.7a). The images are reconstructed from 4 tiles. The step size between each tile is 100 µm, such that there is sufficient overlap between the tiles to correct for the elliptic shape of the primary ion beam spot during the reconstruction of the image. In both positive and negative mode, 20,000 frames per tile are collected. One measurement takes 80,000 frames compared to the single tile imaging with the gold primary ion source that took more than 300,000 frames to achieve similar image quality. This means that as a result of the improvements, ~80% fewer frames are needed to measure an area that is roughly four times the size as the previously reported microscope mode SIMS image with the Timepix detector. Further, the increased secondary ion yield of the C_{60} source reduces the measurement time to only half of the time reported earlier for the single tile microscope mode SIMS measurement. Also, intact phospholipids are detected from the tissue (see Figure 4.8).

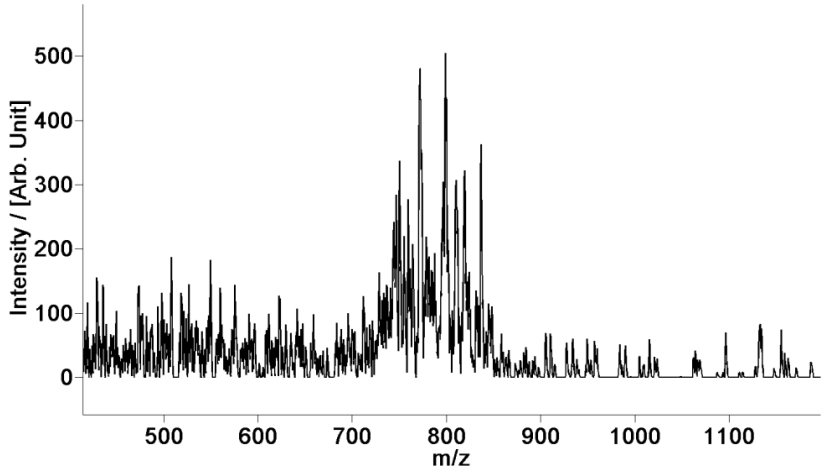

Figure 4.8. Mass spectrum from the positive mode tissue imaging experiment. The spectrum shows the detected intact phospholipids from the tissue

It is possible to distinguish the anterior commissure in both positive and negative mode. The positive mode selected ion images show the distribution of the sodium ion at *m/z* 23, which has higher abundance in the tissue surrounding the anterior commissure and the cholesterol fragment $[M+H-H_2O]^+$ at *m/z* 369, which localizes in the anterior commissure. The ions selected for the negative mode images are $(CH)^-$ at *m/z* 13 with a homogenous distribution in the imaged area of the tissue and $(PO_3)^-$ at *m/z* 79, which is localized in the tissue around the anterior commissure.

4.4 Conclusions

For the first time, the combination of a C_{60} primary ion source and a pixelated detector system with ion post acceleration capabilities was used for high spatial resolution microscope mode SIMS imaging in both positive and negative ion mode. The combination of the higher secondary ion yield of the C_{60} primary ion source and the higher ion post acceleration possibilities of the new Timepix setup resulted in an increased signal-to-noise ratio and wider mass range compared to the earlier microscope mode SIMS experiments. The acquisition time necessary to achieve high quality data was also significantly reduced. The image quality, namely the spatial resolving power, is comparable to the earlier Timepix based microscope

mode SIMS studies. It is also possible, for the first time, to measure microscope mode SIMS images in negative mode with a pixelated detector.

Timepix based microscope mode SIMS imaging opens up new possibilities, such as the fast 3D imaging of complex samples with sub-cellular spatial resolution. However, several challenges such as the speed of the readout system and the single-stop nature of the pixels remain that require further improvements on the detector level. These include a faster, 1 kHz readout system, multi-hit capabilities and a new, compact data format. Also, online, on-the-fly data analysis capability integrated on the chips or on-board the readout electronics would be advantageous for future applications and are subject to present and future studies. Microscope mode SIMS imaging with a pixelated detector shows promising results for high resolution mass spectrometry imaging of biological systems.

Chapter 5

Lipid imaging by secondary ion mass spectrometry in cardiac tissue following myocardial infarction

Although acute myocardial infarction is consistently among the top causes of death worldwide, the spatial distribution of lipids and small atomic ions following myocardial infarction remains to be elucidated. This work presents the investigation of an in vivo rat model of myocardial infarction using high resolution secondary ion mass spectrometry imaging and multivariate data analysis. Secondary ion mass spectrometry imaging was conducted on cardiac tissue following a 24 hour left anterior descending coronary artery ligation to analyze the distribution of lipids and small ions. The spatial distribution of diacylglycerols and triacylglycerols, cholesterol and small atomic ions such as sodium or potassium was determined in positive-ion mode. The higher abundance of diacylglycerols in the at-risk area of the tissue suggests increased activity of phospholipase D. Secondly, negative-ion mode mass spectrometry imaging was performed for complementary information. The higher ion intensities of fatty acids imply the overexpression of the enzyme phospholipase A2 that has an important role in inflammation.

5.1 Introduction

Coronary heart disease (CHD) has been consistently among the leading causes of death worldwide[177]. Many of these deaths in patients with CHD arise from acute myocardial infarction (MI), also known as a heart attack. MI is most often the result of atherosclerosis[178], where the wall of the coronary arteries thickens due to the accumulation of cholesterol and triglycerides in obstructive plaques. Thus, the blood supply to cardiac

tissue is restricted. The lack of oxygenated blood to cardiac tissue results in severe hypoxia and often irreversible damage that may ultimately lead to heart failure. To date, two biomarker concentrations are monitored in blood to detect MI related necrosis; troponins and creatin kinase. However, the concentration of these compounds return to the normal levels within days after a heart attack[179].

Better understanding of the biochemical processes involved in MI can lead to new diagnostic biomarkers and new treatment options to limit tissue damage. Thus, the study of CHD and especially MI has high importance and impact. Mass spectrometry is the main analytical tool used for these studies. MS was utilized as early as 1996 to characterize protein epitopes[180] for MI as well as alterations in fatty acid metabolism in ischemic myocardium[181]. Since these early experiments, MS has been utilized to study changes in the proteome[182-184] and lipidome[185] of various bodily fluids such as serum, plasma and urine. In addition, an extensive list of potential protein markers in serum was recently compiled[186]. However, the number of studies aimed to determine the location of these compounds in intact heart tissue is low. Thus, an analytical method with the possibility to spatially map multiple biomolecules on intact heart tissue can yield a valuable additional insight in the biochemical processes involved in myocardial infarction.

Mass spectrometry imaging[41, 42] (MSI) is a tool that is well suited for the study of the biochemical processes behind complex diseases such as CHD, since it permits the simultaneous detection, (tentative) identification and localization of multiple biomolecules from thin tissue sections. The two main ionization methods used for imaging mass spectrometry are Matrix Assisted Laser Desorption/Ionization (MALDI) and Secondary Ion Mass Spectrometry (SIMS). MALDI uses a focused laser beam to desorbe and ionize biomolecules from a surface. Since it is a soft ionization method it is well suited for the study of lipids, peptides and proteins. However, the maximum spatial resolution reported with MALDI is around 5 µm[76]. Myocardial infarction on a rat heart attack model was previously investigated by Menger et al. with MALDI imaging mass spectrometry[187]. In this work it was concluded that the level of creatine and many phosphocholines decreases in MI while the level of lysophosphocholines and lysophosphatidylethanolamines increases. They also found that several of the intact PCs that decreased in the infarcted tissue contained arachidonic

acid in sn2 position. This can be explained by the increased activity of phospholipase A2 enzyme following MI.

SIMS uses a highly focused high energy ion beam to ionize the sample. It was one of the first ion sources used for imaging mass spectrometry[3]. However, because of the high fragmentation rate of the secondary ions it was originally employed exclusively for studies in solid state physics and surface physics. The introduction of polyatomic ion sources such as the liquid metal ion sources (Au_m^{n+} and Bi_n^{m+})[44, 151] and the C_{60}^{+}[150] ion source, as well as new surface treatment strategies[55, 59, 149] to reduce secondary ion fragmentation have opened up SIMS for biomedical research as well. Its main advantage is the high spatial resolution which can be routinely in the sub-micron range. It is well suited for the high spatial resolution study of atomic ions, lipids and small lipid fragments. Ji-Won Park *et al* have used SIMS to study molecular changes in MI and the effects of mesenchymal stem cell treatment of MI[188]. They concluded that the amount of phosphocholine and fatty acids was lower in the infarcted tissue compared to the healthy tissue while the glucose signal increased as a result of MI. However, the samples were measured without any additional surface treatment and the entire tissue section was not analyzed; only the infarcted part of the MI sample was measured and compared to a healthy sample.

MS imaging of an entire infarcted heart tissue following a model such as a left anterior descending (LAD) coronary artery ligation has the advantage that there are perfused (nonaffected) and affected areas within a single tissue section. Thus, this model eliminates much of the variability inherent in tissue-to-tissue comparisons and also permits the study of changes between hypoxic and necrotic regions of the affected tissue. It was shown already that surface treatment methods such as gold coating can change the ionization efficiency of certain types of molecules[55]. Thus, metal assisted (MetA) SIMS provides complementary information to regular SIMS. This work reports the use of positive- and negative-ion mode MetA-SIMS and multivariate data analysis to study the distribution of lipids and small atomic ions such as Na^+ and K^+ in cardiac tissue following LAD coronary artery ligation induced MI.

5.2 Materials and methods

5.2.1 Sample preparation

All animal procedures were conducted in accordance with guidelines published in the Guide for the Care and Use of Laboratory Animals (National Research Council, National Academy Press, Washington, DC, 2010) and were approved by the Animal Care Committee of Saint Louis University. Ligation of the LAD was performed as previously described[189]. In brief, male Sprague−Dawley rats (250−300 g body weight) were injected with ketamine/xylazine (55 mg/mL, 7 mg/mL; 0.1 mL/100 g, i.p.). Rats were subsequently intubated and injected with Buprenex (0.05 mg/mL; 0.1 mL/100 g, i.p.). Animals were then ventilated with air at a tidal volume of 3−4 mL and a rate of 50−60 breaths/min (Harvard Apparatus). A left lateral thoracotomy was then performed. The thoracic cage was exposed and the intercostal space between ribs 4 and 5 was separated with a retractor. The left atrial appendage was retracted, and a 6−0 suture was placed around the proximal LAD. This LAD suture was tied tightly or loosely (controls) to produce an infarction or sham surgery, respectively. Then, the thoracic incision was closed with a 5−0 suture. After recovery from surgery, rats were weighed and individually housed. Twenty-four hours following LAD occlusion (or control sham surgery), rats were euthanized with pentobarbital (~800 mg/kg, i.p.), and subsequently hearts were removed and flash-frozen in liquid nitrogen. Organs were stored at −80 °C until further preparation. Heart tissue was bisected along a transverse plane that passed through the left and right ventricles. The upper half of the heart was subjected to 2,3,5-Triphenyltetrazolium chloride (TTC) staining[190] to distinguish perfused and damaged tissue.

The remaining lower half of the heart was utilized for SIMS MSI. These samples were sectioned to 12 μm thick sections in a Microm HM525 cryomicrotome (Thermo Fisher Scientific, Walldorf, Germany) and thaw-mounted on indium-tin oxide (ITO) coated slides (4-8 Ω resistance, Delta Technologies, Stillwater, MN, USA). The sections were stored at -80 ^{o}C until further use. Before measurement, they were dried in a vacuum desiccator for 30 min and then coated with 1 nm gold layer in a sputter coater equipped with a FT7607 quartz crystal microbalance stage and a FT690 film thickness monitor (Quorum Technologies SC7640, New Haven, East Sussex, United Kingdom).

5.2.2 Mass spectrometry

The samples were measured with a TRIple Focusing Time-of-Flight mass spectrometer (TRIFT II, Physical Electronics Inc., Chanhassen, MN, USA) equipped with a 22 keV gold primary ion source. The tile size used to measure the samples was between 100 µm and 175 µm. Every tile was measured for 3 s and consisted of 256x256 pixels. The ion current was kept below the static limit (~10^{13} ions/cm^2) for the whole measurement. For both conditions (infarction and sham), three serial sections were measured and the same section was measured both in positive- and negative-ion mode. Data acquisition was performed by Wincadence 4.4 software.

5.2.3 Data analysis

All MS imaging raw data were converted to the generic MS imaging data format data cube (x, y, *m/z*) using in-house developed software. Images were generated with the publicly available Datacube Explorer software (FOM Institute AMOLF, Amsterdam, The Netherlands)[191]. Principal component analysis (PCA) was performed using the in-house developed ChemomeTricks toolbox developed in MATLAB version 2010b (The MathWorks, Natick, MA, USA). PCA is a multivariate data analysis method described in details in several publications[192]. In short, it reduces the dimensions of a dataset. For this, a new set of variables, the principal components, are created by the linear combination of the original variables. Closely correlated variables (i.e., mass channels originating from the same chemical compound) are grouped into the same principal component. The principal components are hierarchically sorted by the amount of the total variance they describe. The first principal component represents the largest amount of the total variance; noise-related signals are found in the higher-ranked principal components. Discarding these higher-ranked principal components from further data processing greatly reduces the noise in the data.

5.3 Results and discussion

5.3.1 Positive-Ion mode SIMS imaging

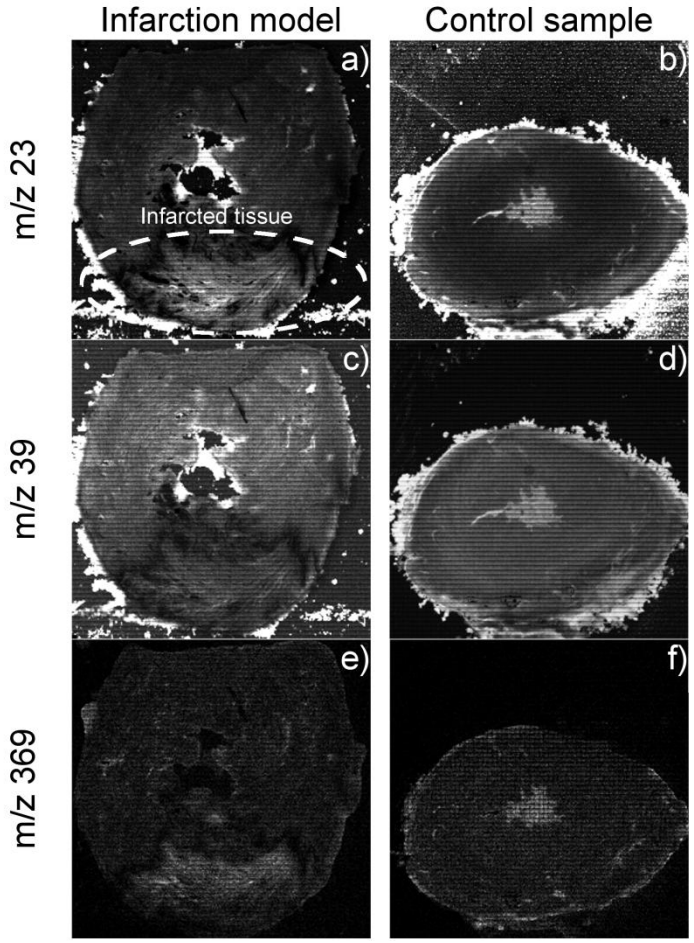

Figure 5.1 Selected ion images of sodium (*m/z* 23, a and b), potassium (*m/z* 39, c and d) and the water loss fragment of cholesterol (*m/z* 369, e and f) from the SIMS imaging experiment of the MI model (a, c, e) and the control (b, d, f) sample

One of the advantages of SIMS over MALDI is the capability to directly measure small elemental ions such as potassium or sodium. Figure 5.1 shows the distribution of sodium (*m/z* 23), potassium (*m/z* 39) and the water loss fragment of cholesterol (*m/z* 369) in the MI sample compared to the distribution of the same ions in the control sample. The cholesterol and sodium are present in higher abundance in the necrotic region of the tissue,

which is on the bottom of the image, while the potassium concentration is higher in the non-affected area of the heart section. In contrast, the same ions show a more homogeneous distribution in the control sample. They only show higher abundance in the center of the control sample where some blood remained after sample preparation and around the edge of the tissue. This confirms that the molecular changes detected in the infarcted tissue are due to the tissue damage associated with the lack of oxygen and are not the results of the surgery itself. Similar distribution of sodium and potassium was already demonstrated in some hypoxic/necrotic breast cancer sections by SIMS imaging[193]. Cancer tissues can undergo hypoxia induced necrosis in a similar process to myocardial infarction. These similar processes lead to comparable molecular and cellular changes in the two diseases.

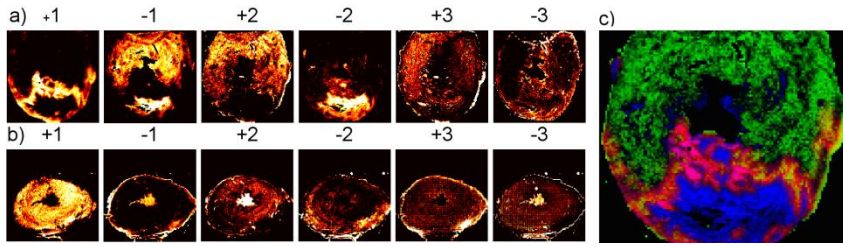

Figure 5.2 Results of the principal component analysis of the positive-ion mode SIMS imaging dataset of the MI (a) and the control (b) sample and the RGB overlay (c) of the +1 (red), +2 (green) and -2 (blue) principal components of the MI dataset

The univariate analysis of the SIMS datasets presented in Figure 5.1 with the most common ions detected by SIMS provides useful insight in the molecular changes initiated by myocardial infarction. However, the complexity of the datasets necessitates the use of unsupervised multivariate data analysis methods such as principal component analysis. The principal component analysis was performed twice on every dataset. The first principal component of the first PCA run separates the tissue from the background of the ITO slide, as this is the main source of variance in the dataset. Thus, this enables the selection and removal of the ITO background from the dataset that is used for the second round of the PCA by turning *off* the pixels identified as background. The changes inside the tissue are much more prominent without the interference of the ITO background in the data analysis process[194].

Figure 5.2 shows the results of the second PCA performed on one of the positive-ion mode MI (Figure 5.2a) and control samples (Figure 5.2b). The first principal component (PC) of the MI sample differentiates between the so called “at-risk area” and the rest of the tissue section, while the second PC differentiates the damaged tissue from the rest of the tissue. The at-risk area is part of the infarcted tissue. This region surrounds the necrotic region of the tissue and it consists of cells that are hypoxic but have not turned necrotic yet. This region is characterized by inflammation[195] and it can be saved if the blood flow in the coronary artery is restored in time. The second principal component of the MI sample differentiates the necrotic and non-necrotic tissue. The combination of SIMS imaging and multivariate data analysis enables the differentiation of this tissue region from the necrotic tissue. The RGB overlay (Figure 5.2c) of the +1, +2 and -2 principal components also confirms the annotation of the three different tissue types, where red is the at-risk area, green is un-affected tissue, and blue is the necrotic tissue . On the other hand, the control sample does not show any similar separation upon PCA analysis, as shown in Figure 5.2b. For example, the first principal component separates the blood containing areas of the tissue from the rest in the control sample.

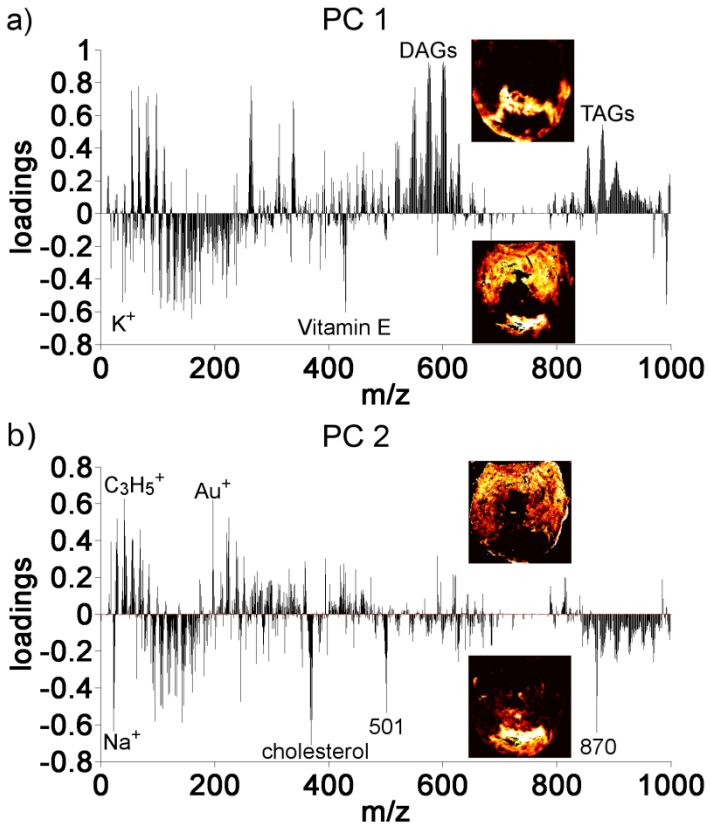

Figure 5.3 Loadings spectra of the first (a) and second (b) principal components from the positive-ion mode SIMS imaging experiment of the MI model sample

Figure 5.3 shows the loadings spectra of the first and second principal components from the PCA of the positive-ion mode MI dataset. The ions with high loadings in the positive part of the first PC, and thus in the at-risk area, are mostly lipid species such as diacylglycerols (DAGs) and triacylglycerols (TAGs), as shown in the top of Figure 5.3a. Also, some of the small fragments, such as the ion at *m/z* 98, have been commonly identified as a DAG related fragment. One of the important features of an ischemic heart tissue is the appearance of lipid droplets containing TAGs due to the decreased lipid metabolism of the cells. On the other hand, the higher abundance of DAGs can be a sign of the increased activity of phospholipase enzymes, specifically enzymes from the phospholipase D family, which was already suggested by several works[196]. According to one theory, DAGs are produced from phospholipids by first their

conversion into phosphatidic acids by phospholipase D enzymes and then their subsequent dephosphorylation by phosphatidate phosphohydrolase. DAGs have a crucial role in the left ventricular remodeling of the heart tissue after myocardial infarction as they function as signaling molecules in this process[197]. Ventricular remodeling includes cardiomyocyte necrosis, scar formation and cardiomyocyte hypertrophy, which can lead to the dysfunction of the cardiac tissue and to subsequent mortality. In contrast, the negative part of the first PC (Figure 5.3a, bottom) shows compounds that have lower abundance in the at-risk area. Some of the ions with high loadings in this PC include potassium at *m/z* 39 and vitamin E at *m/z* 429.

The negative part of the loadings spectrum from the second PC (Figure 5.3b, bottom) shows ions such as sodium (*m/z* 23) and the cholesterol fragment (*m/*z 369) with high loadings. This is in good agreement with the univariate results presented earlier in this chapter, where these ions were indicated to be in higher abundance in the necrotic region of the tissue. The two other ions with high negative loadings in the second PC are at *m/z* 501 and *m/z* 870 but the identification of these ions is challenging due to the lack of MS/MS capabilities on the SIMS instrument employed in this study.

5.3.2 Negative-ion mode SIMS imaging

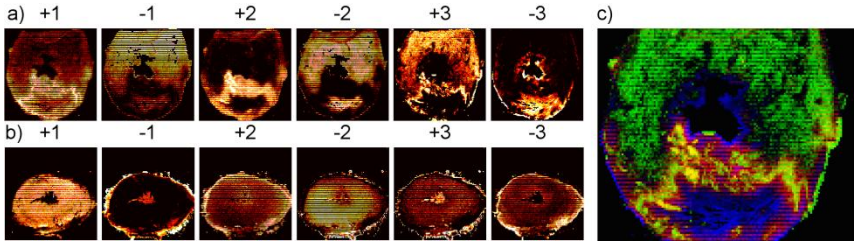

Figure 5.4 Results of the principal component analysis of the negative-ion mode SIMS imaging dataset of the MI (a) and the control (b) sample and the RGB overlay (c) of the +2 (red), +3 (green) and -3 (blue) principal components of the MI dataset

Negative-ion mode SIMS imaging of the same samples provide complementary information to the positive-ion mode data. Negative-ion mode is well suited to study the distribution of fatty acids and small negative ions in the MI sample. Figure 5.4 contains the results of the PCA analysis of a negative-ion mode SIMS imaging dataset of a myocardial infarction model (Figure 5.4a) and a control sample (Figure 5.4b). In negative-ion mode, the first PC separates the affected tissue from the not affected tissue region. On the other hand, the second PC separates the at-risk area from the rest of the tissue, while the negative part of the third PC shows the necrotic area. The PCA results of the control sample show the blood containing areas of the tissue in the second PC and a shading artifact in the third PC. If we compare the first three PCs of the control dataset to the MI data there are no similarities in ion distribution between the control and MI samples. We can clearly distinguish the affected areas on the molecular level.

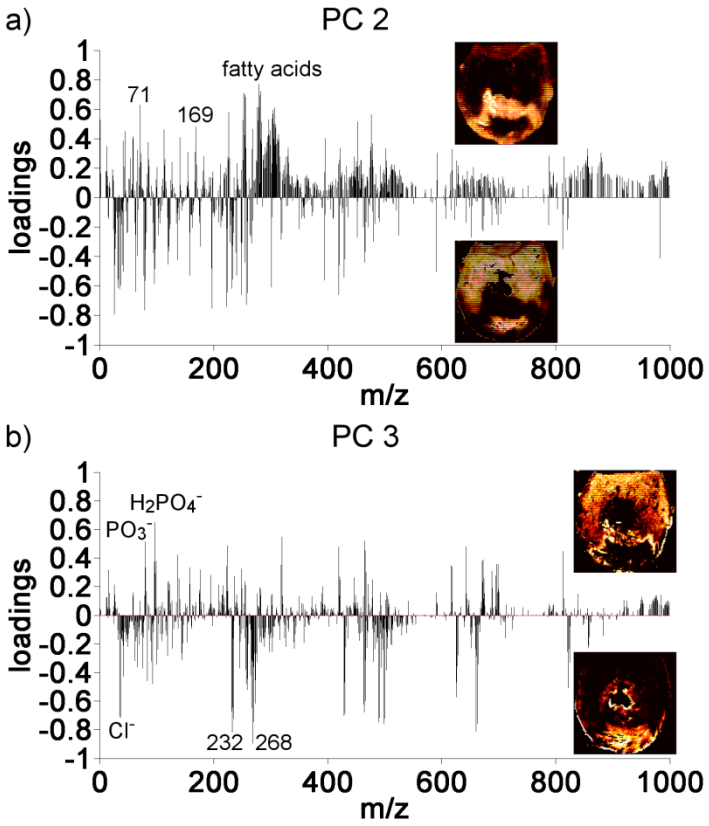

Figure 5.5 Loadings spectra of the second (a) and third (b) principal components from the negative-ion mode SIMS imaging experiment of the MI model sample

Figure 5.5 shows the loadings spectra of the second and third principal components of the negative-ion mode MI dataset. The compounds localized with high loadings in the positive part of the second PC (Figure 5.5a, top) and thus in the at-risk area of the tissue are fatty acids including arachidonic acid at *m/z* 303. This suggests the overexpression of the enzyme phospholipase A2 under the hypoxic conditions characteristic for the at-risk area. This enzyme is responsible for the cleavage of fatty acids at the sn2 position of phospholipids which leads to the production of lysophospholipids and free fatty acids. Thus, PLA2 most importantly cleaves arachidonic acid from the phospholipids, which is the main driving force behind the overexpression of the enzyme. Arachidonic acid is subsequently converted to eicosanoids. Some of these compounds are important vasodilators and their production is a way to increase the blood

flow to the ischemic tissue and thus to compensate for the hypoxia. Therefore, the higher abundance of arachidonic acid in the at-risk area of the tissue is in agreement with the role of PLA2. This importance of the PLA2 enzyme in the process of myocardial infarction was already suggested in several publications[196, 198, 199]. Also, the previously published MALDI results supported this claim by the detection of higher abundance of lysophospholipids in the affected area of the heart tissue which implies higher activity of PLA2. Other important ions with high loadings present in the positive part of the second PC are the ions at *m/z* 71 and *m/z* 169. Both of these ions were identified in an earlier work as DAG and TAG related fragments and their higher abundance corroborates the distribution of intact DAGs and TAGs observed in positive-ion mode.

The negative part of the third PC (Figure 5.5b, bottom) shows the necrotic area of the tissue. Some of the ions with high loadings in this principal component are the two chlorine isotopes at *m/z* 35 and 37 and the ions at *m/z* 232 and *m/z* 268. On the other hand in the viable tissue, which is represented in the positive part of the third PC (Figure 5.5b, top), ions at *m/z* 79 and *m/z* 97 display high loadings. These two ions are both phosphate related peaks; the ion at *m/z* 79 is the PO_3^- ion while the ion at *m/z* 97 is commonly identified as $H_2PO_4^-$. The abundance of phospholipids was indicated to be higher in the viable tissue by both MALDI and SIMS imaging in previous studies. These observations are in agreement with the observed phosphate distribution in the negative-ion mode SIMS images.

5.4 Conclusion

This work presents the first large area high resolution MetA-SIMS imaging study of a myocardial infarction model. The combination of SIMS imaging and multivariate data analysis promises new insight into the molecular changes induced by complex diseases such as myocardial infarction. It was possible to differentiate the necrotic, at-risk and viable region of the tissue. The distribution of several small ions and lipid species characteristic to each of these regions was visualized by mass spectrometry imaging. In positive-ion mode SIMS imaging, a higher ion intensity of TAGs and DAGs in the ischemic tissue was detected. The accumulation of DAGs implicates the overexpression of phospholipase D enzymes. Also,

DAGs are important signaling molecules in the pathway that leads to ventricular remodeling after heart attack. Thus, the process that produces DAGs and DAGs themselves are the potential therapeutic targets to prevent further tissue damage through ventricular remodeling.

The negative-ion mode SIMS imaging provided complementary information to the positive-ion mode measurement. In negative-ion mode the increased abundance of fatty acids was detected in the at-risk area of the tissue that implies the increased activity of phospholipase A2. This enzyme is involved in the inflammatory process in the heart tissue. Also, the lower ion intensities of phosphates in the infarcted region of the tissue were found. These negative-ion mode results support earlier findings by MALDI MS imaging which showed lower abundance of phospholipids in the infarcted area of the tissue.

Chapter 6

Top-Down Mass Spectrometry Imaging of Intact Proteins by LAESI FT-ICR MS

Laser Ablation Electrospray Ionization is a recent development in mass spectrometry imaging. It has been shown that lipids and small metabolites can be imaged in various samples such as plant material, tissue sections or bacterial colonies without any sample pre-treatment. Further, laser ablation electrospray ionization has been shown to produce multiply charged protein ions from liquids or solid surfaces. This presents a means to address one of the biggest challenges in mass spectrometry imaging; the identification of proteins directly from biological tissue surfaces. Such identification is hindered by the lack of multiply charged proteins in common MALDI ion sources and the difficulty of performing tandem MS on such large, singly charged ions. We present here top-down identification of intact proteins from tissue with a LAESI ion source combined with a hybrid ion-trap FT-ICR mass spectrometer. The performance of the system was first tested with a standard protein with ECD and IRMPD fragmentation to prove the viability of LAESI FT-ICR for top-down proteomics. Finally, the imaging of a tissue section was performed, where a number of intact proteins were measured and the hemoglobin α chain was identified directly from tissue using collision-induced dissociation and infrared multiphoton dissociation fragmentation.

6.1 Introduction

The importance of mass spectrometry (MS) based proteomics in the field of biological research has grown constantly over the past two decades and has become a powerful tool for biological analysis. The two main

approaches in the field of proteomics are bottom-up and top-down proteomics. Bottom-up proteomics uses different proteolytic enzymes, such as trypsin, to digest the intact proteins into smaller peptide fragments. These peptides are then typically separated and identified by the combination of liquid chromatography and mass spectrometry. Despite its widespread successful application, the method has several drawbacks. First, it is challenging to retain labile post translational modifications (PTM) and to identify different proteoforms[200]. Secondly, in bottom-up proteomics, the sequence coverage of a protein is limited due to the poor fragmentation of some of the peptides and the discrimination of the proteases for certain amino acid residues.

Top-down proteomics[201], however, analyzes intact proteins without any prior protease treatment. Thus, labile PTMs are retained during mass spectrometric analysis. However, multiply charged ions are necessary for most mass spectrometers to enable detection and effective fragmentation of intact proteins. In the overwhelming majority of experiments, this is typically achieved by electrospray ionization (ESI)[20, 202, 203]. A mass spectrometer with high mass resolving power is necessary to resolve the isotopic envelopes of the high charge states of the precursor and fragment ions produced in a top-down proteomics experiment. This is required for the proper deconvolution of the complex spectra produced in top-down proteomics. This means that typically Fourier Transform mass spectrometers, such as Fourier Transform Ion Cyclotron Resonance (FT-ICR)[204] and orbital trapping[205, 206] (i.e. the Thermo Fisher Orbitrap) mass spectrometers, are used for top-down proteomics research. These types of instruments combine exceptional mass resolving power with several fragmentation methods, such as collision-induced dissociation (CID), electron capture dissociation (ECD), electron transfer dissociation (ETD) and infrared multiphoton dissociation (IRMPD).

Mass spectrometry imaging (MSI)[41, 42] is a method to simultaneously map the distribution of multiple molecules on complex surfaces. The main advantage of the technique over other imaging techniques is its label free nature. One of the main challenges in the application of MSI for proteomics is the identification of detected protein or peptide ions[207]. The traditional ion sources for mass spectrometry imaging are matrix-assisted laser desorption/ionization (MALDI) and secondary ion mass spectrometry (SIMS). However, these ion sources are not suitable for

top-down proteomics measurements because they predominantly produce singly charged ions. Thus, proteins are traditionally identified by the bottom-up approach in mass spectrometry imaging experiments. A recent work by Schey *et al.* combines top-down protein identification and mass spectrometry imaging [208]. In this work, after the imaging of the tissue section by MALDI time-of-flight MS, proteins were isolated by microextraction from certain areas of the tissue, which was followed by a traditional top-down MS proteomics workflow. The proteins identified in the top-down MS experiments were subsequently matched to those measured in the MALDI MS imaging experiment, but no identification from the tissue surface was performed.

Recently, ambient pressure ion sources have begun to gain more popularity in the mass spectrometry imaging community. These sources have several advantages over vacuum sources (like MALDI). They allow the analysis of samples that are not vacuum compatible and they simplify sample and source exchange. An additional reason for the elevated interest in ambient ionization sources is their ability to produce multiply charged ions. Most of these ion sources employ electrospray as the main ionization mechanism such as MALDESI[209, 210], DESI[211], nano-DESI[212] and LAESI[213] or have similar ionization mechanisms to ESI, such as Laserspray[214]. The latter has demonstrated to be capable of imaging multiply charged proteins from tissue samples offering promise for top-down proteomic imaging experiments. One example of these is the work done by Inutan *et al*[215], where multiply charged proteins were detected both from standard and tissue with Laserspray ionization and ETD was used for fragmentation. However, they were unable to identify the intact proteins detected from the tissue. While no successful top-down imaging of multiply charged proteins from tissue sections has been published, both nano-DESI and MALDI with special matrices show promise for top-down MS imaging.

Laser Ablation Electrospray Ionization is an ambient pressure ionization method developed in 2007 by the Vertes group[213]. This ionization method employs a mid-infrared laser with the wavelength of 2.94 μm to ablate material from a sample surface. After the initial ablation event, the ablated material interacts with the plume of an electrospray source. This results in the incorporation of the analytes in the charged droplets and the subsequent ionization of the material from the sample surface. Due to the ionization mechanism, multiply charged ions can be produced. The main

advantage of LAESI is its matrix free nature. The wavelength of the infrared laser is in the region of the stretching vibrations of the OH groups. Thus, LAESI uses the sample's natural water content as a matrix. LAESI has been used to image or profile several different substrates such as different plant material[216-218], tissue sections[219-221], cell cultures[222], bacterial colonies[223] and textile fabrics[224]. Most of these experiments were done on time-of-flight mass spectrometers. However, the Muddiman group built a LAESI FT-ICR system and demonstrated the systems capability to detect multiply charged proteins such as cytochrome C and myoglobin from both solid and liquid standard samples[225]. In the same work they presented the first example of CID fragmentation of intact protein ions produced with a LAESI ion source from standard samples. The same group later published a modified version of the source for tissue imaging where lipids could be imaged from various tissue sections[226].

Here we present the results of interfacing a commercial LAESI source with an FT-ICR mass spectrometer. For the first time, LAESI is used for imaging of multiply charged proteins directly from biological tissue sections. Subsequent top-down analysis by CID and IRMPD is used for protein identification in the imaging mode. Further, the top-down analysis of proteins from standard liquid surfaces by ECD and IRMPD is presented.

6.2 Materials and methods

6.2.1 Samples

An 80 µM solution of Cytochrome C standard prepared in water was used for IRMPD and ECD top-down analysis with the LAESI source. For every measurement, 10 µl of the solution was spotted on a 96 well plate and was measured directly from the surface of the liquid droplets. For tissue imaging experiments, mouse lung (female 9 CFW-1 mouse, Harlan Laboratories, Boxmeer, The Netherlands) was sectioned to 50 µm thick sections in a Microm HM525 cryomicromtome (Thermo Fisher Scientific, Walldorf, Germany) and was deposited on standard microscope slides (Thermo Fisher Scientific, Braunschweig, Germany). The tissue sections were stored at -20 °C until further use and were measured frozen and without any additional sample preparation. A 1:1 mixture of MeOH and H_2O with 0.1 % acetic acid was used as the electrospray solvent in all measurements.

6.2.2 Mass spectrometry

Measurements were done on an LTQ-FT hybrid mass spectrometer (Thermo Fisher Scientific, Bremen, Germany) equipped with the IRMPD and ECD option. The LAESI DP-1000 (Protea Biosciences, Inc, Morgantown, WV) ion source was used for all LAESI measurements. A flow rate of 1.5 µl/min and ESI voltage of 4200 V was used for all experiments. The sample was positioned 11 mm below the inlet capillary of the mass spectrometer and 50 mm from the lens of the infrared laser (z-direction). The distance between the ESI needle and the inlet capillary was set to 10 mm.

For the imaging experiments the stage step size was set to 300 µm. At every pixel the ions from 5 laser shots were collected at a laser repetition rate of 10 Hz. The mass spectrometer has been run with the automatic gain control (AGC) turned off. The injection time was set to 900 ms and 1 microscan was collected at every position. The mass resolution was set to 200 000 at *m/z* 400. The tissue imaging experiments have been done in SIM mode, with the mass range set between *m/*z 500 and 1100. This is the mass range where most of the proteins and protein fragments are expected. Additionally, with these settings most of the chemical background ions produced by the ESI source are not injected into the FT-ICR cell which has a beneficial effect on both the spectral quality and the sensitivity of the instrument since the ion-trap and FT-ICR cell are not overfilled with low mass ions. The programmable trigger from the LTQ-FT was used at the start of the analytical scan to synchronize the mass spectrometer, laser firing and X-Y stage movement. For the MS/MS imaging experiments an isolation window of 10 Da was used and the precursor ion was isolated in the ion trap. The CID fragmentation was performed in the ion trap as well with the normalized collision energy (NCE) set to 20. The fragments were detected in the FT-ICR. The IRMPD spectra were measured with the energy set to 20 and the duration to 100 ms. The ECD experiments were done with the energy at 5, the delay set to 30 ms and the duration of 20 ms.

The mass spectrometry data was collected with the Xcalibur software in the Thermo Raw file format. Individual scans were also stored in the MIDAS file format. The spectra were deconvoluted and peaklists were created with the THRASH algorithm[227] built in the MIDAS 3.21

(National High Magnetic Field Laboratory, Tallahassee, FL) data analysis software[228]. ProSight PTM 2.0[229] was used for database search and protein identification. The imaging datasets were converted from the MIDAS raw files to AMOLF developed Datacube format with the Chameleon software package[230] and were analyzed with the Datacube explorer software (FOM Institute AMOLF, Amsterdam, The Netherlands) and in-house developed Matlab code (The MathWorks Inc., Natick, MA).

6.2.3 Synchronization of the mass spectrometer and the LAESI source

In the original LAESI design the source sends a trigger signal to the mass spectrometer at the beginning of the experiment to start the data acquisition simultaneously with the start of the imaging experiment. However, the individual scans are not synchronized with the laser shots of the ion source. The two devices run asynchronously after the start of the measurement. This approach works well with mass analyzers such as ion traps because they scan fast enough to collect ions from each ionization event. However, the scan cycle of an FT-ICR is much longer. Thus, without the synchronization of every scan with the ionization events of the ion source, part of the pixels would not be measured in an imaging experiment. Consequently, the synchronization of the ion source and the mass spectrometer is necessary for a successful LAESI FT-ICR imaging experiment.

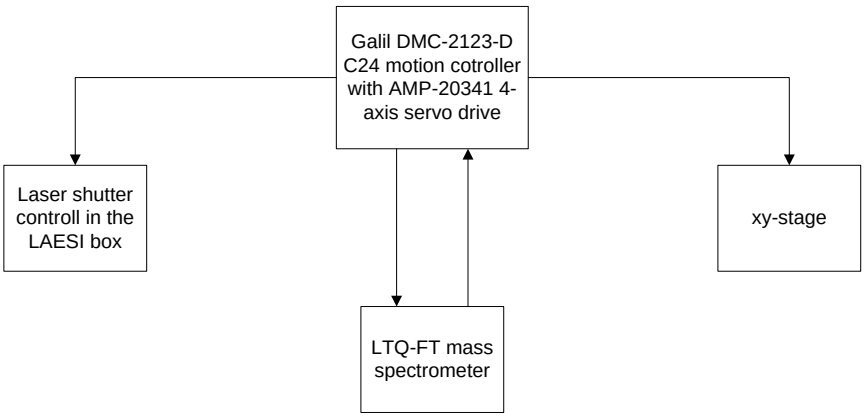

Figure 6.1 Scheme of the connections between the different components of the LAESI FT-ICR system.

Figure 6.1 shows a schematic of the synchronized LAESI FT-ICR system. For the synchronization of the ion source and the mass spectrometer a Galil DMC-2123-DC24 motion controller was used. This device has 8 digital inputs and 8 digital outputs. Thus, it is able to control multiple devices at the same time. One of the digital outputs was connected to the laser shutter control in the LAESI source, a second digital out was connected to the start-in connector on the LTQ mass spectrometer while the programmable trigger from the LTQ was connected to one of the digital inputs via a pulse generator. This pulse generator was used to lengthen the programmable trigger pulse width to ~ 50 ms because the original trigger from the programmable trigger was too short to be recognized by the motion controller.

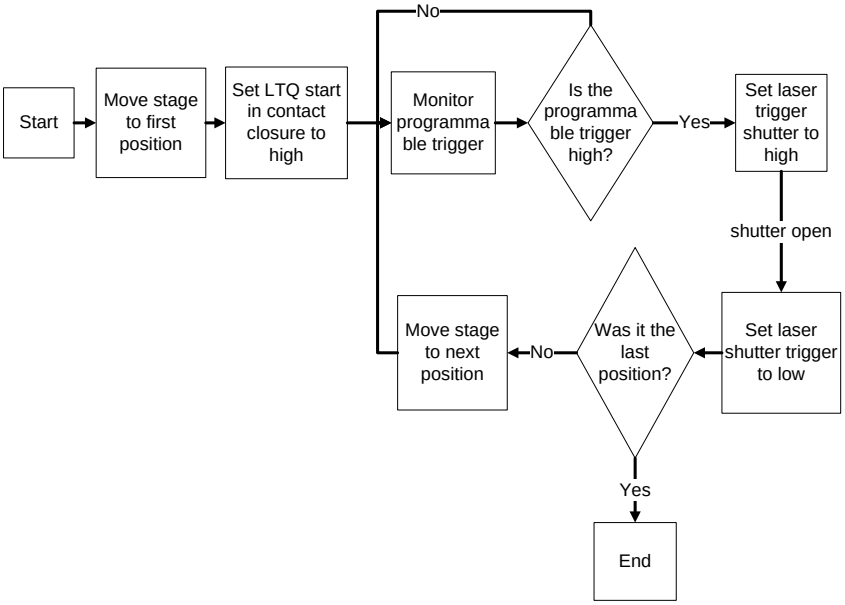

Figure 6.2 Flow chart of the LAESI FT-ICR MS imaging measurement sequence

The whole system has been controlled by the in-house built AWG software[114, 231, 232]. The sequence used for the imaging experiments can be seen in Figure 6.2. First, the stage moves to the starting position and then the motion controller sets the mass spectrometer's "Start In" contact closure to high, thus starting the measurement. After this, the workflow waits until the programmable trigger of the LTQ is set to high, which is set to the start of the analytical scan. Then the motion controller sends a trigger signal to the laser shutter to open for a set amount of time for the desorption and

ionization event. When the set time is up the laser shutter trigger is set to low and the stage moves to the next position. The measurement cycle starts again when the next scan starts.

6.3 Results and discussion

6.3.1 ESI and LAESI of a protein standard

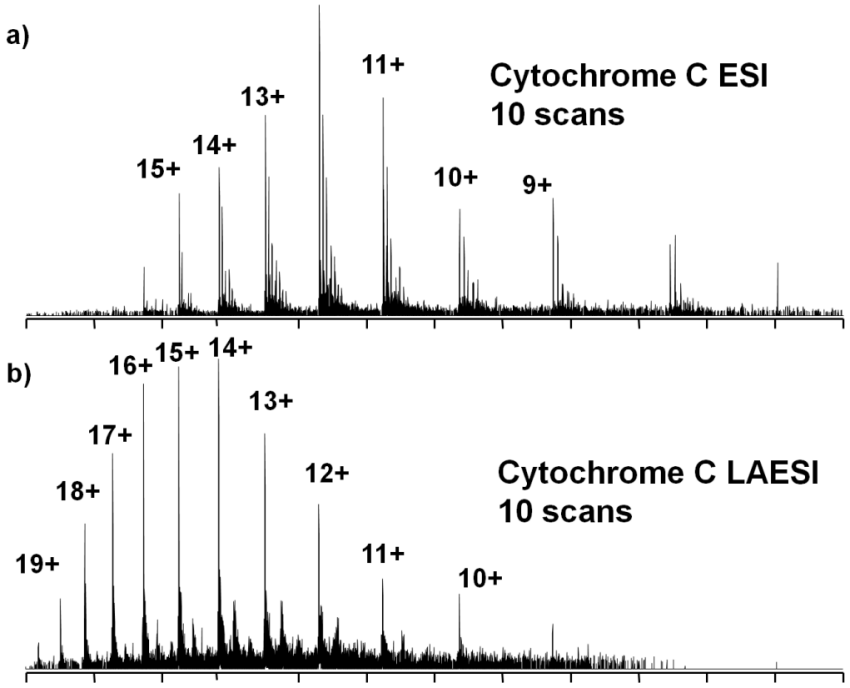

Figure 6.3. Comparison of the mass spectrum of Cytochrome C standard solution acquired with ESI (a) and LAESI (b). The electrospray spectra were measured with the IonMax source at a flow rate of 5 µl/min and an electrospray voltage of 4.2 kV.

Cytochrome C standard solution was measured in both direct infusion electrospray mode and directly from the surface of a single liquid droplet with the LAESI ion source to compare the two ionization methods. Figure 6.3 shows the comparison of the electrospray and the LAESI spectra. Both measurements provided several different charge states of the protein between 10+ and 19+ charges. These results demonstrate that LAESI is able to provide similar protein spectra as electrospray ionization. However, the

LAESI spectrum is shifted to slightly higher charge states. This can be explained by subtle differences in the electrospray conditions between the two sources, or by IR laser induced denaturation.

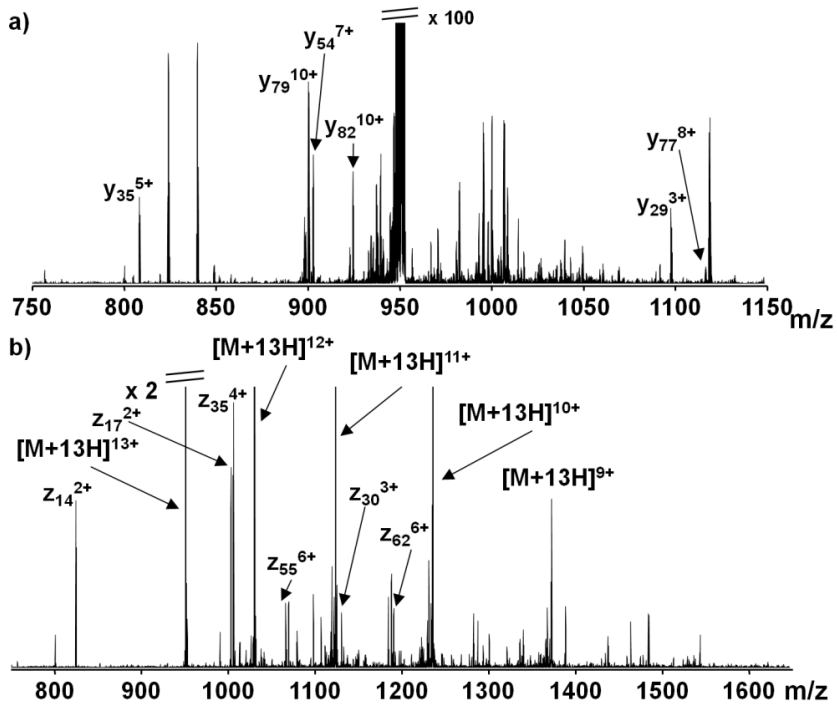

Figure 6.4 Mass spectra from the IRMPD (a) and ECD (b) fragmentation of Cytochrome C measured with a LAESI FT-ICR MS directly from liquid droplets.

The precursor ion of cytochrome C at *m/z* 951 was fragmented by IRMPD and ECD to prove the suitability of the combination of LAESI and these fragmentation methods for top-down proteomics. As IRMPD and ECD have different fragmentation mechanism they provide complementary information on the protein sequence. IRMPD fragmentation produces b and y protein fragments while ECD fragmentation results in c and z fragments. Also, in ECD fragmentation an extensive charge loss of the precursor ion can be observed. Both the IRMPD and the ECD spectra are shown on Figure 6.4. The database search after deconvolution of the fragment spectra resulted in the identification of cytochrome C in both cases. As it is shown on Figure 6.4, several of the y fragment ions in various charge states were annotated in the IRMPD spectrum and z fragments in the ECD spectrum. The results shown in Figure 6.4 confirm that the combination of LAESI

with FT-ICR can be used for successful top-down analysis of intact proteins.

6.3.2 MS imaging of intact proteins

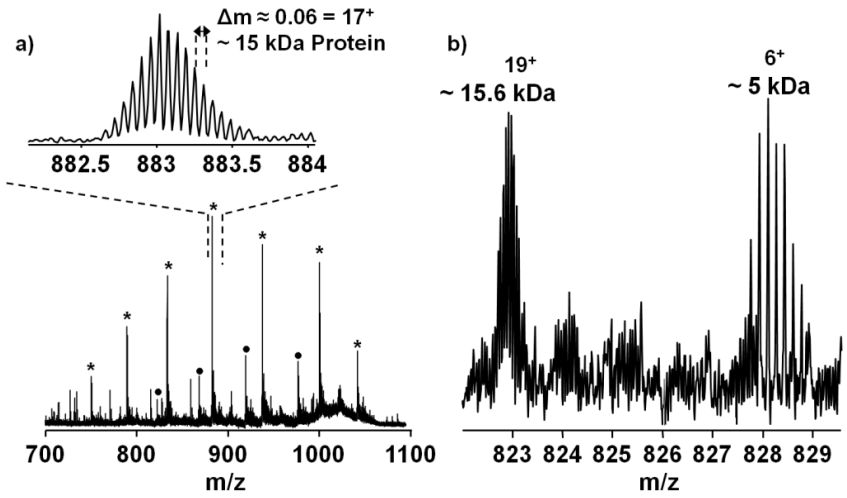

Figure 6.5 Summed full mass spectrum from LAESI FT-ICR MS imaging of a mouse lung section with the charge state series of a 15 kDa protein (*) and 15.6 kDa protein (•) marked (a) and two multiply charged protein ions between *m/z* 820 and 830 (b). The inset at the top-left shows the resolved isotope structure of the protein ion at *m/z* 883

Figure 6.5 shows the summed mass spectrum from an MS imaging experiment on a mouse lung tissue section. The spectrum contains one main charge state series. The mass difference between the isotope peaks of the ion at *m/z* 883 from this charge state series is ~0.06 Da, which means that this ion has 17 charges. Thus the main charge state series is related to a 15 kDa protein. Besides this protein there is also a second charge state series visible which is related to a different protein which has a mass of ~15.6 kDa. Figure 6.5b shows the 19^+ charge state from the lower intensity charge state series and an additional protein detected with 6 charges, which has a mass of ~5 kDa. Figure 6.5 demonstrates the viability of LAESI for the analysis of several, unknown intact proteins directly from biological tissue sections. The high mass resolving power of the FT-ICR MS is required to resolve the isotopic distributions and enable proper mass deconvolution.

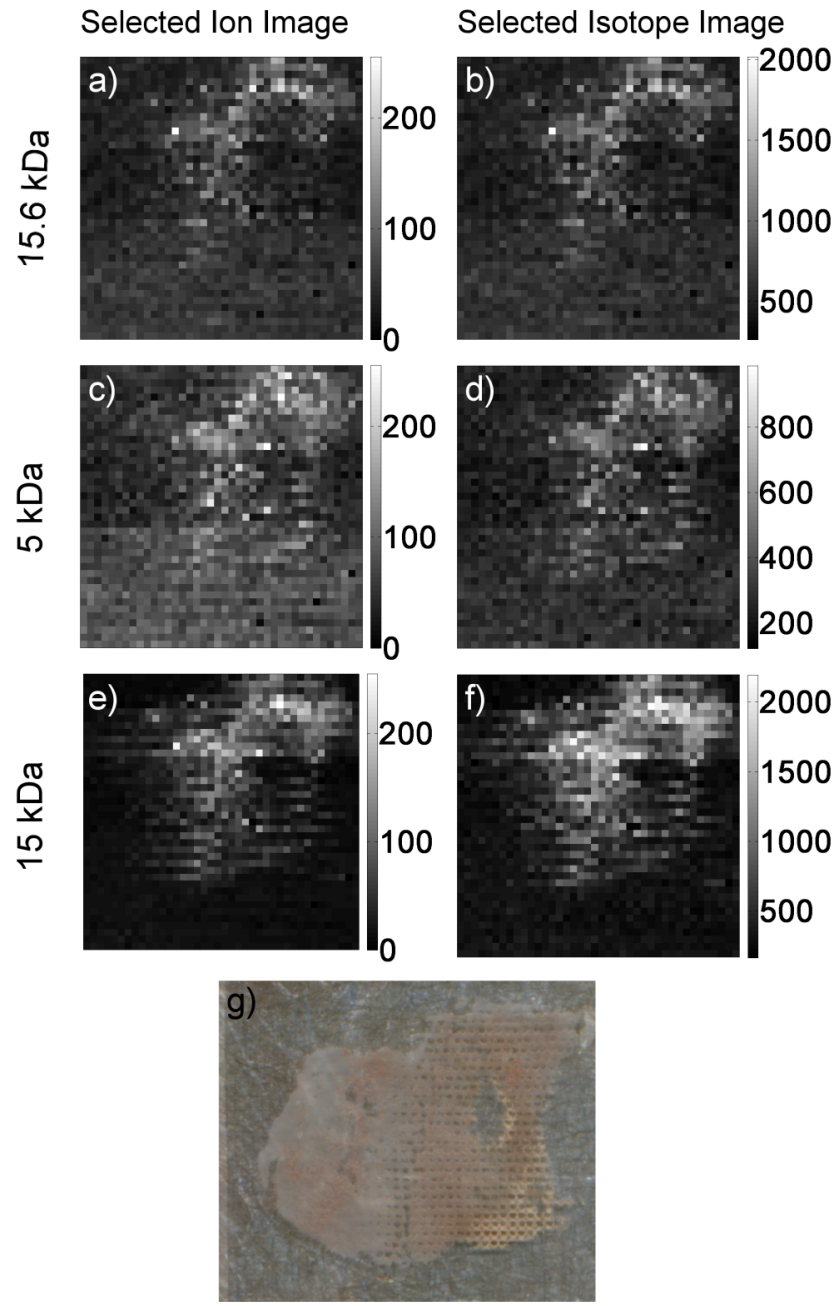

Figure 6.6 Optical (g), selected ion images (a, c, e) and selected isotope images (b, d, f) from a LAESI FT-ICR MS imaging experiment of a mouse lung section. The MS images show the distribution of the ions at *m/z* 822 (15.6 kDa: a, b), 827 (5 kDa: c, d) and 883 (15.6 kDa: e, f)

Figure 6.6 shows selected ion images for the ions at *m/z* 823 (15.6 kDa), 827 (5 kDa) and 883 (15 kDa). The images show the distribution of these compounds on the tissue sample, where the hole in the middle of the lung tissue is visible. The compounds are mostly localized in the brown colored areas of the lung section, which means they are likely blood related proteins. Two different approaches were used to plot the distribution of these three ion species. First, the entire isotope distribution was selected for the image. The second approach yields the so called "selected isotope images". This means that the isotope peaks are selected individually and these isotope images are summed together to create the selected isotope image. This second approach is made possible by the high mass resolving power of the FT-ICR mass spectrometer, because it is able to resolve the individual isotope peaks of the highly charged protein ions. As it can be seen on Figure 6.6, the selected isotope images provide a better contrast. The selected isotope images additionally minimize the contribution of underlying interferences. Because of the aforementioned advantages the selected isotope images were selected for all the images presented further in this chapter.

6.3.3 CID imaging of an intact protein

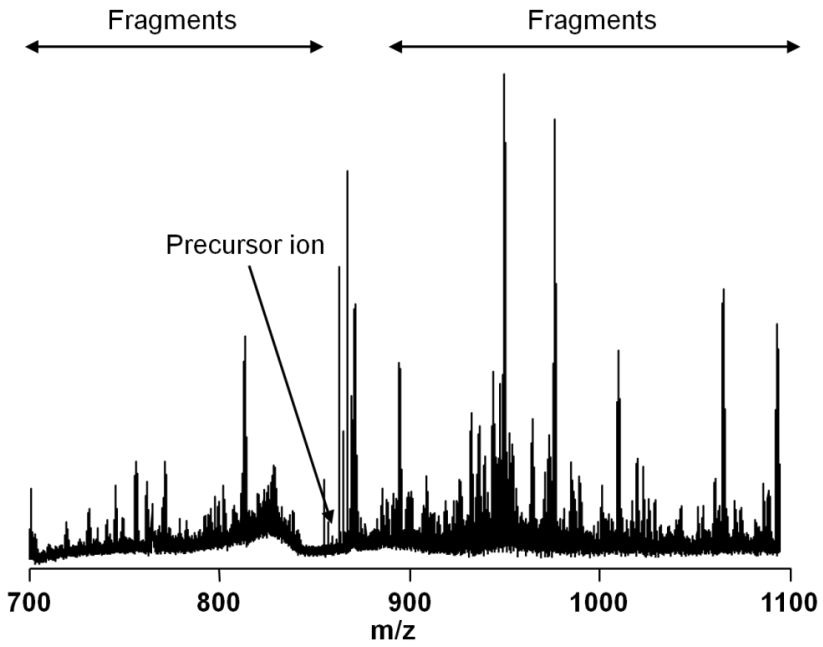

Figure 6.7 Full summed mass spectrum from the CID MS imaging experiment of mouse lung.

The biggest challenge in mass spectrometry imaging of proteins is their identification directly from tissue sections. Thus, the ion at *m/z* 883 has been selected for a CID MS imaging experiment for protein identification. Figure 6.8 shows the summed mass spectrum between *m/z* 880 and 950 from this CID MS/MS imaging experiment (the broadband mass spectrum is provided on Figure 6.7). These MS/MS imaging experiments have two main advantages over profiling MS/MS experiments. First, all fragment ions have an image and secondly the larger number of MS/MS scans result in better statistics and thus better mass spectra. Therefore, the signal-to-noise of the fragment ions is better in the imaging experiments. The spectrum proved to be very information rich. After deconvolution and a subsequent database search in Prosight PTM 2.0, the protein was identified as hemoglobin α with a p value of $1.52*10^{-10}$ and with 19 fragments identified in absolute mass search mode. If the peaklist is searched against the acetylated hemoglobin α sequence from the Uniprot database in single protein mode, then the p value improves to $4{,}22*10^{-30}$ and 52 fragment ions are identified. The acetylation site was identified as

the serine at the 68 position. The number of annotated fragment ions was further improved by the comparison of the identified fragments from the CID fragmentation and the list of the identified fragments from an IRMPD imaging experiment discussed in details in the next paragraph. In this way, the fragment ions where the difference between the theoretical and the experimental mass values was ± 1 Da, due to the deconvolution of the multiply charged ion peak, can be manually annotated.

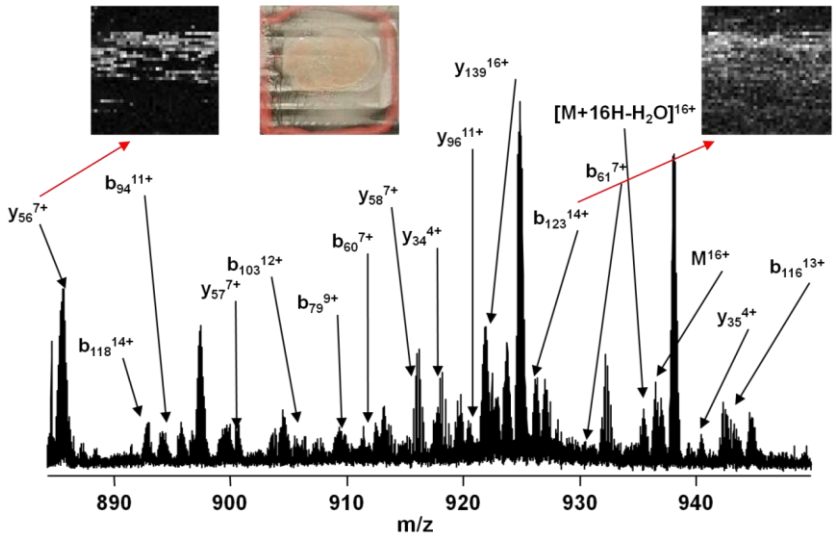

Figure 6.8 Zoomed summed mass spectrum from the CID MS imaging experiment of a mouse lung tissue section. Insets show selected isotope images of two fragments and the optical image of the lung section

The identity of the protein is in good agreement with the results from the MS imaging experiment which showed that the protein has a higher intensity in the brown colored areas of the sample. This color is mostly related to blood in tissue sections. Also, this identification is in accordance with the biological role of the tissue, where oxygen is transported into the blood stream. In the mass spectrum shown in Figure 6.8, several y and b fragment ions are annotated. These ions have a wide range of charge states between 4^+ and 16^+. As it can be seen on Figure 6.9, these different fragments can overlap, where the mass difference between the isotopes of the two different fragments is 20 mDa. Thus, a mass spectrometer with high mass resolving power (resolving power of ~47 000 at mass 936) is needed to resolve these overlapping charge states and to properly deconvolute the spectrum. Also, these overlapping peaks show the

advantage of using the selected isotope images which makes it possible to image the individual charge states with the added benefit of the full image contrast from the summed individual isotope peak intensities. Since this was an MS/MS imaging experiment, the images of the fragment ions can be plotted. The examples on Figure 6.8 show the selected isotope images of the ions at *m/z* 885.7678 (y_{56}^{7+} fragment) and at *m/z* 926.5439 (b_{123}^{14+} fragment). Although these fragments show the same distribution on the tissue, the possibility to map the distribution of protein fragments from a top-down proteomics experiment on a tissue section offers the prospect to image the distribution of different proteoforms. This can give new insight in the mechanism of biological processes where protein modifications are involved.

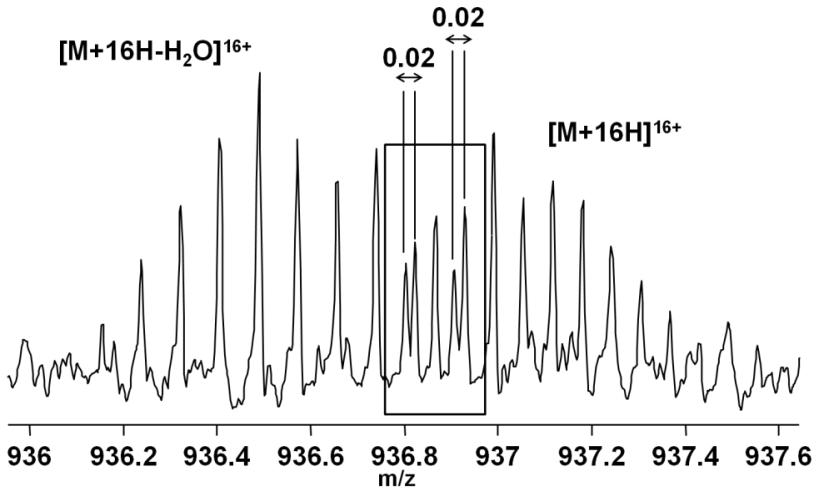

Figure 6.9 Zoom mass spectrum from the CID MS imaging experiment of mouse lung showing two overlapping fragment ions.

6.3.4 IRMPD imaging of an intact protein

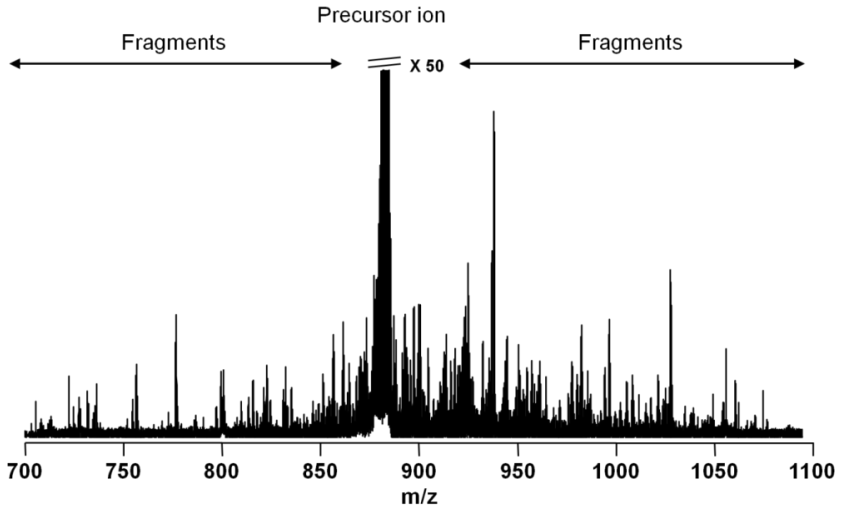

Figure 6.10 Full summed spectrum from the IRMPD MS imaging experiment of mouse lung.

Figure 6.11 presents the results of an IRMPD MS/MS imaging experiment of the same precursor ion at *m/z* 883 (the broadband spectrum is shown on Figure 6.10). After deconvolution of the summed spectrum, the database search resulted in the identification of the protein as hemoglobin α, with a p value of $1.25*10^{-5}$ in absolute mass search mode with 12 annotated fragments and $2*10^{-11}$ in single protein search with 19 identified fragments of the acetylated hemoglobin α. This result is in agreement with the result of the CID fragmentation. Thus, it improves the confidence of the protein identification. IRMPD has a similar fragmentation mechanism as CID. Thus, similar b and y ions were expected, as shown in Table A1 and A2 in the Appendix, which list the annotated fragments from the CID and IRMPD experiments, respectively. There is a substantial overlap between the fragment ions produced by the two fragmentation methods. Nevertheless, seven fragments are exclusively present in the IRMPD spectrum; see the Venn diagram in Figure 6.11. Thus, the two fragmentation methods provide complementary datasets. However, the fragmentation efficiency of IRMPD is lower than of CID as it is proven by the lower number of fragments produced by IRMPD fragmentation.

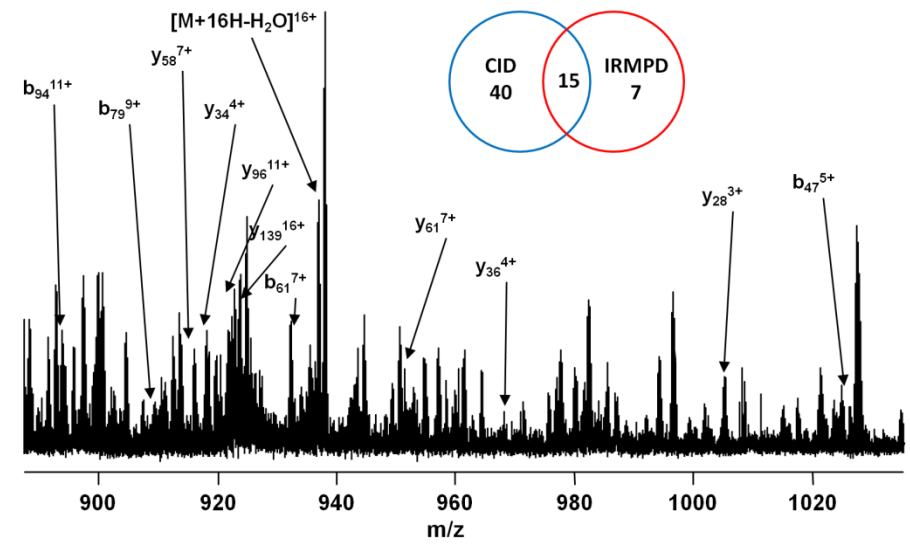

Figure 6.11 Zoomed summed mass spectrum from an IRMPD MS imaging experiment of a mouse lung section. The Venn-diagram shows the number of unique fragments annotated from the CID and the IRMPD experiment

6.4 Conclusion

This work presents the first example of top-down mass spectrometry imaging with a LAESI ion source. The protein identified in this work is hemoglobin which is among the most abundant proteins in a tissue sample. For the analysis of lower abundance proteins further instrumental developments are needed. The most important of these is to increase the sensitivity of the LAESI FT-ICR system. This can include the improvement of the ion source and capacitive coupling of the FT-ICR cell which is estimated to result in two-fold sensitivity increase. Further possible improvements also include different commonly used tissue washing methods to remove lipids to enhance protein and peptide signal. Also, the investigation of potential IR matrices, such as glycerol or succinic acid, might result in further increases in the sensitivity of the LAESI FT-ICR system. These improvements are also required to be able to decrease the laser spot size and thus to increase the spatial resolution of the system. In addition, ECD/ETD fragmentation of intact proteins would be a good compliment to CID and IRMPD fragmentation. It has a different fragmentation mechanism compared to CID or IRMPD and it produces c and z protein fragments and is more gentle to allow labile PTMs to be retained. Thus it would provide complementary information to the other fragmentation methods.

This chapter presents that imaging and identification of intact proteins and their modifications is achievable directly from tissue with the combination of high mass resolution mass spectrometers and an ambient imaging ion source. Multiply charged proteins were fragmented with IRMPD and ECD and identified directly from liquid standards. In addition, multiply charged proteins directly from frozen tissue sections were imaged by LAESI FT-ICR MS and identified without any additional sample preparation. In addition, a post-translational modification (acetylation) was identified for the first time directly from tissue and the position of the post-translational modification in the protein sequence was determined. This MS-based top-down proteomics imaging approach opens up new possibilities in biological research. The study of the distribution of protein proteoforms and labile post translational modifications directly from tissue provide new insight in the role of the different proteoforms in biological processes and diseases.

References

[1] www.nobelprize.org. *Nobel prizes in physics and in chemistry*.

[2] www.nobelprize.org. *Nobel lecture of John B. Fenn*.

[3] H. Liebl. Ion Microprobe Mass Analyzer. *Journal of Applied Physics* **1967**, *38*, 5277.

[4] R. M. Caprioli, T. B. Farmer, J. Gile. Molecular imaging of biological samples: Localization of peptides and proteins using MALDI-TOF MS. *Analytical Chemistry* **1997**, *69*, 4751.

[5] E. Rutherford. Velocity and Rate of Recombination of the Ions of Gases Exposed to Röntgen Radiation. *Phil. Mag.* **1897**, *44*, 422.

[6] E. W. McDaniel, D. W. Martin, W. S. Barnes. Drift-tube mass spectrometer for studies of low-energy ion-molecule reactions. *Review of Scientific Instruments* **1962**, *33*.

[7] K. B. J. McAfee, D. P. Sipler, D. Edelson. Mobilities and reactions of ions in argon. *Physical Review* **1967**, *160*.

[8] L. G. McKnight, K. B. McAfee, D. P. Sipler. Low-field drift velocities and reactions of nitrogen ions in nitrogen. *Physical Review* **1967**, *164*.

[9] F. W. Karasek, M. J. Cohen, D. I. Carroll. Trace studies of alcohols in the plasma chromatography-mass spectrometer. *Journal of Chromatographic Science* **1971**, *9*.

[10] C. Wu, W. F. Siems, G. R. Asbury, H. H. Hill. Electrospray ionization high-resolution ion mobility spectrometry - Mass spectrometry. *Analytical Chemistry* **1998**, *70*, 4929.

[11] C. S. Creaser, M. Benyezzar, J. R. Griffiths, J. W. Stygall. A tandem ion trap/ion mobility spectrometer. *Analytical Chemistry* **2000**, *72*, 2724.

[12] C. S. Hoaglund, S. J. Valentine, D. E. Clemmer. An ion trap interface for ESI-ion mobility experiments. *Analytical Chemistry* **1997**, *69*, 4156.

[13] B. H. Clowers, H. H. Hill. Influence of cation adduction on the separation characteristics of flavonoid diglycoside isomers using dual gate-ion mobility-quadrupole ion trap mass spectrometry. *Journal of Mass Spectrometry* **2006**, *41*, 339.

[14] B. K. Bluhm, K. J. Gillig, D. H. Russell. Development of a Fourier-transform ion cyclotron resonance mass spectrometer-ion mobility spectrometer. *Review of Scientific Instruments* **2000**, *71*, 4078.

[15] D. C. Parent, M. T. Bowers. Temperature dependence of ion mobilities: experiment and theory. *Chemical Physics* **1981**, *60*.

[16] X. T. Tang, J. E. Bruce, H. H. Hill. Design and performance of an atmospheric pressure ion mobility Fourier transform ion cyclotron resonance mass spectrometer. *Rapid Communications in Mass Spectrometry* **2007**, *21*, 1115.

[17] M. Karas, U. Bahr, F. Hillenkamp. Uv Laser Matrix Desorption Ionization Mass-Spectrometry of Proteins in the 100 000 Dalton Range. *International Journal of Mass Spectrometry and Ion Processes* **1989**, *92*, 231.

[18] M. Karas, U. Bahr, A. Ingendoh, F. Hillenkamp. Laser Desorption Ionization Mass-Spectrometry of Proteins of Mass 100 000 to 250 000 Dalton. *Angewandte Chemie-International Edition in English* **1989**, *28*, 760.

[19] M. Karas, F. Hillenkamp. Laser Desorption Ionization of Proteins with Molecular Masses Exceeding 10000 Daltons. *Analytical Chemistry* **1988**, *60*, 2299.

[20] J. B. Fenn, M. Mann, C. K. Meng, S. F. Wong, C. M. Whitehouse. Electrospray Ionization for Mass-Spectrometry of Large Biomolecules. *Science* **1989**, *246*, 64.

[21] S. F. Wong, C. K. Meng, J. B. Fenn. Multiple Charging in Electrospray Ionization of Poly(Ethylene Glycols). *Journal of Physical Chemistry* **1988**, *92*, 546.

[22] D. E. Clemmer, R. R. Hudgins, M. F. Jarrold. Naked Protein Conformations - Cytochrome-C in the Gas-Phase. *Journal of the American Chemical Society* **1995**, *117*, 10141.

[23] B. T. Ruotolo, K. Giles, I. Campuzano, A. M. Sandercock, R. H. Bateman, C. V. Robinson. Evidence for macromolecular protein rings in the absence of bulk water. *Science* **2005**, *310*, 1658.

[24] C. Uetrecht, R. J. Rose, E. van Duijn, K. Lorenzen, A. J. R. Heck. Ion mobility mass spectrometry of proteins and protein assemblies. *Chemical Society Reviews* **2010**, *39*, 1633.

[25] S. N. Jackson, M. Ugarov, T. Egan, J. D. Post, D. Langlais, J. A. Schultz, A. S. Woods. MALDI-ion mobility-TOFMS imaging of lipids in rat brain tissue. *Journal of Mass Spectrometry* **2007**, *42*, 1093.

[26] S. N. Jackson, M. Ugarov, J. D. Post, T. Egan, D. Langlais, J. A. Schultz, A. S. Woods. A Study of Phospholipids by Ion Mobility TOFMS. *Journal of the American Society for Mass Spectrometry* **2008**, *19*, 1655.

[27] S. N. Jackson, H. Y. J. Wang, A. S. Woods. Direct tissue analysis of phospholipids in rat brain using MALDI-TOFMS and MALDI-ion mobility-TOFMS. *Journal of the American Society for Mass Spectrometry* **2005**, *16*, 133.

[28] W. B. Ridenour, M. Kliman, J. A. McLean, R. M. Caprioli. Structural Characterization of Phospholipids and Peptides Directly from Tissue Sections by MALDI Traveling-Wave Ion Mobility-Mass Spectrometry. *Analytical Chemistry* **2010**, *82*, 1881.

[29] S. Trimpin, B. Tan, B. C. Bohrer, D. K. O'Dell, S. I. Merenbloom, M. X. Pazos, D. E. Clemmer, J. M. Walker. Profiling of phospholipids and related lipid structures using multidimensional ion mobility spectrometry-mass spectrometry. *International Journal of Mass Spectrometry* **2009**, *287*, 58.

[30] A. S. Woods, M. Ugarov, T. Egan, J. Koomen, K. J. Gillig, K. Fuhrer, M. Gonin, J. A. Schultz. Lipid/peptide/nucleotide separation with MALDI-ion mobility-TOF MS. *Analytical Chemistry* **2004**, *76*, 2187.

[31] P. Dwivedi, B. Bendiak, B. H. Clowers, H. H. Hill. Rapid resolution of carbohydrate isomers by electrospray ionization ambient pressure ion mobility spectrometry-time-of-flight mass spectrometry (ESI-APIMS-TOFMS). *Journal of the American Society for Mass Spectrometry* **2007**, *18*, 1163.

[32] L. S. Fenn, J. A. McLean. Enhanced carbohydrate structural selectivity in ion mobility-mass spectrometry analyses by boronic acid derivatization. *Chemical Communications* **2008**, 5505.

[33] M. D. Plasencia, D. Isailovic, S. I. Merenbloom, Y. Mechref, D. E. Clemmer. Resolving and Assigning N-Linked Glycan Structural Isomers from Ovalbumin by IMS-MS. *Journal of the American Society for Mass Spectrometry* **2008**, *19*, 1706.

[34] S. Y. Vakhrushev, J. Langridge, I. Campuzano, C. Hughes, J. Peter-Katlinic. Ion mobility mass spectrometry analysis of human glycourinome. *Analytical Chemistry* **2008**, *80*, 2506.

[35] B. Bothner, G. Siuzdak. Electrospray ionization of a whole virus: Analyzing mass, structure, and viability. *Chembiochem* **2004**, *5*, 258.

[36] J. J. Thomas, B. Bothner, J. Traina, W. H. Benner, G. Siuzdak. Electrospray ion mobility spectrometry of intact viruses. *Spectroscopy-an International Journal* **2004**, *18*, 31.

[37] C. Uetrecht, C. Versluis, N. R. Watts, P. T. Wingfield, A. C. Steven, A. J. R. Heck. Stability and shape of hepatitis B virus capsids in vacuo. *Angewandte Chemie-International Edition* **2008**, *47*, 6247.

[38] P. Dwivedi, C. Wu, L. M. Matz, B. H. Clowers, W. F. Siems, H. H. Hill. Gas-phase chiral separations by ion mobility spectrometry. *Analytical Chemistry* **2006**, *78*, 8200.

[39] J. R. Enders, J. A. McLean. Chiral and Structural Analysis of Biomolecules Using Mass Spectrometry and Ion Mobility-Mass Spectrometry. *Chirality* **2010**, *21*, E253.

[40] A. E. Holliday. ANYL 392-Chiral separations using ion mobility spectrometry. *Abstracts of Papers of the American Chemical Society* **2008**, *236*.

[41] K. Chughtai, R. M. A. Heeren. Mass Spectrometric Imaging for Biomedical Tissue Analysis. *Chemical Reviews* **2010**, *110*, 3237.

[42] L. A. McDonnell, R. M. A. Heeren. Imaging mass spectrometry. *Mass Spectrometry Reviews* **2007**, *26*, 606.

[43] A. F. M. Altelaar, J. van Minnen, C. R. Jimenez, R. M. A. Heeren, S. R. Piersma. Direct molecular Imaging of Lymnaea stagnalis nervous tissue at subcellular spatial resolution by mass spectrometry. *Analytical Chemistry* **2005**, *77*, 735.

[44] N. Winograd. The magic of cluster SIMS. *Analytical Chemistry* **2005**, *77*, 142a.

[45] Z. Postawa. Sputtering simulations of organic overlayers on metal substrates by monoatomic and clusters projectiles. *Applied Surface Science* **2004**, *231*, 22.

[46] A. Carado, J. Kozole, M. Passarelli, N. Winograd, A. Loboda, J. Bunch, J. Wingate, J. Hankin, R. Murphy. Biological tissue imaging with a hybrid cluster SIMS quadrupole time-of-flight mass spectrometer. *Applied Surface Science* **2008**, *255*, 1572.

[47] A. Carado, J. Kozole, M. Passarelli, N. Winograd, A. Loboda, J. Wingate. Cluster SIMS with a hybrid quadrupole time-of-light mass spectrometer. *Applied Surface Science* **2008**, *255*, 1610.

[48] A. Carado, M. K. Passarelli, J. Kozole, J. E. Wingate, N. Winograd, A. V. Loboda. C-60 Secondary Ion Mass Spectrometry with a Hybrid-Quadrupole Orthogonal Time-of-Flight Mass Spectrometer. *Analytical Chemistry* **2008**, *80*, 7921.

[49] C. F. Ijames, C. L. Wilkins. An External Secondary Ion-Source for Fourier-Transform Mass-Spectrometry. *Journal of the American Society for Mass Spectrometry* **1990**, *1*, 208.

[50] M. P. Irion, A. Selinger, R. Wendel. Secondary Ion Fourier-Transform Mass-Spectrometry - a New Approach Towards the Study of Metal Cluster Ion Chemistry. *International Journal of Mass Spectrometry and Ion Processes* **1990**, *96*, 27.

[51] S. M. Mccullough, E. Gard, C. B. Lebrilla. A 3t External Source Quadrupole Fourier-Transform Mass-Spectrometer for Ion Molecule Reactions and Analysis. *International Journal of Mass Spectrometry and Ion Processes* **1991**, *107*, 91.

[52] S. Maharrey, R. Bastasz, R. Behrens, A. Highley, S. Hoffer, G. Kruppa, J. Whaley. High mass resolution SIMS. *Applied Surface Science* **2004**, *231*, 972.

[53] D. F. Smith, E. W. Robinson, A. V. Tolmachev, R. M. A. Heeren, L. Pasa-Tolic. C-60 Secondary Ion Fourier Transform Ion Cyclotron Resonance Mass Spectrometry. *Analytical Chemistry* **2011**, *83*, 9552.

[54] D. F. Smith, A. Kiss, F. E. Leach, E. W. Robinson, L. Pasa-Tolic, R. M. A. Heeren. High mass accuracy and high mass resolving power FT-ICR secondary ion mass spectrometry for biological tissue imaging. *Analytical and Bioanalytical Chemistry* **2013**, *405*, 6069.

[55] A. F. M. Altelaar, I. Klinkert, K. Jalink, R. P. J. de Lange, R. A. H. Adan, R. M. A. Heeren, S. R. Piersma. Gold-enhanced biomolecular surface imaging of cells and tissue by SIMS and MALDI mass spectrometry. *Analytical Chemistry* **2006**, *78*, 734.

[56] A. Delcorte, P. Bertrand. Interest of silver and gold metallization for molecular SIMS and SIMS imaging. *Applied Surface Science* **2004**, *231–232*, 250.

[57] A. Heile, D. Lipinsky, N. Wehbe, A. Delcorte, P. Bertrand, A. Felten, L. Houssiau, J. J. Pireaux, R. De Mondt, L. Van Vaeck, H. F. Arlinghaus. Metal-assisted SIMS and cluster ion bombardment for ion yield enhancement. *Applied Surface Science* **2008**, *255*, 941.

[58] A. Delcorte. Matrix-enhanced secondary ion mass spectrometry: The Alchemist's solution? *Applied Surface Science* **2006**, *252*, 6582.

[59] K. J. Wu, R. W. Odom. Matrix-enhanced secondary ion mass spectrometry: A method for molecular analysis of solid surfaces. *Analytical Chemistry* **1996**, *68*, 873.

[60] H. T. Jonkman, J. Michl, R. N. King, J. D. Andrade. Low-temperature secondary positive ion mass spectrometry of neat and argon-diluted organic solids. *Analytical Chemistry* **1978**, *50*, 2078.

[61] L. K. Liu, K. L. Busch, R. G. Cooks. Matrix-assisted secondary ion mass spectra of biological compounds. *Analytical Chemistry* **1981**, *53*, 109.

[62] M. M. Ross, R. J. Colton. Carbon as a sample substrate in secondary ion mass spectrometry. *Analytical Chemistry* **1983**, *55*, 150.

[63] D. Touboul, F. Halgand, A. Brunelle, R. Kersting, E. Tallarek, B. Hagenhoff, O. Laprevote. Tissue molecular ion imaging by gold cluster ion bombardment. *Analytical Chemistry* **2004**, *76*, 1550.

[64] M. W. Huang, H. L. Chei, J. P. Huang, J. Shiea. Application of organic solvents as matrixes to detect air-sensitive and less polar compounds using low-temperature secondary ion mass spectrometry. *Analytical Chemistry* **1999**, *71*, 2901.

[65] A. Wucher, S. X. Sun, C. Szakal, N. Winograd. Molecular depth profiling of histamine in ice using a buckminsterfullerene probe. *Analytical Chemistry* **2004**, *76*, 7234.

[66] J. Cheng, N. Winograd. Depth profiling of peptide films with TOF-SIMS and a C-60 probe. *Analytical Chemistry* **2005**, *77*, 3651.

[67] R. G. Cooks, K. L. Busch. Matrix effects, internal energies and MS/MS spectra of molecular ions sputtered from surfaces. *International Journal of Mass Spectrometry and Ion Physics* **1983**, *53*, 111.

[68] A. Delcorte, B. J. Garrison. Particle-induced desorption of kilodalton molecules embedded in a matrix: A molecular dynamics study. *Journal of Physical Chemistry B* **2003**, *107*, 2297.

[69] T. W. Jaskolla, M. Karas. Compelling Evidence for Lucky Survivor and Gas Phase Protonation: The Unified MALDI Analyte Protonation Mechanism. *Journal of the American Society for Mass Spectrometry* **2011**, *22*, 976.

[70] T. W. Jaskolla, W. D. Lehmann, M. Karas. 4-Chloro-alpha-cyanocinnamic acid is an advanced, rationally designed MALDI matrix. *Proceedings of the National Academy of Sciences of the United States of America* **2008**, *105*, 12200.

[71] T. W. Jaskolla, D. G. Papasotiriou, M. Karas. Comparison between the Matrices alpha-Cyano-4-hydroxycinnamic Acid and 4-Chloro-alpha-cyanocinnamic Acid for Trypsin, Chymotrypsin, and Pepsin

Digestions by MALDI-TOF Mass Spectrometry. *Journal of Proteome Research* **2009**, *8*, 3588.

[72] K. Teuber, J. Schiller, B. Fuchs, M. Karas, T. W. Jaskolla. Significant sensitivity improvements by matrix optimization: a MALDI-TOF mass spectrometric study of lipids from hen egg yolk. *Chemistry and Physics of Lipids* **2010**, *163*, 552.

[73] J. Soltwisch, T. W. Jaskolla, F. Hillenkamp, M. Karas, K. Dreisewerd. Ion Yields in UV-MALDI Mass Spectrometry As a Function of Excitation Laser Wavelength and Optical and Physico-Chemical Properties of Classical and Halogen-Substituted MALDI Matrixes. *Analytical Chemistry* **2012**, *84*, 6567.

[74] M. Karas, D. Bachmann, F. Hillenkamp. Influence of the wavelength in high-irradiance ultraviolet laser desorption mass spectrometry of organic molecules. *Analytical Chemistry* **1985**, *57*, 2935.

[75] U. Bahr, M. Karas, F. Hillenkamp. ANALYSIS OF BIOPOLYMERS BY MATRIX-ASSISTED LASER-DESORPTION IONIZATION (MALDI) MASS-SPECTROMETRY. *Fresenius Journal of Analytical Chemistry* **1994**, *348*, 783.

[76] S. Guenther, A. Rompp, W. Kummer, B. Spengler. AP-MALDI imaging of neuropeptides in mouse pituitary gland with 5 mu m spatial resolution and high mass accuracy. *International Journal of Mass Spectrometry* **2011**, *305*, 228.

[77] L. S. Fenn, M. Kliman, A. Mahsut, S. R. Zhao, J. A. McLean. Characterizing ion mobility-mass spectrometry conformation space for the analysis of complex biological samples. *Analytical and Bioanalytical Chemistry* **2009**, *394*, 235.

[78] P. R. Kemper, N. F. Dupuis, M. T. Bowers. A new, higher resolution, ion mobility mass spectrometer. *International Journal of Mass Spectrometry* **2009**, *287*, 46.

[79] K. Tang, A. A. Shvartsburg, H. N. Lee, D. C. Prior, M. A. Buschbach, F. M. Li, A. V. Tolmachev, G. A. Anderson, R. D. Smith. High-sensitivity ion mobility spectrometry/mass spectrometry using electrodynamic ion funnel interfaces. *Analytical Chemistry* **2005**, *77*, 3330.

[80] F. J. Knorr, R. L. Eatherton, W. F. Siems, H. H. Hill, Jr. Fourier transform ion mobility spectrometry. *Analytical Chemistry* **1985**, *57*, 402.

[81] B. H. Clowers, W. F. Siems, H. H. Hill, S. M. Massick. Hadamard transform ion mobility spectrometry. *Analytical Chemistry* **2006**, *78*, 44.

[82] A. W. Szumlas, S. J. Ray, G. M. Hieftje. Hadamard transform ion mobility spectrometry. *Analytical Chemistry* **2006**, *78*, 4474.

[83] S. I. Merenbloom, R. S. Glaskin, Z. B. Henson, D. E. Clemmer. High-Resolution Ion Cyclotron Mobility Spectrometry. *Analytical Chemistry* **2009**, *81*, 1482.

[84] R. T. Kurulugama, F. M. Nachtigall, S. Lee, S. J. Valentine, D. E. Clemmer. Overtone Mobility Spectrometry: Part 1. Experimental Observations. *Journal of the American Society for Mass Spectrometry* **2009**, *20*, 729.

[85] S. J. Valentine, S. T. Stokes, R. T. Kurulugama, F. M. Nachtigall, D. E. Clemmer. Overtone Mobility Spectrometry: Part 2. Theoretical Considerations of Resolving Power. *Journal of the American Society for Mass Spectrometry* **2009**, *20*, 738.

[86] S. L. Koeniger, S. I. Merenbloom, D. E. Clemmer. Evidence for many resolvable structures within conformation types of electrosprayed ubiquitin ions. *Journal of Physical Chemistry B* **2006**, *110*, 7017.

[87] S. I. Merenbloom, S. L. Koeniger, S. J. Valentine, M. D. Plasencia, D. E. Clemmer. IMS-IMS and IMS-IMS-IMS/MS for separating peptide and protein fragment ions. *Analytical Chemistry* **2006**, *78*, 2802.

[88] S. J. Valentine, R. T. Kurulugama, B. C. Bohrer, S. I. Merenbloom, R. A. Sowell, Y. Mechref, D. E. Clemmer. Developing IMS-IMS-MS for rapid characterization of abundant proteins in human plasma. *International Journal of Mass Spectrometry* **2009**, *283*, 149.

[89] N. J. Kirchner. *US Patent 5(206):506*, **1993**.

[90] K. Giles, S. D. Pringle, K. R. Worthington, D. Little, J. L. Wildgoose, R. H. Bateman. Applications of a travelling wave-based radio-frequencyonly stacked ring ion guide. *Rapid Communications in Mass Spectrometry* **2004**, *18*, 2401.

[91] S. D. Pringle, K. Giles, J. L. Wildgoose, J. P. Williams, S. E. Slade, K. Thalassinos, R. H. Bateman, M. T. Bowers, J. H. Scrivens. An investigation of the mobility separation of some peptide and protein ions using a new hybrid quadrupole/travelling wave IMS/oa-ToF instrument. *International Journal of Mass Spectrometry* **2007**, *261*, 1.

[92] A. A. Shvartsburg, R. D. Smith. Fundamentals of Traveling Wave Ion Mobility Spectrometry. *Analytical Chemistry* **2008**, *80*, 9689.

[93] K. Thalassinos, M. Grabenauer, S. E. Slade, G. R. Hilton, M. T. Bowers, J. H. Scrivens. Characterization of Phosphorylated Peptides Using Traveling Wave-Based and Drift Cell Ion Mobility Mass Spectrometry. *Analytical Chemistry* **2009**, *81*, 248.

[94] J. P. Williams, J. H. Scrivens. Coupling desorption electrospray ionisation and neutral desorption/extractive electrospray ionisation with a travelling-wave based ion mobility mass spectrometer for the analysis of drugs. *Rapid Communications in Mass Spectrometry* **2008**, *22*, 187.

[95] M. P. Gorshkov. *USSR inventors certificate no 966583*, **1982**.

[96] I. A. Buryakov, E. V. Krylov, E. G. Nazarov, U. K. Rasulev. A New Method of Separation of Multi-Atomic Ions by Mobility at Atmospheric-Pressure Using a High-Frequency Amplitude-Asymmetric Strong Electric-Field. *International Journal of Mass Spectrometry and Ion Processes* **1993**, *128*, 143.

[97] R. A. Miller, G. A. Eiceman, E. G. Nazarov, A. T. King. A novel micromachined high-field asymmetric waveform-ion mobility spectrometer. *Sensors and Actuators B-Chemical* **2000**, *67*, 300.

[98] R. Guevremont. High-field asymmetric waveform ion mobility spectrometry: A new tool for mass spectrometry. *Journal of Chromatography A* **2004**, *1058*, 3.

[99] R. Guevremont, R. W. Purves. Atmospheric pressure ion focusing in a high-field asymmetric waveform ion mobility spectrometer. *Review of Scientific Instruments* **1999**, *70*, 1370.

[100] A. A. Shvartsburg, F. M. Li, K. Q. Tang, R. D. Smith. High-resolution field asymmetric waveform ion mobility spectrometry using new planar geometry analyzers. *Analytical Chemistry* **2006**, *78*, 3706.

[101] R. Mabrouki, R. T. Kelly, D. C. Prior, A. A. Shvartsburg, K. Q. Tang, R. D. Smith. Improving FAIMS Sensitivity Using a Planar Geometry with Slit Interfaces. *Journal of the American Society for Mass Spectrometry* **2009**, *20*, 1768.

[102] G. A. Eiceman, E. V. Krylov, E. G. Nazarov, R. A. Miller. Separation of ions from explosives in differential mobility spectrometry by vapor-modified drift gas. *Analytical Chemistry* **2004**, *76*, 4937.

[103] G. A. Eiceman, J. A. Stone. Ion mobility spectrometers in national defense. *Analytical Chemistry* **2004**, *76*, 390a.

[104] K. Q. Tang, F. M. Li, A. A. Shvartsburg, E. F. Strittmatter, R. D. Smith. Two-dimensional gas-phase separations coupled to mass Spectrometry for analysis of complex mixtures. *Analytical Chemistry* **2005**, *77*, 6381.

[105] A. A. Shvartsburg, R. D. Smith, A. Wilks, A. Koehl, D. Ruiz-Alonso, B. Boyle. Ultrafast Differential Ion Mobility Spectrometry at Extreme Electric Fields in Multichannel Microchips. *Analytical Chemistry* **2009**, *81*, 6489.

[106] A. A. Shvartsburg, K. Q. Tang, R. D. Smith, M. Holden, M. Rush, A. Thompson, D. Toutoungi. Ultrafast Differential Ion Mobility Spectrometry at Extreme Electric Fields Coupled to Mass Spectrometry. *Analytical Chemistry* **2009**, *81*, 8048.

[107] A. A. Shvartsburg, W. F. Danielson, R. D. Smith. High-Resolution Differential Ion Mobility Separations Using Helium-Rich Gases. *Analytical Chemistry* **2010**, *82*, 2456.

[108] A. A. Shvartsburg, K. Q. Tang, R. D. Smith. Differential Ion Mobility Separations of Peptides with Resolving Power Exceeding 50. *Analytical Chemistry* **2010**, *82*, 32.

[109] G. Vonhelden, T. Wyttenbach, M. T. Bowers. Inclusion of a Maldi Ion-Source in the Ion Chromatography Technique - Conformational Information on Polymer and Biomolecular Ions. *International Journal of Mass Spectrometry and Ion Processes* **1995**, *146*, 349.

[110] J. M. Koomen, B. T. Ruotolo, K. J. Gillig, J. A. McLean, D. H. Russell, M. J. Kang, K. R. Dunbar, K. Fuhrer, M. Gonin, J. A. Schultz. Oligonucleotide analysis with MALDI-ion-mobility-TOFMS. *Analytical and Bioanalytical Chemistry* **2002**, *373*, 612.

[111] J. A. McLean, D. H. Russell. Sub-femtomole peptide detection in ion mobility-time-of-flight mass spectrometry measurements. *Journal of Proteome Research* **2003**, *2*, 427.

[112] J. A. McLean, B. T. Ruotolo, K. J. Gillig, D. H. Russell. Ion mobility-mass spectrometry: a new paradigm for proteomics. *International Journal of Mass Spectrometry* **2005**, *240*, 301.

[113] S. Sundarapandian, J. C. May, J. A. McLean. Dual Source Ion Mobility-Mass Spectrometer for Direct Comparison of Electrospray Ionization and MALDI Collision Cross Section Measurements. *Analytical Chemistry* **2010**, *82*, 3247.

[114] I. M. Taban, A. F. M. Altelaar, Y. E. M. Van der Burgt, L. A. McDonnell, R. M. A. Heeren, J. Fuchser, G. Baykut. Imaging of peptides in the rat brain using MALDI-FTICR mass spectrometry. *Journal of the American Society for Mass Spectrometry* **2007**, *18*, 145.

[115] J. A. McLean, W. B. Ridenour, R. M. Caprioli. Profiling and imaging of tissues by imaging ion mobility-mass spectrometry. *Journal of Mass Spectrometry* **2007**, *42*, 1099.

[116] T. C. Rohner, D. Staab, M. Stoeckli. MALDI mass spectrometric imaging of biological tissue sections. *Mechanisms of Ageing and Development* **2005**, *126*, 177.

[117] M. Stoeckli, D. Staab, A. Schweitzer. Compound and metabolite distribution measured by MALDI mass spectrometric imaging in whole-body tissue sections. *International Journal of Mass Spectrometry* **2007**, *260*, 195.

[118] P. J. Trim, C. M. Henson, J. L. Avery, A. McEwen, M. F. Snel, E. Claude, P. S. Marshall, A. West, A. P. Princivalle, M. R. Clench. Matrix-Assisted Laser Desorption/Ionization-Ion Mobility Separation-Mass Spectrometry Imaging of Vinblastine in Whole Body Tissue Sections. *Analytical Chemistry* **2008**, *80*, 8628.

[119] M. C. Djidja, E. Claude, M. F. Snel, P. Scriven, S. Francese, V. Carolan, M. R. Clench. MALDI-Ion Mobility Separation-Mass Spectrometry Imaging of Glucose-Regulated Protein 78 kDa (Grp78) in Human Formalin-Fixed, Paraffin-Embedded Pancreatic Adenocarcinoma Tissue Sections. *Journal of Proteome Research* **2009**, *8*, 4876.

[120] J. Stauber, L. MacAleese, J. Franck, E. Claude, M. Snel, B. K. Kaletas, I. M. V. D. Wiel, M. Wisztorski, I. Fournier, R. M. A. Heeren. On-Tissue Protein Identification and Imaging by MALDI-Ion Mobility Mass Spectrometry. *Journal of the American Society for Mass Spectrometry* **2010**, *21*, 338.

[121] M. C. Djidja, E. Claude, M. F. Snel, S. Francese, P. Scriven, V. Carolan, M. R. Clench. Novel molecular tumour classification using MALDI-mass spectrometry imaging of tissue micro-array. *Analytical and Bioanalytical Chemistry* **2010**, *397*, 587.

[122] S. Prasad, K. Q. Tang, D. Manura, D. Papanastasiou, R. D. Smith. Simulation of Ion Motion in FAIMS through Combined Use of SIMION and Modified SDS. *Analytical Chemistry* **2009**, *81*, 8749.

[123] B. Wang, S. Valentine, M. Plasencia, S. Raghuraman, X. A. Zhang. Artificial neural networks for the prediction of peptide drift time in ion mobility mass spectrometry. *Bmc Bioinformatics* **2010**, *11*.

[124] L. MacAleese, J. Stauber, R. M. A. Heeren. Perspectives for imaging mass spectrometry in the proteomics landscape. *Proteomics* **2009**, *9*, 819.

[125] J. Stauber, L. MacAleese, J. Franck, E. Claude, M. Snel, B. K. Kaletas, I. Wiel, M. Wisztorski, I. Fournier, R. M. A. Heeren. On-

Tissue Protein Identification and Imaging by MALDI-Ion Mobility Mass Spectrometry. *Journal of the American Society for Mass Spectrometry* **2010**, *21*, 338.

[126] C. Hu, R. van der Heijden, M. Wang, J. van der Greef, T. Hankemeier, G. Xu. Analytical strategies in lipidomics and applications in disease biomarker discovery. *Journal of Chromatography B* **2009**, *877*, 2836.

[127] N. Goto-Inoue, T. Hayasaka, N. Zaima, M. Setou. Imaging mass spectrometry for lipidomics. *Biochimica Et Biophysica Acta* **2011**, *1811*, 961.

[128] R. C. Murphy, A. H. Merrill, Jr. Lipidomics and imaging mass spectrometry. *Biochimica Et Biophysica Acta* **2011**, *1811*, 635.

[129] M. Bedair, L. W. Sumner. Current and emerging mass-spectrometry technologies for metabolomics. *TrAC Trends in Analytical Chemistry* **2008**, *27*, 238.

[130] D. Y. Lee, B. P. Bowen, T. R. Northen. Mass spectrometry-based metabolomics, analysis of metabolite-protein interactions, and imaging. *Biotechniques* **2010**, *49*, 557.

[131] T. Greer, R. Sturm, L. Li. Mass spectrometry imaging for drugs and metabolites. *Journal of Proteomics* **2011**, *74*, 2617.

[132] B. Långström, P. Andrén, Ö. Lindhe, M. Svedberg, H. Hall. <i>In Vitro</i> Imaging Techniques in Neurodegenerative Diseases. *Molecular Imaging and Biology* **2007**, *9*, 161.

[133] L. A. McDonnell, G. L. Corthals, S. M. Willems, A. van Remoortere, R. J. M. van Zeijl, A. M. Deelder. Peptide and protein imaging mass spectrometry in cancer research. *Journal of Proteomics* **2010**, *73*, 1921.

[134] D. R. Ifa, N. E. Manicke, A. L. Dill, R. G. Cooks. Latent Fingerprint Chemical Imaging by Mass Spectrometry. *Science* **2008**, *321*, 805.

[135] D. Ifa, A. Jackson, G. Paglia, R. Cooks. Forensic applications of ambient ionization mass spectrometry. *Analytical and Bioanalytical Chemistry* **2009**, *394*, 1995.

[136] S. Chandra, D. R. Smith, G. H. Morrison. Peer Reviewed: A Subcellular Imaging by Dynamic SIMS Ion Microscopy. *Analytical Chemistry* **2000**, *72*, 104 A.

[137] I. V. Veryovkin, W. F. Calaway, C. E. Tripa, M. J. Pellin. Mass spectrometry on the nanoscale with ion sputtering based techniques: What is feasible. *Nuclear Instruments & Methods in*

Physics Research Section B-Beam Interactions with Materials and Atoms **2007**, *261*, 508.

[138] J. A. Bradshaw, O. S. Ovchinnikova, K. A. Meyer, D. E. Goeringer. Combined chemical and topographic imaging at atmospheric pressure via microprobe laser desorption/ionization mass spectrometry-atomic force microscopy. *Rapid Communications in Mass Spectrometry* **2009**, *23*, 3781.

[139] M. Koestler, D. Kirsch, A. Hester, A. Leisner, S. Guenther, B. Spengler. A high-resolution scanning microprobe matrix-assisted laser desorption/ionization ion source for imaging analysis on an ion trap/Fourier transform ion cyclotron resonance mass spectrometer. *Rapid Communications in Mass Spectrometry* **2008**, *22*, 3275.

[140] S. L. Luxembourg, T. H. Mize, L. A. McDonnell, R. M. A. Heeren. High-spatial resolution mass spectrometric imaging of peptide and protein distributions on a surface. *Analytical Chemistry* **2004**, *76*, 5339.

[141] O. Hadjar, G. Johnson, J. Laskin, G. Kibelka, S. Shill, K. Kuhn, C. Cameron, S. Kassan. IonCCD (TM) for Direct Position-Sensitive Charged-Particle Detection: from Electrons and keV Ions to Hyperthermal Biomolecular Ions. *Journal of the American Society for Mass Spectrometry* **2011**, *22*, 612.

[142] L. A. Klerk, N. P. Lockyer, A. Kharchenko, L. MacAleese, P. Y. W. Dankers, J. C. Vickerman, R. M. A. Heeren. C-60(+) Secondary Ion Microscopy Using a Delay Line Detector. *Analytical Chemistry* **2010**, *82*, 801.

[143] T. Jalowy, R. Neugebauer, M. Hattass, J. Fiol, F. Afaneh, J. A. M. Pereira, V. Collado, E. F. da Silveira, H. Schmidt-Bocking, K. O. Groeneveld. Dynamics of secondary ion emission: Novel energy and angular spectrometry. *Nuclear Instruments & Methods in Physics Research Section B-Beam Interactions with Materials and Atoms* **2002**, *193*, 762.

[144] J. H. Jungmann, L. MacAleese, R. Buijs, F. Giskes, A. de Snaijer, J. Visser, J. Visschers, M. J. J. Vrakking, R. M. A. Heeren. Fast, High Resolution Mass Spectrometry Imaging Using a Medipix Pixelated Detector. *Journal of the American Society for Mass Spectrometry* **2010**, *21*, 2023.

[145] C. Bamberger, U. Renz, A. Bamberger. Digital Imaging Mass Spectrometry. *Journal of the American Society for Mass Spectrometry* **2011**, *22*, 1079.

[146] J. H. Jungmann, L. MacAleese, J. Visser, M. J. J. Vrakking, R. M. A. Heeren. High Dynamic Range Bio-Molecular Ion Microscopy with the Timepix Detector. *Analytical Chemistry* **2011**, *83*, 7888.

[147] J. H. Jungmann, D. F. Smith, L. MacAleese, I. Klinkert, J. Visser, R. M. A. Heeren. Biological Tissue Imaging with a Position and Time Sensitive Pixelated Detector. *Journal of the American Society for Mass Spectrometry* **2012**, *23*, 1679.

[148] Julia H. Jungmann, Donald F. Smith, Luke MacAleese, Ivo Klinkert, Jan Visser, R. M. A. Heeren. Biological Tissue Imaging with a Position and Time Sensitive Pixelated Detector. *Journal of the American Society for Mass Spectrometry* **2012**.

[149] F. N. Svara, A. Kiss, T. W. Jaskolla, M. Karas, R. M. A. Heeren. High-Reactivity Matrices Increase the Sensitivity of Matrix Enhanced Secondary Ion Mass Spectrometry. *Analytical Chemistry* **2011**, *83*, 8308.

[150] D. Weibel, S. Wong, N. Lockyer, P. Blenkinsopp, R. Hill, J. C. Vickerman. A C-60 primary ion beam system for time of flight secondary ion mass spectrometry: Its development and secondary ion yield characteristics. *Analytical Chemistry* **2003**, *75*, 1754.

[151] J. Xu, S. Ostrowski, C. Szakal, A. G. Ewing, N. Winograd. ToF-SIMS imaging with cluster ion beams. *Applied Surface Science* **2004**, *231*, 159.

[152] F. M. Wanlass. *US Patent 3,356,858*, **1967**.

[153] M. Campbell, M. Collaboration. 10 years of the Medipix2 Collaboration. *Nuclear Instruments & Methods in Physics Research Section a-Accelerators Spectrometers Detectors and Associated Equipment* **2011**, *633*, S1.

[154] X. Llopart, R. Ballabriga, M. Campbell, L. Tlustos, W. Wong. Timepix, a 65k programmable pixel readout chip for arrival time, energy and/or photon counting measurements. *Nuclear Instruments & Methods in Physics Research Section a-Accelerators Spectrometers Detectors and Associated Equipment* **2007**, *581*, 485.

[155] X. Llopart, M. Campbell, R. Dinapoli, D. S. Segundo, E. Pemigotti. Medipix2: a 64-k pixel readout chip with 55 mu m square elements working in single photon counting mode. *Ieee Transactions on Nuclear Science* **2002**, *49*, 2279.

[156] J. Visser, B. van der Heijden, S. J. A. Weijers, R. de Vries, J. L. Visschers. A Gigabit per second read-out system for Medipix Quads. *Nuclear Instruments & Methods in Physics Research*

Section a-Accelerators Spectrometers Detectors and Associated Equipment **2011**, *633*, S22.

[157] Z. Vykydal, J. Visschers, D. S. Tezcan, K. De Munck, T. Borgers, W. Ruythooren, P. De Moor. The RELAXd project: Development of four-side tilable photon-counting imagers. *Nuclear Instruments & Methods in Physics Research Section a-Accelerators Spectrometers Detectors and Associated Equipment* **2008**, *591*, 241.

[158] D. Turecek, T. Holy, J. Jakubek, S. Pospisil, Z. Vykydal. Pixelman: a multi-platform data acquisition and processing software package for Medipix2, Timepix and Medipix3 detectors. *Journal of Instrumentation* **2011**, *6*.

[159] T. Holy, J. Jakubek, S. Pospisil, J. Uher, D. Vavrik, Z. Vykydal. Data acquisition and processing software package for Medipix2. *Nuclear Instruments & Methods in Physics Research Section a-Accelerators Spectrometers Detectors and Associated Equipment* **2006**, *563*, 254.

[160] T. L. Colliver, C. L. Brummel, M. L. Pacholski, F. D. Swanek, A. G. Ewing, N. Winograd. Atomic and Molecular Imaging at the Single-Cell Level with TOF-SIMS. *Analytical Chemistry* **1997**, *69*, 2225.

[161] R. Kersting, B. Hagenhoff, F. Kollmer, R. Mollers, E. Niehuis. Influence of primary ion bombardment conditions on the emission of molecular secondary ions. *Applied Surface Science* **2004**, *231*, 261.

[162] A. M. Piwowar, J. C. Vickerman. The role of molecular weight on the ToF-SIMS spectra of PMMA using Au+ and C-60(+) primary ions. *Surface and Interface Analysis* **2010**, *42*, 1387.

[163] D. E. Weibel, N. Lockyer, J. C. Vickerman. C-60 cluster ion bombardment of organic surfaces. *Applied Surface Science* **2004**, *231*, 146.

[164] S. C. C. Wong, R. Hill, P. Blenkinsopp, N. P. Lockyer, D. E. Weibel, J. C. Vickerman. Development of a C-60(+) ion gun for static SIMS and chemical imaging. *Applied Surface Science* **2003**, *203*, 219.

[165] A. Wucher. Molecular secondary ion formation under cluster bombardment: A fundamental review. *Applied Surface Science* **2006**, *252*, 6482.

[166] B. Cillero-Pastor, G. Eijkel, A. Kiss, F. J. Blanco, R. M. A. Heeren. Time-of-Flight Secondary Ion Mass Spectrometry-Based Molecular

Distribution Distinguishing Healthy and Osteoarthritic Human Cartilage. *Analytical Chemistry* **2012**, *84*, 8909.

[167] D. Debois, K. Hamze, V. Guerineau, J. P. Le Caer, I. B. Holland, P. Lopes, J. Ouazzani, S. J. Seror, A. Brunelle, O. Laprevote. In situ localisation and quantification of surfactins in a Bacillus subtilis swarming community by imaging mass spectrometry. *Proteomics* **2008**, *8*, 3682.

[168] N. Desbenoit, I. Schmitz-Afonso, C. Baudouin, O. Laprevote, D. Touboul, F. Brignole-Baudouin, A. Brunelle. Localisation and quantification of benzalkonium chloride in eye tissue by TOF-SIMS imaging and liquid chromatography mass spectrometry. *Analytical and bioanalytical chemistry* **2013**, *405*, 4039.

[169] L. Fornai, A. Angelini, I. Klinkert, F. Giskes, A. Kiss, G. Eijkel, E. A. Amstalden-van Hove, L. A. Klerk, M. Fedrigo, G. Pieraccini, G. Moneti, M. Valente, G. Thiene, R. M. A. Heeren. Three-dimensional molecular reconstruction of rat heart with mass spectrometry imaging. *Analytical and bioanalytical chemistry* **2012**, *404*, 2927.

[170] L. A. Klerk, P. Y. W. Dankers, E. R. Popa, A. W. Bosman, M. E. Sanders, K. A. Reedquist, R. M. A. Heeren. TOF-Secondary Ion Mass Spectrometry Imaging of Polymeric Scaffolds with Surrounding Tissue after in Vivo Implantation. *Analytical Chemistry* **2010**, *82*, 4337.

[171] S. L. Luxembourg, L. A. McDonnell, T. H. Mize, R. M. A. Heeren. Infrared mass spectrometric imaging below the diffraction limit. *Journal of Proteome Research* **2005**, *4*, 671.

[172] M. Froesch, S. L. Luxembourg, D. Verheijde, R. M. A. Heeren. Imaging mass spectrometry using a delay-line detector. *European Journal of Mass Spectrometry* **2010**, *16*, 35.

[173] J. H. Jungmann, A. Gijsbertsen, J. Visser, J. Visschers, R. M. A. Heeren, M. J. J. Vrakking. A new imaging method for understanding chemical dynamics: Efficient slice imaging using an in-vacuum pixel detector. *Review of Scientific Instruments* **2010**, *81*.

[174] J. H. Jungmann, D. F. Smith, A. Kiss, L. MacAleese, R. Buijs, R. M. A. Heeren. An in-vacuum, pixelated detection system for mass spectrometric analysis and imaging of macromolecules. *International Journal of Mass Spectrometry* **2013**, *341–342*, 34.

[175] A. Kiss, J. H. Jungmann, D. F. Smith, R. M. A. Heeren. Microscope mode secondary ion mass spectrometry imaging with a Timepix detector. *Review of Scientific Instruments* **2013**, *84*.

[176] X. Llopart, M. Campbell. First test measurements of a 64k pixel readout chip working in single photon counting mode. *Nuclear Instruments & Methods in Physics Research Section a-Accelerators Spectrometers Detectors and Associated Equipment* **2003**, *509*, 157.

[177] www.who.int. *The top 10 causes of death in 2011*.

[178] G. K. Hansson. Inflammation, atherosclerosis, and coronary artery disease - Reply. *New England Journal of Medicine* **2005**, *353*, 429.

[179] N. W. G. MEMBERS, D. A. Morrow, C. P. Cannon, R. L. Jesse, L. K. Newby, J. Ravkilde, A. B. Storrow, A. H. B. Wu, R. H. Christenson, N. C. MEMBERS, F. S. Apple, G. Francis, W. Tang. National Academy of Clinical Biochemistry Laboratory Medicine Practice Guidelines: Clinical Characteristics and Utilization of Biochemical Markers in Acute Coronary Syndromes. *Clinical Chemistry* **2007**, *53*, 552.

[180] M. Macht, W. Fiedler, K. Kürzinger, M. Przybylski. Mass Spectrometric Mapping of Protein Epitope Structures of Myocardial Infarct Markers Myoglobin and Troponin T†. *Biochemistry* **1996**, *35*, 15633.

[181] D. A. Ford, X. Han, C. C. Horner, R. W. Gross. Accumulation of Unsaturated Acylcarnitine Molecular Species During Acute Myocardial Ischemia: Metabolic Compartmentalization of Products of Fatty Acyl Chain Elongation in the Acylcarnitine Pool†. *Biochemistry* **1996**, *35*, 7903.

[182] J. Marshall, P. Kupchak, W. M. Zhu, J. Yantha, T. Vrees, S. Furesz, K. Jacks, C. Smith, I. Kireeva, R. Zhang, M. Takahashi, E. Stanton, G. Jackowski. Processing of serum proteins underlies the mass spectral fingerprinting of myocardial infarction. *Journal of Proteome Research* **2003**, *2*, 361.

[183] C. Delles, E. Schiffer, C. von zur Muhlen, K. Peter, P. Rossing, H. H. Parving, J. A. Dymott, U. Neisius, L. U. Zimmerli, J. K. Snell-Bergeon, D. M. Maahs, R. E. Schmieder, H. Mischak, A. F. Dominiczak. Urinary proteomic diagnosis of coronary artery disease: identification and clinical validation in 623 individuals. *Journal of Hypertension* **2010**, *28*, 2316.

[184] C. von zur Muhlen, E. Schiffer, P. Zuerbig, M. Kellmann, M. Brasse, N. Meert, R. C. Vanholder, A. F. Dominiczak, Y. C. Chen, H. Mischak, C. Bode, K. Peter. Evaluation of Urine Proteome Pattern Analysis for Its Potential To Reflect Coronary Artery Atherosclerosis in Symptomatic Patients. *Journal of Proteome Research* **2008**, *8*, 335.

[185] H. Y. Zhang, X. Chen, P. Hu, Q. L. Liang, X. P. Liang, Y. M. Wang, G. A. Luo. Metabolomic profiling of rat serum associated with isoproterenol-induced myocardial infarction using ultra-performance liquid chromatography/time-of-flight mass spectrometry and multivariate analysis. *Talanta* **2009**, *79*, 254.

[186] L. Anderson. Candidate-based proteomics in the search for biomarkers of cardiovascular disease. *The Journal of Physiology* **2005**, *563*, 23.

[187] R. F. Menger, W. L. Stutts, D. S. Anbukumar, J. A. Bowden, D. A. Ford, R. A. Yost. MALDI Mass Spectrometric Imaging of Cardiac Tissue Following Myocardial Infarction in a Rat Coronary Artery Ligation Model. *Analytical Chemistry* **2012**, *84*, 1117.

[188] J. W. Park, M. J. Cha, H. K. Shon, S. H. Kim, T. G. Lee, D. W. Moon, K. C. Hwang. ToF-SIMS analysis of myocardial infarcted tissue. *Surface and Interface Analysis* **2011**, *43*, 350.

[189] M. C. Fishbein, D. Maclean, P. R. Maroko. Experimental myocardial infarction in the rat: qualitative and quantitative changes during pathologic evolution. *Am J Pathol* **1978**, *90*, 57.

[190] A. Benedek, K. Moricz, Z. Juranyi, G. Gigler, G. Levay, L. G. Harsing, P. Matyus, G. Szenasi, M. Albert. Use of TTC staining for the evaluation of tissue injury in the early phases of reperfusion after focal cerebral ischemia in rats. *Brain Research* **2006**, *1116*, 159.

[191] I. Klinkert, L. A. McDonnell, S. L. Luxembourg, A. F. M. Altelaar, E. R. Amstalden, S. R. Piersma, R. M. A. Heeren. Tools and strategies for visualization of large image data sets in high-resolution imaging mass spectrometry. *Review of Scientific Instruments* **2007**, *78*.

[192] I. T. Jolliffe. *Principal Component Analysis*, Second Edition ed., Springer, **2002**.

[193] E. R. A. van Hove, T. R. Blackwell, I. Klinkert, G. B. Eijkel, R. M. A. Heeren, K. Glunde. Multimodal Mass Spectrometric Imaging of Small Molecules Reveals Distinct Spatio-Molecular Signatures in Differentially Metastatic Breast Tumor Models. *Cancer Research* **2010**, *70*, 9012.

[194] G. B. Eijkel, B. K. Kaletas, I. M. van der Wiel, J. M. Kros, T. M. Luider, R. M. A. Heeren. Correlating MALDI and SIMS imaging mass spectrometric datasets of biological tissue surfaces. *Surface and Interface Analysis* **2009**, *41*, 675.

[195] N. G. Frangogiannis, C. W. Smith, M. L. Entman. The inflammatory response in myocardial infarction. *Cardiovascular Research* **2002**, *53*, 31.

[196] D. A. Ford. Alterations in myocardial lipid metabolism during myocardial ischemia and reperfusion. *Progress in Lipid Research* **2002**, *41*, 6.

[197] T. Niizeki, Y. Takeishi, T. Arimoto, H. Takahashi, T. Shishido, Y. Koyama, K. Goto, R. A. Walsh, I. Kubota. Cardiac-specific overexpression of diacylglycerol kinase zeta attenuates left ventricular remodeling and improves survival after myocardial infarction. *American Journal of Physiology-Heart and Circulatory Physiology* **2007**, *292*, H1105.

[198] D. A. Ford, S. L. Hazen, J. E. Saffitz, R. W. Gross. The Rapid and Reversible Activation of a Calcium-Independent Plasmalogen-Selective Phospholipase-A2 during Myocardial-Ischemia. *Journal of Clinical Investigation* **1991**, *88*, 331.

[199] D. J. Mancuso, D. R. Abendschein, C. M. Jenkins, X. L. Han, J. E. Saffitz, R. B. Schuessler, R. W. Gross. Cardiac ischemia activates calcium-independent phospholipase A(2)beta, precipitating ventricular tachyarrhythmias in transgenic mice - Rescue of the lethal electrophysiologic phenotype by mechanism-based inhibition. *Journal of Biological Chemistry* **2003**, *278*, 22231.

[200] L. M. Smith, N. L. Kelleher, C. T. D. Proteomics. Proteoform: a single term describing protein complexity. *Nature Methods* **2013**, *10*, 186.

[201] N. L. Kelleher. Top-down proteomics. *Analytical Chemistry* **2004**, *76*, 197A.

[202] M. Yamashita, J. B. Fenn. Electrospray ion source. Another variation on the free-jet theme. *The Journal of Physical Chemistry* **1984**, *88*, 4451.

[203] C. K. Meng, M. Mann, J. B. Fenn. Of protons or proteins. *Zeitschrift für Physik D Atoms, Molecules and Clusters* **1988**, *10*, 361.

[204] A. G. Marshall, C. L. Hendrickson, G. S. Jackson. Fourier transform ion cyclotron resonance mass spectrometry: A primer. *Mass Spectrometry Reviews* **1998**, *17*, 1.

[205] A. Makarov. Electrostatic axially harmonic orbital trapping: A high-performance technique of mass analysis. *Analytical Chemistry* **2000**, *72*, 1156.

[206] R. A. Zubarev, A. Makarov. Orbitrap Mass Spectrometry. *Analytical Chemistry* **2013**, *85*, 5288.

[207] N. E. Mascini, R. M. A. Heeren. Protein identification in mass-spectrometry imaging. *Trac-Trends in Analytical Chemistry* **2012**, *40*, 28.

[208] K. L. Schey, D. M. Anderson, K. L. Rose. Spatially-Directed Protein Identification from Tissue Sections by Top-Down LC-MS/MS with Electron Transfer Dissociation. *Analytical Chemistry* **2013**.

[209] J. S. Sampson, A. M. Hawkridge, D. C. Muddiman. Generation and detection of multiply-charged peptides and proteins by matrix-assisted laser desorption electrospray ionization (MALDESI) Fourier transform ion cyclotron resonance mass spectrometry. *Journal of the American Society for Mass Spectrometry* **2006**, *17*, 1712.

[210] J. Shiea, M. Z. Huang, H. J. HSu, C. Y. Lee, C. H. Yuan, I. Beech, J. Sunner. Electrospray-assisted laser desorption/ionization mass spectrometry for direct ambient analysis of solids. *Rapid Communications in Mass Spectrometry* **2005**, *19*, 3701.

[211] Z. Takats, J. M. Wiseman, B. Gologan, R. G. Cooks. Mass spectrometry sampling under ambient conditions with desorption electrospray ionization. *Science* **2004**, *306*, 471.

[212] P. J. Roach, J. Laskin, A. Laskin. Nanospray desorption electrospray ionization: an ambient method for liquid-extraction surface sampling in mass spectrometry. *Analyst* **2010**, *135*, 2233.

[213] P. Nemes, A. Vertes. Laser ablation electrospray ionization for atmospheric pressure, in vivo, and imaging mass spectrometry. *Analytical Chemistry* **2007**, *79*, 8098.

[214] S. Trimpin, E. D. Inutan, T. N. Herath, C. N. McEwen. Laserspray Ionization, a New Atmospheric Pressure MALDI Method for Producing Highly Charged Gas-phase Ions of Peptides and Proteins Directly from Solid Solutions. *Molecular & Cellular Proteomics* **2010**, *9*, 362.

[215] E. D. Inutan, A. L. Richards, J. Wager-Miller, K. Mackie, C. N. McEwen, S. Trimpin. Laserspray Ionization, a New Method for Protein Analysis Directly from Tissue at Atmospheric Pressure with Ultrahigh Mass Resolution and Electron Transfer Dissociation. *Molecular & Cellular Proteomics* **2011**, *10*.

[216] P. Nemes, A. A. Barton, Y. Li, A. Vertes. Ambient molecular imaging and depth profiling of live tissue by infrared laser ablation

electrospray ionization mass spectrometry. *Analytical Chemistry* **2008**, *80*, 4575.

[217] A. Vertes, P. Nemes, B. Shrestha, A. A. Barton, Z. Y. Chen, Y. Li. Molecular imaging by Mid-IR laser ablation mass spectrometry. *Applied Physics a-Materials Science & Processing* **2008**, *93*, 885.

[218] P. Nemes, A. A. Barton, A. Vertes. Three-Dimensional Imaging of Metabolites in Tissues under Ambient Conditions by Laser Ablation Electrospray Ionization Mass Spectrometry. *Analytical Chemistry* **2009**, *81*, 6668.

[219] P. Nemes, A. S. Woods, A. Vertes. Simultaneous Imaging of Small Metabolites and Lipids in Rat Brain Tissues at Atmospheric Pressure by Laser Ablation Electrospray Ionization Mass Spectrometry. *Analytical Chemistry* **2010**, *82*, 982.

[220] B. Shrestha, P. Nemes, J. Nazarian, Y. Hathout, E. P. Hoffman, A. Vertes. Direct analysis of lipids and small metabolites in mouse brain tissue by AP IR-MALDI and reactive LAESI mass spectrometry. *Analyst* **2010**, *135*, 751.

[221] A. Vaikkinen, B. Shrestha, J. Nazarian, R. Kostiainen, A. Vertes, T. J. Kauppila. Simultaneous Detection of Nonpolar and Polar Compounds by Heat-Assisted Laser Ablation Electrospray Ionization Mass Spectrometry. *Analytical Chemistry* **2013**, *85*, 177.

[222] J. A. Stolee, A. Vertes. Toward Single-Cell Analysis by Plume Collimation in Laser Ablation Electrospray Ionization Mass Spectrometry. *Analytical Chemistry* **2013**, *85*, 3592.

[223] G. Parsiegla, B. Shrestha, F. Carriere, A. Vertes. Direct Analysis of Phycobilisomal Antenna Proteins and Metabolites in Small Cyanobacterial Populations by Laser Ablation Electrospray Ionization Mass Spectrometry. *Analytical Chemistry* **2012**, *84*, 34.

[224] K. H. Cochran, J. A. Barry, D. C. Muddiman, D. Hinks. Direct Analysis of Textile Fabrics and Dyes Using Infrared Matrix-Assisted Laser Desorption Electrospray Ionization Mass Spectrometry. *Analytical Chemistry* **2013**, *85*, 831.

[225] J. S. Sampson, K. K. Murray, D. C. Muddiman. Intact and Top-Down Characterization of Biomolecules and Direct Analysis Using Infrared Matrix-Assisted Laser Desorption Electrospray Ionization Coupled to FT-ICR, Mass Spectrometry. *Journal of the American Society for Mass Spectrometry* **2009**, *20*, 667.

[226] G. Robichaud, J. A. Barry, K. P. Garrard, D. C. Muddiman. Infrared Matrix-Assisted Laser Desorption Electrospray Ionization (IR-MALDESI) Imaging Source Coupled to a FT-ICR Mass

Spectrometer. *Journal of the American Society for Mass Spectrometry* **2013**, *24*, 92.

[227] D. M. Horn, R. A. Zubarev, F. W. McLafferty. Automated reduction and interpretation of high resolution electrospray mass spectra of large molecules. *Journal of the American Society for Mass Spectrometry* **2000**, *11*, 320.

[228] M. W. Senko, J. D. Canterbury, S. H. Guan, A. G. Marshall. A high-performance modular data system for Fourier transform ion cyclotron resonance mass spectrometry. *Rapid Communications in Mass Spectrometry* **1996**, *10*, 1839.

[229] L. Zamdborg, R. D. LeDuc, K. J. Glowacz, Y.-B. Kim, V. Viswanathan, I. T. Spaulding, B. P. Early, E. J. Bluhm, S. Babai, N. L. Kelleher. ProSight PTM 2.0: improved protein identification and characterization for top down mass spectrometry. *Nucleic Acids Research* **2007**, *35*, W701.

[230] D. F. Smith, A. Kharchenko, M. Konijnenburg, I. Klinkert, L. Pasa-Tolic, R. M. A. Heeren. Advanced Mass Calibration and Visualization for FT-ICR Mass Spectrometry Imaging. *Journal of the American Society for Mass Spectrometry* **2012**, *23*, 1865.

[231] T. H. Mize, I. Taban, M. Duursma, M. Seynen, M. Konijnenburg, A. Vijftigschild, C. V. Doornik, G. V. Rooij, R. M. A. Heeren. A modular data and control system to improve sensitivity, selectivity, speed of analysis, ease of use, and transient duration in an external source FTICR-MS. *International Journal of Mass Spectrometry* **2004**, *235*, 243.

[232] D. F. Smith, K. Aizikov, M. C. Duursma, F. Giskes, D. J. Spaanderman, L. A. McDonnell, P. B. O'Connor, R. M. A. Heeren. An External Matrix-Assisted Laser Desorption Ionization Source for Flexible FT-ICR Mass Spectrometry Imaging with Internal Calibration on Adjacent Samples. *Journal of the American Society for Mass Spectrometry* **2011**, *22*, 130.

Appendix

Table A1 List of annotated CID fragments

Annotated ions	Charge state	Experimental monoisotopic mass	Deconvoluted experimental mass	Theoretical monoisotopic mass	Error (Da)	Error (ppm)
b45	6	808.3980	4850.388	4850.392	-0.004	-0.82
b47	6	852.0772	5112.463	5112.487	-0.024	-4.68
b60	7	912.1633	6385.143	6385.156	-0.013	-2.01
b61	8	814.1519	6513.215	6513.251	-0.036	-5.47
b63	8	835.2934	6682.347	6683.356	-1.009	6.20
b64	8	849.6713	6797.371	6798.383	-1.013	5.59
b74	8	968.3539	7746.831	7746.850	-0.019	-2.45
b78	8	1015.998	8127.980	8129.035	-1.055	-0.55
b79	9	911.0048	8199.044	8200.072	-1.029	2.68
b103	12	907.5473	10890.57	10891.57	-1.002	4.42
b116	13	942.1721	12248.24	12249.25	-1.013	3.07
b118-H_2O	13	959.8743	12478.37	12479.36	-0.990	4.82
b118	14	892.5979	12496.37	12497.37	-0.996	4.34
b118	13	961.2596	12496.37	12497.37	-0.992	4.69
b123	14	926.5439	12971.61	12972.62	-1.007	3.36
b126	14	949.0561	13286.79	13287.76	-0.979	5.40
b127	14	958.2056	13414.88	13415.86	-0.980	5.24
b130	15	916.4662	13746.99	13747.05	-0.056	-4.06
y12	2	655.3613	1310.723	1310.721	0.001	0.96
y19	3	695.0475	2085.142	2085.149	-0.006	-3.10
y20	3	740.7350	2222.205	2222.208	-0.003	-1.25
y23	3	829.7870	2489.361	2489.366	-0.005	-2.03
y28	4	755.1494	3020.598	3020.599	-0.001	-0.50
y28	3	1006.867	3020.601	3020.599	0.002	0.59
y29	4	789.4123	3157.649	3157.658	-0.009	-2.79
y32	4	862.9439	3451.776	3452.786	-1.010	11.6
y34	5	733.1817	3665.908	3666.918	-1.009	11.2
y34	4	916.7271	3666.908	3666.918	-0.009	-2.57
y35	4	941.2432	3764.973	3765.986	-1.013	9.95
y35	5	753.1947	3765.973	3765.986	-0.013	-3.37

Annotated ions	Charge state	Experimental monoisotopic mass	Deconvoluted experimental mass	Theoretical monoisotopic mass	Error (Da)	Error (ppm)
y36	5	775.6125	3878.062	3879.070	-1.008	11.0
y36	4	969.7637	3879.055	3879.070	-0.015	-4.01
y38	5	819.0312	4095.156	4095.164	-0.008	-1.83
y47	6	854.9565	5129.739	5130.750	-1.011	7.67
y47	5	1025.948	5129.739	5130.750	-1.011	7.79
y56	8	775.0436	6200.349	6200.365	-0.016	-2.50
y56	7	885.7678	6200.374	6200.365	0.010	1.58
y57	7	902.1964	6315.375	6315.392	-0.017	-2.62
y58	7	914.6278	6402.395	6402.424	-0.029	-4.51
y58	6	1067.068	6402.410	6402.424	-0.014	-2.15
y58	8	800.3015	6402.412	6402.424	-0.011	-1.79
y59	7	930.6409	6514.486	6515.508	-1.021	4.48
y59	8	814.3112	6514.489	6515.508	0.032	4.97
y60	8	823.1901	6585.521	6586.545	0.027	4.04
y61	7	953.2221	6672.555	6673.577	0.029	4.32
y62	7	969.3717	6785.602	6786.661	-0.008	-1.19
y63	7	979.5217	6856.652	6857.698	0.005	0.72
y63	8	857.2091	6857.673	6857.698	-0.025	-3.64
y74-H_2O	8	989.2410	7913.928	7915.179	-0.203	-25.6
y74	8	991.4943	7931.954	7933.191	-0.187	-23.5
y74	8	991.5241	7932.193	7933.191	0.052	6.58
y96	11	921.3953	10135.35	10136.34	0.057	5.64
y128	15	911.6003	13674.00	13674.03	-0.030	-2.18
y139	16	923.3462	14773.54	14774.58	0.009	0.62
M-H_2O	16	935.4185	14966.70	14967.63	0.119	7.94

Table A2 List of annotated IRMPD fragments

Annotated ions	Charge state	Experimental monoisotopic mass	Deconvoluted experimental mass	Theoretical monoisotopic mass	Error (Da)	Error (ppm)
b94	11	895.9072	9854.979	9855.983	0.047	4.77
y23	3	829.7873	2489.362	2489.366	-0.004	-1.72
y28	3	1006.8642	3020.593	3020.599	-0.006	-2.10
y28	4	755.1479	3020.591	3020.599	-0.008	-2.51
y32	4	862.9419	3451.768	3452.786	0.032	9.34
y34	4	916.7274	3666.910	3666.918	-0.008	-2.23
y35	5	753.1932	3765.966	3765.986	-0.020	-5.37
y36	4	969.5154	3878.062	3879.070	0.042	10.87
y47	5	1026.1466	5130.733	5130.750	-0.017	-3.29
y47	6	855.1212	5130.727	5130.750	-0.023	-4.43
y56	7	885.7657	6200.360	6200.365	-0.005	-0.78
y56	8	775.0420	6200.336	6200.365	-0.028	-4.56
y58	7	914.6281	6402.397	6402.424	-0.027	-4.17
y59	7	930.6412	6514.488	6515.508	0.031	4.83
y61	7	953.3633	6673.543	6673.575	-0.031	-4.68
y61	8	834.0672	6672.537	6673.575	0.013	1.97
y81	10	860.0537	8600.537	8601.577	0.011	1.26
y96	11	921.3956	10135.35	10136.34	0.061	5.99
y125	15	886.7871	13301.81	13302.84	0.019	1.45
M-2H_2O	17	879.3894	14949.62	14950.71	-0.038	-2.55
M-H_2O	17	880.4510	14967.67	14968.72	-0.001	-0.10
precursor ion	17	881.5081	14985.64	14986.73	-0.042	-2.78

Summary

There is a constantly growing interest in biomedical research to visualize changes in the location of various biomolecules in tissue sections as a result of complex diseases. Mass spectrometry imaging is one of the techniques that enable the mapping of molecules on a 2D surface. However, the technique has several limitations that should be addressed by developments in ion generation and ion detection. This thesis presents work on instrument development in the field of mass spectrometry imaging. The improvements presented include both the ion source and the ion detection part of the mass spectrometer.

Mass spectrometry imaging is introduced in **Chapter 2**. This chapter evaluates MALDI and SIMS, the two main ionization techniques for mass spectrometry imaging. Also, recent developments in matrix-enhanced SIMS are discussed, namely the application of derivatized versions of common MALDI matrices such as halogenated derivatives of α-cyano-4-hydroxycinnamic acid for SIMS imaging. Most of these matrices show better ionization performance due to their decreased gas phase basicity. Thus, these results prove the correlation between the proton affinity of the matrix and the ionization efficiency in matrix-enhanced-SIMS. As a result, the most acidic matrix, 4-NO_2-CCA exhibits outstanding results among all tested experimental and classical matrix compounds. The second part of the chapter reviews the evolution of ion mobility methods and its application in combination with mass spectrometry for mass spectrometry imaging. The combination of the two methods opens new possibilities in mass spectrometry imaging by enabling the gas phase separation of nominally isobaric ions. Thus, by the combination of the two techniques better selectivity can be achieved which is advantageous for both qualitative and quantitative imaging of biomolecules. Also, the additional ion mobility separation enables the imaging of structural changes such as changes in protein or peptide conformation in a tissue sample.

Chapters 3-5 concentrate on developments in secondary ion mass spectrometry and the application of SIMS for biomedical research. **Chapter 3** and **4** discusses the implementation of an active pixel detector, the Timepix detector for microscope mode SIMS imaging which detector

promises increased speed, spatial resolution and sensitivity for mass spectrometry imaging. On the other hand **Chapter 5** demonstrates the application of high resolution SIMS imaging in biomedical research.

The work presented in **Chapter 3** is the first example of microscope mode secondary ion mass spectrometry imaging with a pixelated detector. The superior spatial resolution of the method is demonstrated over the current microprobe mode, TDC based systems but also the limitations of the system are discussed due to the lack of ion post-acceleration, the low secondary ion yield of the gold primary ion source used for the experiments and the low frame rate of the detector's read-out system. Furthermore, microscope mode SIMS imaging of a biological sample with an active-pixel detector is shown for the first time.

In **Chapter 4** a different ion source and an improved Timepix detector setup is implemented for microscope mode SIMS imaging. The enhanced sensitivity and mass range of the new high voltage detector setup combined with the higher secondary ion yield and lower fragmentation of the C_{60} primary ion source results in increased spectral quality for microscope mode SIMS imaging. In addition, the new detector setup enables the collection of negative ion mode SIMS data for the first time with the Timepix detector. The enhanced speed, sensitivity and mass range of the system is demonstrated with the imaging of a brain section in both positive and negative ion mode. Besides the small ions, intact phospholipids are detected directly from the tissue sample.

Chapter 5 presents an example for the application of high spatial resolution SIMS imaging in biomedical research. SIMS imaging is used to differentiate the different regions of a heart tissue section after myocardial infarction. Also, the changes in lipid metabolism due to heart attack are studied both in positive and negative ion mode. The increased diacylglycerol ion intensities in positive ion mode and the increased fatty acid abundance in negative ion mode indirectly suggest the overexpression of various phospholipase enzymes. These enzymes play important role in inflammatory processes and ventricular remodeling after the heart attack. Thus, SIMS imaging gives a new insight into the molecular changes following myocardial infarction.

Chapter 6 focuses on a different aspect of increasing the information content of a mass spectrometry imaging experiment. The

chapter presents a recently developed ambient pressure ion source, the Laser Ablation Electrospray Ionization source. A commercial version of this ion source is modified to interface it with an FT-ICR mass spectrometer. Thus, both the advantages of an ambient pressure ion source and the superior mass accuracy and mass resolving power of an FT-ICR mass spectrometer are employed to enable the top-down imaging of multiply charged intact proteins. The systems capabilities are demonstrated with protein solutions that are measured in combination with IRMPD and ECD fragmentation directly from a liquid droplet. Additionally, intact proteins are imaged directly from a frozen lung tissue section and are identified by CID and IRMPD imaging experiments. This work also presents the first example of imaging the distribution of a post-translational modification of a protein.

The new developments in ion detection and ion production for mass spectrometry imaging presented in this thesis have the potential to significantly increase the speed, spatial resolution and information content of this technique. Thus, these new developments have the potential to open up new application areas for mass spectrometry imaging.

Samenvatting

Er is een continu groeiende belangstelling voor biomedisch onderzoek om de visualisatie mogelijk te maken van de veranderde locatie van uiteenlopende soorten biomoleculen van complexe ziektes in weefselcoupes. Massaspectrometrie imaging is één van de technieken die het in kaart brengen van moleculen op een 2D oppervlak mogelijk maakt. De techniek heeft echter enige beperkingen, die opgelost kunnen worden met ontwikkelingen in ionengeneratie en –detectie. Dit proefschrift presenteert de instrumentontwikkeling die heeft plaatsgevonden op het gebied van de massaspectrometrie imaging. Deze ontwikkelingen betreffen verbeteringen in de ionenbron en het ionendetectie gedeelte van de massaspectrometer.

Een inleiding in massaspectrometrie imaging wordt gegeven in **Hoofdstuk 2**. Dit hoofdstuk evalueert MALDI en SIMS, de twee belangrijkste ionisatietechnieken voor massaspectrometrie imaging. Ook worden recente ontwikkelingen in *matrix-enhanced* SIMS besproken, namelijk het voor SIMS imaging toepassen van gederivatiseerde MALDI matrixen zoals gehalogeneerde derivaten van CHCA. De meeste van deze matrixen tonen een betere ionisatie-efficiëntie vanwege hun verminderde basiciteit in de gasfase. Deze resultaten bewijzen het verband tussen de proton-affiniteit van de matrix en de ionisatie-efficiëntie in *matrix-enhanced* SIMS. Meer specifiek laat de meeste zure matrix, 4-NO_2-CCA, uitstekende resultaten zien onder alle geteste experimentele en klassieke matrixen. Het tweede deel van dit hoofdstuk beschrijft de ontwikkeling van methoden voor ionenmobiliteitsscheiding, en de toepassing hiervan in combinatie met massaspectrometrie voor massaspectrometrie imaging. De combinatie van deze twee methoden opent nieuwe mogelijkheden voor massaspectrometrie imaging, door het in de gasfase scheiden van nominaal isobarische ionen. Dus door de combinatie van de twee technieken kan een betere selectiviteit worden verkregen die nuttig is voor zowel de kwalitatieve als kwantitatieve imaging van biomoleculen. Tevens maakt de extra ionenmobiliteitsscheiding het afbeelden van structuurveranderingen mogelijk, zoals veranderingen in de conformatie van eiwitten of peptiden in weefselmonsters.

De **Hoofdstukken 3-5** concentreren zich op ontwikkelingen in secundaire ionen massaspectrometrie en de toepassing ervan in biomedisch onderzoek. **Hoofdstuk 3** en **4** bespreekt de implementatie van de Timepix detector, een actieve pixeldetector die gebruikt wordt voor *microscope mode* SIMS imaging. Van deze detector wordt verwacht dat hij massaspectrometrie imaging experimenten mogelijk zal maken met een hogere snelheid, spatiële resolutie en gevoeligheid. Daarnaast laat **Hoofdstuk 5** de toepassing zien van hoge spatiële resolutie van SIMS imaging in biomedisch onderzoek.

In **Hoofdstuk 3** wordt het eerste voorbeeld van *microscope mode* secundaire ionen massaspectrometrie imaging met een pixeldetector beschreven. De superieure spatiële resolutie van deze methode wordt aangetoond met de huidige *microprobe mode* op een TDC-gebaseerd systeem. Ook worden de beperkingen van dit systeem besproken zoals het gebrek aan ionennaversnelling, het lage secundaire ionen rendement van de goud primaire ionenbron welke gebruikt wordt voor de experimenten en de lage framesnelheid van het uitleessysteem. Tevens wordt voor de eerste keer *microscope mode* SIMS imaging van een biologisch monster met een actieve pixeldetector gepresenteerd.

In **Hoofdstuk 4** staat een implementatie beschreven van een andere ionenbron en een verbeterde Timepix detectoropstelling voor *microscope mode* SIMS imaging. De hogere gevoeligheid en het grotere massabereik van de nieuwe hoogspanningsdetector-opstelling, in combinatie met het hogere secundaire ionen rendement en verminderde fragmentatie van de C_{60} primaire ionenbron, resulteert in een hogere spectrale kwaliteit voor *microscope mode* SIMS imaging. Bovendien maakt deze nieuwe detectoropstelling het meten met SIMS in de negatieve ionen modus met de Timepix detector voor de eerste keer mogelijk. De hogere snelheid en gevoeligheid en het grotere massabereik van het systeem worden aangetoond met imaging-experimenten van een weefselcoupe, zowel in de positieve als negatieve ionen modus. Behalve lichte ionen, worden ook intacte fosfolipiden direct uit het weefselmonster gedetecteerd.

Hoofdstuk 5 geeft een voorbeeld van de toepassing van hoge spatiële resolutie SIMS imaging in biomedisch onderzoek. SIMS imaging wordt gebruikt om de verschillende regio's van een hartweefselcoupe na een myocardiaal infarct te onderscheiden. Ook worden veranderingen in het

lipidemetabolisme veroorzaakt door een hartaanval onderzocht, zowel in de positieve en negatieve ionen modus. De verhoogde diacylglycerol ionintensiteiten in de positieve ionen modus, en de toegenomen hoeveelheid vetzuur in de negatieve ionen modus, wijzen op de overexpressie van verschillende fosfolipases. Deze enzymen spelen een belangrijke rol in ontstekingsprocessen en de ventriculaire remodeling na een hartaanval. SIMS imaging geeft dus een vernieuwd inzicht in de moleculaire veranderingen na een hartaanval.

Hoofdstuk 6 concentreert zich op een ander aspect van de verhoging van de informatiedichtheid van een massaspectrometrie imaging experiment. Het hoofdstuk toont de recente ontwikkelling van een ionenbron die werkt bij atmosferische druk, de '*Laser Ablation ElectroSpray Ionisation*' (LAESI) ionenbron. Een commerciële versie van deze ionenbron is gemodificeerd om deze met een FT-ICR massaspectrometer te kunnen combineren. Zo worden de voordelen van een ionenbron bij atmosferische druk en de superieure nauwkeurigheid en resolutie van een FT-ICR massaspectrometer gebruikt om de *top-down* imaging van meervoudig geladen intacte eiwitten mogelijk te maken. De mogelijkheden van het systeem worden aangetoond met eiwitoplossingen die rechtstreeks zijn gemeten uit een vloeibare druppel in combinatie met IRMPD and ECD fragmentatie. Daarnaast worden intacte eiwitten van een bevroren longweefselcoupe direct afgebeeld en worden ze geïdentificeerd door CID en IRMPD imaging experimenten. Ook wordt het eerste voorbeeld getoond van het afbeeldenvan de ruimtelijke verdeling van een posttranslationele modificatie van een eiwit.

De nieuwe ontwikkelingen in ionendetectie en -productie voor massaspectrometrie imaging die in dit proefschrift gepresenteerd worden, hebben het potentieel om de snelheid, de spatiële resolutie en de informatie-inhoud van deze techniek aanzienlijk te verbeteren. Deze nieuwe ontwikkelingen bieden daarom perspectief voor nieuwe toepassingsmogelijkheden in de massaspectrometrie imaging.

Acknowledgements

The work presented in a thesis requires efforts from multiple people. As that first of all I would like to express my gratitude to those who played some role in my scientific career and are not mentioned below.

I would like to thank my supervisor, Ron Heeren for his support and guidance during the PhD process. Ron, I am very grateful for giving me the amazing opportunity to be a member of your group and for all your help. Your energy, enthusiasm, curiosity and knowledge never stopped to amaze me during these four years I spent at AMOLF.

I also would like to thank my co-supervisor, Don Smith. The fact that he is co-author of most of the publications used in this thesis shows how invaluable his support was in finishing this thesis. Don, I learned a lot from you about mass spectrometry and science in general and I really enjoyed our many discussions.

Julia Jungmann, we worked on several instrumentation projects together and I had a lots of fun working with you. I will always remember the "high-tech" solutions we came up to tackle some of the challenges we were facing during our projects. I am also grateful for both yours and Don's friendship and that you accepted to be one of my paranymphs.

I also would like to thank Erika Amstalden van Hove for training me how to operate the TRIFT system and for always finding time to help me solve issues with the instrument.

I would like to thank Marc Duursma that he always found the time to assist me when I needed help in the lab. I will also miss the lunches with you and Gert. I also would like to thank our group technician, Frans Giskes and the group's electronics engineer Ronald Buis for their technical support on the TRIFT system.

I would like to thank Gert Eijkel for his support with data analysis. Your knowledge about multivariate data analysis methods and your ability to constantly come up with new ideas to analyze challenging datasets never ceased to amaze me. I will really miss our often philosophical discussions about life, the universe and everything.

I would like to thank Ivo Klinkert for his invaluable support regarding some of the softwares used for the Timepix projects and also I am grateful to him

and Nadine Mascini for their help with the Dutch translation of the summary of this thesis.

I would like to thank Marco Konijnenburg and Marco Seynen for their support with the softwares necessary for the success of the LAESI FT-ICR project.

Many thanks for all the help, discussions and the amazing time at AMOLF to the current and former members of the BIMS group: Lennaert Klerk, Luke MacAleese, Lara Fornai, Fabian Svara, Nadine Mascini Kamila Chughtai, Sana Chughtai, Anne Bruinen, Shane Ellis, Florian Marty, Berta Cillero-Pastor, Guzel Kireeva, Bob Hommersom, Mark Jansen, Bryn Flinders, Karolina Skraskova, Sarfaraz Syed, Andreas Nasioudis, Junkan Song, Andriy Kharchenko. I really enjoyed working with you.

During my stay at AMOLF I worked together with several collaborators. The most successful of these collaborations were the works done with members of the Yost lab at the University of Florida. Several of my publications and also one chapter in this thesis is the result of these collaborations for which I am thankful to David Pirmann, Kyle Mino, Rob Menger and Whitney Stutts.

I would like to thank the people at Protea Biosciences for their hospitality and the great time I spent at their facility and for their excellent support with the LAESI project: Matthew Powell, Brent Reschke, Holly Henderson, Trust Razunguzwa, Callee Walsh, Katherine Moss, Alessandro Baldi, Pamela Williams and Gregory Boyce.

Szeretnék köszönetet mondani Pollreisz Ferencnek és Vékey Károlynak, előző témavezetőimnek, akik megismertették velem a tömegspektrometria szépségeit és akiknek nagy szerepe volt abban, hogy ezt a négy évet Ron laborjában tölthettem.

Szeretném megköszönni Ica néninek, hogy megszerettette velem a kémiát és elindított azon az úton, aminek egy nagyon fontos lépése ez a könyv. Soha nem fogom elfelejteni a kémia szakköröket, versenyeket és a gyümölcstortákat. Szintén szeretnék köszönetet mondani a kémia szakkörös barátaimnak, Honvéd Daninak, Meleg Gábornak és Szilágyi Gergőnek.

Végül, de nem utolsó sorban szüleimnek, nagymamámnak és testvéremnek szeretném megköszönni a szeretetet és támogatást ami nélkül ez a doktori disszertáció nem jöhetett volna létre.

List of publications

This thesis is based on the following publications:

A. Kiss, R.M.A. Heeren, *Size, weight and position: Ion mobility spectrometry and imaging MS combined*, Analytical and Bioanalytical Chemistry 399, 8, 2623-2634, 2011 (Chapter 2)

F.N. Svara, A. Kiss, T. Jaskolla, M. Karas and R.M.A. Heeren, *High-reactivity matrices increase the sensitivity of Matrix Enhanced Secondary Ion Mass Spectrometry*, Analytical Chemistry 83, 8308-8313, 2011 (Chapter 2)

A. Kiss, J.H. Jungmann, D.F. Smith and R.M.A. Heeren, *Microscope mode secondary ion mass spectrometry imaging with a Timepix detector*, Review of Scientific Instruments 84, 013704 1-7, 2013 (Chapter 3)

A. Kiss, D. F. Smith, J. H. Jungmann, R. M. A. Heeren, *Cluster SIMS Microscope Mode Mass Spectrometry Imaging*, Rapid Communications in Mass Spectrometry, 27, 2745-2750, 2013 (Chapter 4)

A. Kiss, D. F. Smith, B. R. Reschke, M. J. Powell, R. M.A. Heeren, *Top-Down Mass Spectrometry Imaging of Intact Proteins by LAESI FT-ICR MS*, Proteomics, 2013, Accepted (Chapter 6)

Other publications:

W. L. Stutts, R. F. Menger, A. Kiss, R. M. A. Heeren, R. A Yost, *Characterization of Phosphatidylcholine Oxidation Products by MALDI MS^n*, Analytical Chemistry, 2013, Accepted

J. H. Jungmann, N. E. Mascini, A. Kiss, D. F. Smith, I. Klinkert, G. B. Eijkel, M. C. Duursma, B. Cillero Pastor, K. Chughtai, S. Chughtai, R. M. A. Heeren, *Mass Spectrometry Basics for Young Students: An Interactive Laboratory Tour*, Journal of the American Society of Mass Spectrometry 24, 979-982, 2013

D. F. Smith, A. Kiss, F. E. Leach III, E. W. Robinson, L. Paša-Tolić, R. M. A. Heeren, *High mass accuracy and high mass resolving power FT-ICR secondary ion mass spectrometry for biological tissue imaging*, Analytical and Bioanalytical Chemistry 405, 6069-6076, 2013

J. H. Jungmann, D. F. Smith, A. Kiss, L. MacAleese, R. Buijs, R.M.A. Heeren, *An in-vacuum, pixelated detection system for mass spectrometric analysis and imaging of macromolecules,* International Journal of Mass Spectrometry 341-342, 34-44, 2013

H.F. Wehrl, J. Schwab, K. Hasenbach, G. Reischl, G. Tabatabai, L. Quintanilla-Martinez, F. Jiru, K. Chughtai, A. Kiss, F. Cay, D. Bukala, R.M.A. Heeren, B.J. Pichler and A.W. Sauter, *Multimodal elucidation of the Choline metabolism in a Murine Glioma model using magnetic resonance spectroscopy and ^{11}C-choline positron emission tomography*, Cancer Research, 73, 1470-1480, 2013

D.A. Pirman, A. Kiss, R.M.A. Heeren and R. Yost, *Identifying tissue-specific signal variation in MALDI Mass Spectrometric Imaging by use of an internal standard*, Analytical Chemistry, 85, 1090-1096, 2013

D.A. Pirman, R. Reich, A. Kiss, R.M.A. Heeren and R. Yost, *Quantitative MALDI Tandem Mass Spectrometric Imaging of Cocaine from Brain Tissue with a Deuterated Internal Standard*, Analytical Chemistry, 85, 1081-1089, 2013

A. Bodzon-Kulakowska, A. Kiss, K. Chughtai and R.M.A. Heeren, *Distribution of cholesterol in the brain tissue as an example of TOF-SIMS analysis*, In**:** 8th Münster Conference on Single Cell and Molecule Analysis Nov. 16-17, 2011 : Proceedings /ed. S. König, New York: NOVA Publisher, 1-10, 2012

B. Cillero Pastor, G.B. Eijkel, A. Kiss, F.J. Blanco Garcia and R.M.A. Heeren, *Matrix-assisted laser desorption ionization–imaging mass spectrometry: A new methodology to study human osteoarthritic cartilage* Arthritis and Rheumatism 65, 3, 710-720, 2012

L. Fornai, A. Angelini, I. Klinkert, F.G. Giskes, A. Kiss, G.B. Eijkel, E.R. Amstalden van Hove, L.A. Klerk, M. Fedrigo, G. Pieraccini, G. Moneti, M. Valente, G. Thiene and R.M.A. Heeren, *Three-dimensional molecular reconstruction of rat heart with mass spectrometry imaging*, Analytical and Bioanalytical Chemistry, 404, 2927-2938, 2012

B. Cillero Pastor, G.B. Eijkel, A. Kiss, F.J. Blanco Garcia and R.M.A. Heeren, *Time-of-flight secondary ion mass spectrometry-based molecular distribution distinguishing healthy and osteoarthritic human cartilage*, Analytical Chemistry, 84, 8909-8916, 2012

S. Chughtai, K. Chughtai, B. Cillero Pastor, A. Kiss, P. Agrawal, L. MacAleese and R.M.A. Heeren, *A multimodal mass spectrometry imaging approach for the study of musculoskeletal tissues*, International Journal of Mass Spectrometry, 325-327, 150-160, 2012

Contributions to conferences and seminars:

Oral presentations:

András Kiss, Donald F. Smith, Brent R. Reschke, Matthew J. Powell, Ron M.A. Heeren: *Mass Spectrometry Imaging with a LAESI Hybrid Ion Trap FT-ICR Mass Spectrometer*, 61th ASMS Conference, 2013. June 9-13. Minneapolis, MN, USA

András Kiss, Anna Carrano, Don F. Smith, Saskia M. van der Vies, Ron M. A. Heeren: *Mass spectrometry imaging of brain tissue from patients with Alzheimer's disease*, Spring Meeting of the Dutch Mass Spectrometry Society (NVMS), 2011. April 7. Utrecht, The Netherlands

András Kiss, Anna Carrano, Don F. Smith, Saskia M. van der Vies, Ron M. A. Heeren: *Mass spectrometry imaging of brain tissue from patients with Alzheimer's disease*, Klein Colloquium, AMOLF, 2011. February 7. Amsterdam, The Netherlands

András Kiss, Fabian Svara, Thorsten W. Jaskolla, Michael Karas, Ron M. A. Heeren: *Novel matrices for matrix enhanced SIMS imaging*, 28th Informal Meeting on Mass Spectrometry, 2010. May 2-6. Kőszeg, Hungary

András Kiss, Ferenc Pollreisz, Károly Vékey: *The study of fatty acids, as potential biomarkers for characterizing obesity, with an HPLC-MS method*, 27th Informal Meeting on Mass Spectrometry, 2009. May 3-7. Retz, Austria

Kiss András, Ferenc Pollreisz, Károly Vékey: *Zsírsavak mint elhízást jellemző potenciális biomarkerek HPLC-MS vizsgálata (The study of fatty acids, the potential biomarkers for characterizing obesity, with an HPLC-MS method)*, National Conference of Scientific Students' Associations, Chemistry Section, 2009. April 6-8. Debrecen, Hungary

Kiss András, Sztáray Bálint: *Új arzán- és stibánszubsztituált kobaltkomplexek szintézise és elektronszerkezetük vizsgálata (Synthesis of new arsane and stibane substituted cobalt complexes and the study of their electronic structure)*, National Conference of Scientific Students' Associations, Chemistry Section, 2007. April 2-4. Szeged, Hungary

Posters:

András Kiss, Julia H. Jungmann, Donald F. Smith, Luke MacAleese, Ron M.A. Heeren: *Ion microscopy with the Timepix active pixel detector: Ultrahigh spatial resolution SIMS and MALDI analysis of complex surfaces*, 61th ASMS Conference, 2013. June 9-13. Minneapolis, MN, USA

András Kiss, Don F. Smith, Brent R. Reschke, Matthew J. Powell, Ron M. A. Heeren: *From cocaine to multiply charged proteins – imaging with a LAESI-hybrid iontrap FTICR mass spectrometer*, Netherlands Proteomics Centre (NPC) Progress Meeting, 2013. February 11-12. Utrecht, The Netherlands

András Kiss, Holly D. Henderson, Gregory R. Boyce, Brent R. Reschke, Gert B. Eijkel, Donald F. Smith, Matthew J. Powell, Ron M.A. Heeren: *Evaluation of a novel Laser Ablation Electrospray Ionization ion source for the imaging of bacteria from high salt content liquid medium*, 1st Ourense Conference on Imaging Mass Spectrometry, 2012. September 3-5. Ourense, Spain

András Kiss, Holly D. Henderson, Gregory R. Boyce, Brent R. Reschke, Gert B. Eijkel, Donald F. Smith, Matthew J. Powell, Ron M.A. Heeren: *Evaluation of a novel Laser Ablation Electrospray Ionization ion source for the imaging of bacteria from high salt content liquid medium*, 60th ASMS Conference, 2012. May 19-24. Vancouver, BC, Canada

András Kiss, Donald F. Smith, Diego F. Cobice, Ruth Andrew Ron M. A. Heeren: *Quantitative Secondary Ion Mass Spectrometry measurement of corticosteroids*, 2nd NVMS-BSMS International Conference on Mass Spectrometry, 2012. March 28-30. Kerkrade, The Netherlands

András Kiss, Anna Carrano, Saskia M. van der Vies, Ron M. A. Heeren: *Mass spectrometry imaging of brain tissue from patients with Alzheimer's disease*, 59th ASMS Conference, 2011. June 5-9. Denver, CO, USA

András Kiss, Anna Carrano, Don F. Smith, Saskia M. van der Vies, Ron M. A. Heeren: *Mass spectrometry imaging of brain tissue from patients with Alzheimer's disease*, Netherlands Proteomics Centre (NPC) Progress Meeting, 2011. January 13. Utrecht, The Netherlands

András Kiss, Fabian Svara, Thorsten W. Jaskolla, Michael Karas, Ron M. A. Heeren: *Novel matrices for matrix enhanced SIMS imaging*, 58th ASMS Conference, 2010. May 23-27. Salt Lake City, UT USA

Kiss András, Pollreisz Ferenc, Vékey Károly: Összefüggés a vérben észlelt zsírsavak, az obezitás és a diabétesz között *(Connection between diabetes, obesity and the fatty acid profile of human plasma)*, Separation Science Meeting, Hungarian Society for Separation Sciences, 2008. November 5-7. Sárvár, Hungary

Kiss András, Pollreisz Ferenc, Vékey Károly: *Zsírsavprofil meghatározása HPLC-MS módszerrel (Determination of fatty acid profile using HPLC-MS)*, IX. Congress of the Hungarian Society for the Study of Obesity, 2008. May 23-24. Budapest, Hungary

Curriculum Vitae

András Kiss was born in Tatabánya (Hungary) in 1985. After finishing high school at *Bárdos László Gimnázium*, Tatabánya in 2004 he studied chemistry at the *Eötvös Loránd University*, Budapest. He received his Masters degree in chemistry in 2009. He carried out his Masters research in the *Mass Spectrometry Group of the Chemical Research Center of the Hungarian Academy of Sciences*, Budapest under the supervision of Dr. Ferenc Pollreisz and Dr. Károly Vékey. His Masters project comprised of the study of changes in the fatty acid composition of human plasma due to obesity and type II diabetes using HPLC-MS. In 2009 he joined the *Biomolecular Imaging Mass Spectrometry Group* of Prof. Dr. Ron M. A. Heeren at *FOM Institute AMOLF*, Amsterdam to conduct a PhD research in the instrumentation and application of imaging mass spectrometry. The results of this research are presented in this thesis